Université de Neuchâtel
Institut de Microtechnique

Characterization of Liquid Crystal Light Valves for Neural Network Applications

Thèse

Présentée à la Faculté des sciences
pour obtenir le grade de docteur ès sciences

par

Wei Xue

Neuchâtel, mars 1994

IMPRIMATUR POUR LA THÈSE

Characterization of Liquid Crystal Light Valves for Neural Network Applications

de Monsieur Wei Xue

UNIVERSITÉ DE NEUCHÂTEL

FACULTÉ DES SCIENCES

La Faculté des sciences de l'Université de Neuchâtel
sur le rapport des membres du jury,

Messieurs R. Dändliker, A. Shah et H.J. White (Bristol)

autorise l'impression de la présente thèse.

Neuchâtel, le 11 mai 1994

Le doyen:

H.-H. Nägeli

纳沙特尔大学　　微技术所

液晶光阀的特性研究及其在人工神经网络中的应用

理学博士论文

薛　　唯

瑞　　士　　纳沙特尔

一九九四年三月

To my wife and daughter

献给

我的妻子和女儿

ABSTRACT

Liquid crystal light valve as a nonlinear thresholding and gain element plays a very important role in the optical neural networks. The first part of this thesis presents the theoretical and experimental characterization of liquid crystal light valves with reference to their application in neural networks. The second part deals with the implementation of optical neural networks using liquid crystal light valves.

The characterization of three types of liquid crystal light valves has been performed. From the point of view of optical neural network system, we have chosen a set of characteristic parameters, such as the effective gain, the spatial uniformity, the response speed, and the transfer characteristic represented by a sigmoid function, to evaluate the liquid crystal light valves. Of these parameters, the key is the effective gain which takes account of the sensitivity and the read-out efficiency and indicates the usability of a liquid crystal light valve. The other parameters influence the dynamics of optical neural network systems. We have shown that using a sigmoid function to fit the transfer curve is an effective means of the characterization of LCLVs.

The inherent peculiarity of optical neural networks lies in the fast communication speed between the neurons and the relatively slow response speed of each neuron. We have designed and built an ONN based on the Hopfield model. The ONN shows more complex and rich behavior, including oscillations. The dynamic behavior of the ONN depends on the parameters of the system and on the interconnections. The main parameters are the two ratios: the ratio of the response time to the propagation time and the ratio of the gain of the system to the slope of the transfer curve. The high time ratio increases the probability of oscillations. In our experiments the oscillations occur only when all neurons have similar response speed. Fortunately, the nonuniformity of the LCLV can effectively prevent the oscillation. The ratio of the gain to the slope influences the system's capability for associative memory. Our ONN system gave only one stable state, and no other local minimum was observed because the ratio of the gain to the slope was below a critical value .

The interconnections depend on the neural network model. In our experiments we used the inhibitory model and the inverted model. The interconnections in the two models are all negative, which increases also the probability of oscillations. Moreover, the low feedback efficiency of the two models is disadvantageous for the realization of an associative memory.

摘要

液晶光阀作为非线性阈值反馈元件在光学神经网络中发挥重要作用。本论文的第一部分讨论与光学神经网络应用有关的液晶光阀的理论和实验特性。第二部分讨论使用液晶光阀的光学神经网络系统。

本文研究了三种液晶光阀的特性。根据光学神经网络应用的特点，我们选择了一套评估液晶光阀的特性参量如有效增益，空间均匀度，响应速度，及用Sigmoid函数表征的非线性特性。其中关键是有效增益，它包括了灵敏度和读出效率的影响，可用来衡量液晶光阀的可用性。其它参量影响光学神经网络系统的动力学行为。本文引入Sigmoid函数来拟合特性曲线，从而可以定量地讨论光阀的非线性特性及其对系统动力学的影响。

光学神经网络的本质特性在于神经元之间极快的通讯速度和每一神经元较慢的响应速度。我们完成了一个基于Hopfield模型的光学神经网络系统。这一系统显示了包括振荡在内的非常复杂的动力学行为。系统的动力学行为依赖于系统的参量和神经元之间的互连。主要的参量是两个比值：一个是神经元的响应时间与神经元之间的通讯时间的比；另一个是系统的增益与特性曲线的斜率的比。高时间比增加振荡的可能性。实验表明当所有神经元具有近似相同的响应速度时系统开始振荡。然而液晶光阀的不均匀性可以有效的防止振荡。增益与斜率的比影响系统的联想存贮能力。在我们的光学神经网络系统中，由于这一比值低于一个临界值，所以系统只给出一个稳态，未观察到其它的区域极小。在实验中我们选择了Inhibitory模型和Inverted模型。这两个模型都使用全负互连，因而增加了振荡的可能性。此外，较低的反馈效率也不利于实现联想存贮。

CONTENTS

1

INTRODUCTION

The basic advantages of optics in information processing derives from its intrinsic parallelism and the ability of optical signals to propagate through free space without interaction. It has long been recognized that to realize these advantages in processing application, real-time, reusable, two-dimensional (2-D) devices referred to as Spatial Light Modulators (SLMs) which modify the amplitude, phase, and/or polarization of an optical wave front are essential. A diverse variety of SLMs have been proposed and developed.[1-4]

Optically addressed liquid crystal SLMs, or liquid crystal light valves (LCLV), as they are frequently called, were developed at the Hughes Research Laboratories in the 1970s.[5] The first generation of the LCLV used nematic liquid crystals as the electro-optic material and CdS as the photoreceptor. Since then much improvement has been made in both the liquid crystal material and the photoreceptor, such as the use of ferroelectric liquid crystal materials and amorphous silicon photoreceptors with p-i-n structure.[6] The newest generation of LCLV called Smart SLM has been developed over the past few years.[7,8] Since the LCLVs have the advantages of large working aperture, low power operation and moderate price over other modulators, they have been widely used in many optical systems as input/output displays, spatial filters, incoherent-to-coherent light converters, optical switches, and nonlinear transform/thresholding elements.[9,10]

Over the past few decades, a class of massively parallel and interconnected computational models, generally referred to as neural networks, has been intensively studied. These models are based on the structure and function of the human brain. Much of the interest in this field is due to the fact that human brains are able to solve problems, such as visual object recognition and verbal communication, that are currently very difficult or impossible to solve using digital computers. These models describe the brain as consisting of a highly interconnected network of a huge number of relatively simple neurons. The human brain is believed to have between 10^{11} and 10^{13} neurons, and each neuron has between 10^3 and 10^4 connections to other neurons.[11] Many mathematical models which describe the neural network have been proposed, such as the Hopfield model,[12] the Kohonen model,[13] and the adaptive

resonance theory.[14] These neural networks require completely different implementations than traditional computers. This requirement has led to significant efforts toward implementing neural networks in hardware in both the electronics and optics field.

The optical implementation of neural networks derives from several unique properties of optical systems, such as the three-dimensional (3-D) topology and the ability of optical beams to cross through one another in free space. Therefore the common characteristic of optical implementation of neural networks is the utilization of 3-D global interconnections. However, one can choose different ways to implement the gain and the nonlinear operations required by the neural models. There are two most popular techniques: The first approach uses electronic components where light source arrays and detector arrays are used to switch signals from optical to electronic carriers and vice versa, e.g. the early pioneering work on optical implementation of neural network performed by Farhat[15] and by Jang.[16] The second approach uses entirely optical means where either a liquid crystal light valve[17-19] or refractive crystals[20] are used as the nonlinear thresholding and gain element. Of the two implementations, the former is often called optoelectronic neural network (OENN), while the latter is called optical neural network (ONN). There are other implementations which used the personal computer (PC) instead of the parallel electronic circuits.[21] This kinds of implementations can be regarded as hybrid simulators rather than hardware implementations, because there are actually neither parallel communication channels nor analog nonlinearity, but serial communications and digital algorithms in the systems.

Although the optical neural network (ONN) was born at about the same time as the optoelectronic neural network (OENN), it has never attracted adequate attention. Most of the researchers, who declare themselves working in the field of optical implementation of neural networks, have been only interested in the OENN or the hybrid simulators during the past ten years. There may be many reasons, but the main reason, we believe, is due to the absence of suitable optically addressed SLMs. Although the LCLV has been considered a mature SLM technology, unfortunately one still has a lot of difficulties in finding a LCLV which is usable for ONN. For example, the high gain is vital to ONN, but is often not available for most of commercially available LCLVs. Although there have been many research papers dealt with the performance of LCLVs,[22-25] most of them were based on the isolated devices or the OENN rather than ONN. Therefore it is still an open question, what kind of LCLV is suitable for optical neural networks.

It is widely believed that an ONN should have the same behavior as an OENN or even a hybrid simulator does, if they implement the same model. If so, why are we using optical neural networks (ONN) at all? The optoelectronic neural network (OENN) can easily offer the flexibility, high gain and nonlinearity. The hybrid simulator is even more flexible and handy, particularly, in implementing the learning algorithms. However, we have never seen any analysis or discussion dealt with the equivalence of these implementations. Therefore, the second question arises: what is the inherent peculiarity of the ONN?

ONN is a typical complex dynamic system which is continuous both in neural state and in time. Therefore it is more comparable to the biological neural networks. ONN should exhibit rich and varied dynamics, e.g. oscillation and chaos, besides the fixed point. However, the dynamic behavior of ONN have not been brought to much attention. Lee reported an observation of oscillation in his optical neural network five years ago,[20] but did not give a clear explanation. Thereafter, there has not been any report relating to the dynamics of ONN until recently. Farhat proposed a model called bifurcating neural networks in order to demonstrate the dynamics.[26] They have implemented and characterized a single bifurcating neuron circuit, but have not reported the implementation of the bifurcating neural network. Naturally, one would ask what the dynamic behavior of ONN can do.

Our initial motivation of this work was to answer the first two questions, but the third question came on during the research. In this thesis we will try to answer how to evaluate the performance of LCLV both theoretically and experimentally; what parameters are necessary and appropriate to characterize LCLV for ONN applications; what is the necessary conditions for implementing ONN; how the parameters of LCLV influence the behavior of ONN. We will demonstrate the dynamics of a conventional optical neural network and give an analysis on the relation between the dynamic behavior and the system parameters. Recently, Farhat proposed the concept of "chaotic neurons",[27] and the scientists working in electronics field have begun the research on the exploitation and application of chaos in engineering, such as secure communication, associative memory and control problems. However, there is still a lot of work to be done before we can clearly answer the third question.

The thesis may be divided into two parts: the first part consists of Chapter 2 and Chapter 3 which deal with characterization of LCLVs, and the second part, Chapter 4, deals with the implementation of optical neural networks using LCLVs.

Chapter 2 is the theoretical part relating to the operation and characterization of LCLVs, which deals with the basic configurations of the LCLVs, the operating principles, the drive conditions, and the methods of characterization and analysis of the LCLVs from a system point of view. Section 1 presents the basics for LCLVs, which include a brief introduction of liquid crystals; a description of the structure of LCLVs and the electro-optics of three types of LCLVs. Section 2 discusses the drive waveforms for the LCLVs and the effects on the read/write characteristics. Section 3 discusses how to characterize the LCLVs from a system point of view and introduces a set of parameters for the evaluation of LCLVs. Section 4 gives two mathematical techniques for analyzing LCLV behaviors, which are particularly important in simulating the optical system where LCLVs are used.

Chapter 3 is the experimental part relating to the characterization of LCLVs. Three different types of LCLVs based on twisted nematic, homeotropic nematic and ferroelectric (smectic C*) liquid crystals have been experimentally investigated. The experimental results, procedures and conditions are given in detail. Finally, a comparison of three LCLVs is presented.

Chapter 4 deals with the application of the LCLVs to optical neural networks (ONN). Section 1 presents the Hopfield neural network model (H-model) and two modified H-models which could be implemented using optics. Section 2 discusses the basic principles of ONN design and gives the parameters of the ONN. Section 3 gives the experimental results of the optical implementations of the two neural network models. Section 4 analyses the experimental results and gives the explanations of the system's behavior. Section 5 briefly discusses the limitations of the ONN and the requirements for the LCLV from a system point of view.

2

THE PRINCIPLES OF OPERATION OF LCLVs

This chapter is the theoretical part relating to the operation and characterization of LCLVs, which deals with the basic configurations of the LCLVs, the operating principles, the drive conditions, and the methods of characterization and analysis of the LCLVs from a system point of view.

Section 1 presents the basics for LCLVs, which include a brief introduction of liquid crystals; a description of the structure of LCLVs and the electro-optics of three types of LCLVs.

Section 2 discusses the drive waveforms for the LCLVs and the effects on the read/write characteristics.

Section 3 discusses how to characterize the LCLVs from a system point of view and introduces a set of parameters for the evaluation of LCLVs.

Section 4 gives two mathematical techniques for analyzing LCLV behaviors, which are particularly important in simulating the optical system where LCLVs are used.

2.1 GENERAL DESCRIPTION OF LCLVS

2.1.1 Basics of Liquid Crystals[29,30]

It is commonly know that matter exists in three forms: solid, liquid and gas. For example, crystalline solids have a regular arrangement of the molecules, which is called long range order. Because of this order, crystals have the anisotropic physical properties. When a crystalline solid is heated, it transforms into an isotropic liquid at its melt point. Isotropic liquid does not have a long range order. However, there are certain substances which do not directly pass from

crystalline solid to isotropic liquid but adopt an intermediate phase which flows like a liquid but has the anisotropic physical properties similar to crystalline solid. This type of phase is called liquid crystals. The general definition of a liquid crystal is a liquid consisting of molecules that maintains order over a long distance relative to the molecular scale. Molecules are nanometers in length, so the order is in thousands of nanometers.

A. Phase structure of LC

The liquid crystals are a big family with tens of thousands members. Generally speaking liquid crystal molecules are oils, organic molecules. Liquid crystals can be classified from different standpoints. For example, according to the geometrical structure of the molecules, LCs can be divided into disk-like, lath-like and rod-like. The rod-like LC is the best investigated one and the most important with respect to practical applications such as LCD and LCLV. Therefore we only deal with rod-like liquid crystals in this thesis.

We are interested in the classification of LCs according to the crystalline phase since the electrical and optical properties depend directly on the phase. The phase structure of LC is characterized by the arrangement of the molecules, the conformation of the molecules and the intermolecular interaction. There are three major phases used in LCLV: nematic, smectic A and smectic C.

Nematics are the simplest type of liquid crystals, having only an orientation order. It is convenient to specify the direction of average orientation of the long axes of the molecules by a unit vector called the director n (Fig. 2.1a). All smectics have a layered structure, so they are more ordered than nematics. Smectics have both positional and orientational order which can be indicated by two unit vectors: the director n and the layer normal z. The difference between smectic A and smectic C is the relative orientation of n and z. In smectic A the director n is along the layer normal z but in smectic C the director n is tilted by a angle θ_t with respect to z (Fig. 2.1b and 2.1c). For smectic materials the layer spacing is about the magnitude of a typical length scale of the molecule.

The smectic Cs can be further divided into nonchiral or chiral nnes, the latter are called ferroelectric LCs, or smectic C*s as well. An implication of the added chirality on the structure ordering in the LC is the introduction of a macroscopic helix[3]. If we look at the molecular direction by moving along the z axis, we will see a precession of the director induced by the chirality. The director slightly rotates arnund z from layer to layer. So there is another order which can be

defined by a parameter p (pitch) which is the value of the translation along z needed to find the same molecular direction.

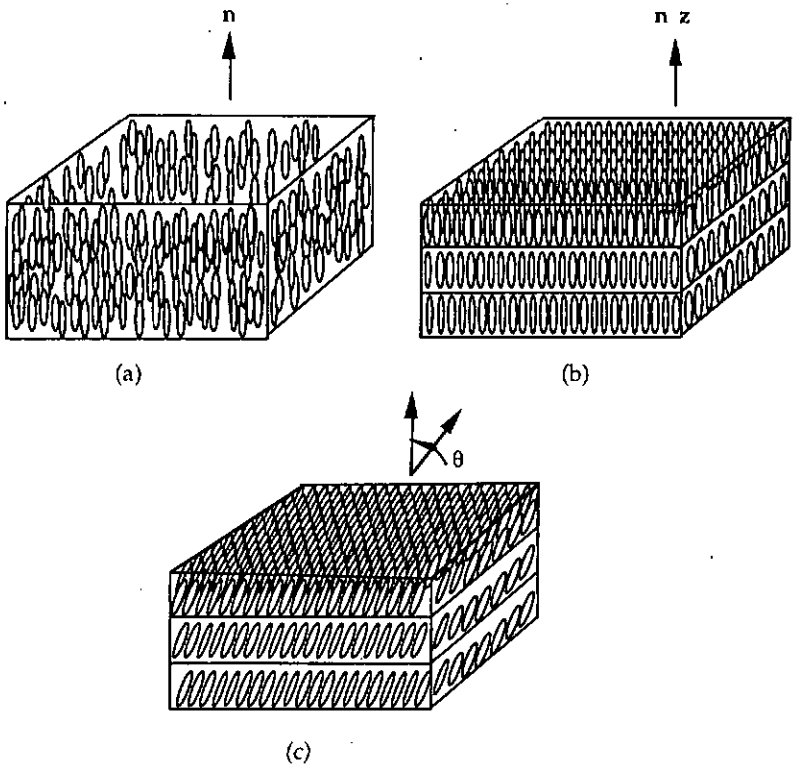

Fig. 2.1 The arrangement of molecules in the nematic (a), smectic A (b) and smectic C (c).

B. Electric and optical properties

As a result of the order, liquid crystals exhibit anisotropy in many of their properties. For example, nematics and smectic As behave optically like uniaxial crystals with the optical axis along the director, whereas smectic C is biaxial. We will limit ourselves to a discussion of the electric and optical properties which are directly related to LCLV operation.

The LC molecule may carry a permanent electric dipole. A macroscopic sample of a LC, however, might or might not be polar (ferroelectric), depending on the symmetry of the dipoles within the sample. So there may be two kinds of

dielectric polarizations in the LC: one is a spontaneous polarization $\mathbf{P_s}$ coming from the permanent dipoles with some symmetry, e.g. in smectic C* phase; another is a induced polarization $\mathbf{P_i}$ coming from the reorientation or the electron cloud distortion of the LC molecules under a external electric field, e.g. in the nematic phase. The strength of the interaction between the external electric field and the induced polarization is described by the dielectric tensor, $\varepsilon_{\alpha\beta}$ (α,β = x, y, z). For uniaxial liquid crystals it is convenient to choose the director as the z axis. In this case, the dielectric anisotropy is given by

$$\Delta\varepsilon_{DC} = \varepsilon_{\parallel} - \varepsilon_{\perp}, \tag{2.1}$$

where $\varepsilon_{\parallel}$ and $\varepsilon_{\perp}$ refer to the dielectric constants parallel and perpendicular to the director, respectively. Liquid crystals can be positive or negative dielectric anisotropy ($\Delta\varepsilon > 0$ or $\Delta\varepsilon < 0$). Values for $\Delta\varepsilon$ of technically useful materials range from -6 to +50.[29] When a external electric field is applied to the liquid crystals, the interaction energy in the liquid crystals (SI unit) is

$$-\int \mathbf{D}\bullet d\mathbf{E} = -\frac{\varepsilon_0 \varepsilon_{\perp}}{2}\mathbf{E}^2 - \frac{\varepsilon_0 \Delta\varepsilon}{2}(\mathbf{n}\bullet\mathbf{E})^2 . \tag{2.2}$$

The energy function should be minimum when LC molecules reach a stable state. Therefore, according to Eq. (2.2), the director tends to be parallel to the field for the positive dielectric anisotropy case, or perpendicular to the field for the negative dielectric anisotropy case. For nematic and smectic A phase, there is no spontaneous polarization, but an induced polarization

$$\mathbf{P_i} = \Delta\varepsilon\,\varepsilon_0\,(\mathbf{n}\bullet\mathbf{E})\mathbf{n} + (\varepsilon_{\perp}-1)\varepsilon_0\mathbf{E}. \tag{2.3}$$

The dielectric anisotropy of smectic C is very complicated. In practice smectic C phase may also be considered to be uniaxial. Indeed, various experiments show that in most smectic C phase the molecules rotate very much like in a nematic phase.[30]

The chiral smectic C phase (C*) can be achieved by adding a chiral material or solute to a smectic C. The C* phase may also be considered to be uniaxial.[31] Due to symmetry considerations, when the molecule is chiral, a spontaneous polarization $\mathbf{P_s}$ exist in each layer and normal to the director **n**. So chiral smectic C phase is also called ferroelectric phase. In this case, the total polarization is

$$\mathbf{P} = \mathbf{P_S} + \mathbf{P_i} = \mathbf{P_s} + \Delta\varepsilon\,\varepsilon_0\,(\mathbf{n}\bullet\mathbf{E})\mathbf{n} + (\varepsilon_{\perp}-1)\varepsilon_0\mathbf{E}. \tag{2.4}$$

Usually ferroelectric LCs with a small negative dielectric anisotropy are used in the devices, and the spontaneous polarization is much greater than the induced

one. So for FLC we neglect the induced polarization's effect. However, a macroscopic sample of C* which freely develops its helix is still not ferroelectric due to the zero value of averaged spontaneous polarization along one pitch of the sample. By applying an electric field normal to the helical axis or using a special geometrical arrangement, such as a very thin cell, the helix can be suppressed and completely unwound. As a result, the sample is poled. The molecules are aligned in a plane perpendicular to E with a tilt θ with respect to the layer normal. When the field is reversed, the polarization P_s reverses direction, and because of the coupling between polarization and tilt, the molecular orientation switches from θ to -θ.[32]

The optical anisotropy or birefringence Δn is given by

$$\Delta n = n_{\parallel} - n_{\perp} = n_e - n_o \tag{2.5}$$

The general relation between Δn and Δε in the optical frequencies is

$$\varepsilon_{\parallel,\infty} = n^2_{\parallel} \; ; \; \varepsilon_{\perp\infty} = n^2_{\perp} \tag{2.6}$$

$$\Delta\varepsilon_{\infty} = n^2_{\parallel} - n^2_{\perp} \tag{2.7}$$

The symbol ∞ denotes very high (optical) frequency. In all known nematic and smectic LCs, Δn > 0, i.e. the value of n_e is greater than that for n_o. The values of n_o is about 1.5 for most materials. On the other hand, the values of n_e can be higher by as much as 0.45 for some materials or only by as 0.06 for the others.[29]

Actually the behavior of LC molecules in the devices are greatly constrained by the boundary conditions. A variety of LCLVs have been fabricated which use different phase deformation and alignment techniques combined with different LC materials. In order to understand the operating modes in different devices we must first discuss the configuration of the LCLV.

2.1.2 Structure of LCLV

The LCLV is an optical-to-optical image transducer which transfers and transposes information from one beam of light (called the write light) to a second beam of light that may be of a different coherence, wavelength or intensity (called the read light). A typical device structure is shown in Fig. 2.2(a). It consists of three main parts, the photoreceptor, the liquid crystal layer and the reflector/light blocking layer, which are sandwiched between transparent electrodes. The reflector/light blocking layer is most commonly a dielectric mirror which both reflects the read beam and reduces the effect of the read beam on the photoreceptor. The transparent electrodes are commonly made of indium-tin-

oxide (ITO: a compound of SnO_2 5% and In_2O_3 95%).

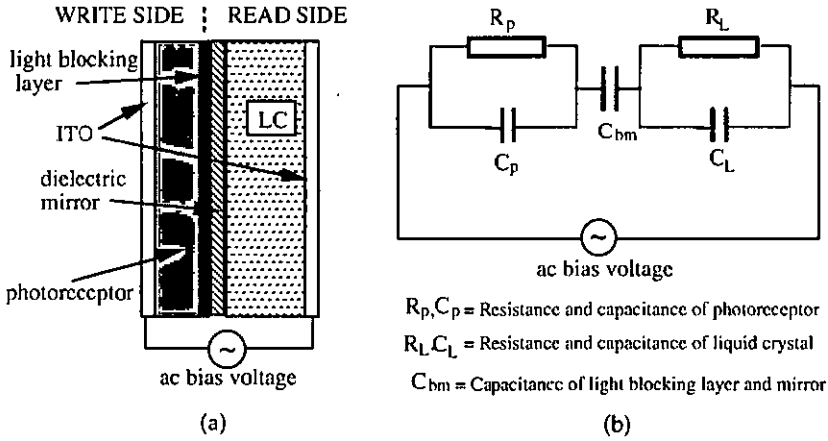

Fig. 2.2 Generic structure of a LCLV (a) and its equivalent circuit model (b).

The method of operation of the valve can be understood by consideration of a simple equivalent circuit as shown in Fig. 2.2(b).[22] If V_s is the rms value of the drive voltage, then from the figure the voltage V_{LC} developed across the liquid crystal cell is given by

$$V_{LC} = \frac{V_s Z_{LC}}{Z_p + Z_{bm} + Z_{LC}}, \tag{2.8}$$

$$Z_p = \frac{1}{i2\pi f C_p + \frac{1}{R_p}} \tag{2.9}$$

$$Z_{LC} = \frac{1}{i2\pi f C_L + \frac{1}{R_L}} \tag{2.10}$$

$$Z_{bm} = \frac{1}{i2\pi f C_{bm}} \tag{2.11}$$

where Z_p, Z_{bm}, Z_{LC} are the impedances of the photoreceptor, the light blocking layer and the liquid crystal layer, respectively. f is the frequency of the drive waveform. The impedance of the light blocking layer and liquid crystal are effectively constant at a particular drive frequency, whereas the impedance of the photoreceptor decreases with light intensity. The change in impedance of photoreceptor changes the voltage split between the photoreceptor and the liquid crystal layer. The AC voltage across the two electrodes is held constant, so that the

change in impedance of the photoreceptor produces a change of voltage across the liquid crystal.

For C_{bm} = 1.5nF, C_{LC} = 1.5nF, R_{LC} = 2.2MΩ, V_s = 10v, C_p = 2.5nF, R_p = $2x10^{10}$ Ω (dark) and 10^4 Ω (bright), then using Eqs. (2.8 - 2.11), the liquid crystal voltages are 5v for the ON-state and 3.8v for the OFF-state, respectively. It can be seen that the voltage on the LC corresponding to the illuminated area is larger than that in the nonilluminated area. It is this difference in the voltage that provides us with the means for controlling the LC electro-optic effect with the photoreceptor.

A write beam with a spatial intensity distribution creates a charge image on the photoreceptor which spatially modulates the voltage across the liquid crystal layer. This voltage modulation locally changes the state of the liquid crystal. The read beam is reflected from the mirror and, in passing twice through the liquid crystal, is modulated according to the state of the liquid crystal. The modulation is most commonly a polarization change.

We have studied three different types of LCLVs. A summary of the particular parts of the LCLVs is given in Table 2.1. In the following we give a brief description of the photoreceptor and reflector/light blocking layer. The liquid crystal layer will be discussed in Section 2.1.3.

Valve	Photoreceptor	Light blocking layer	Liquid crystal	Aperture size (mm)
LCLV1	CdS	CdTe + dielectric mirror	aligned nematic	R=37
LCLV2	a-Si:H	dielectric mirror	twisted nematic	40x40
LCLV3	a-Si:H	pixellated metal mirror	surface stable ferroelectric	30x30

Table 2.1 . Specific structure of the three LCLVs.

A. Photoreceptor

The function of the photoreceptor is to convert a light intensity distribution into an electric field distribution which will then modulate the liquid crystal. There are some basic requirements for the photoreceptor, such as: a low dark conductivity σ_d; a high photoconductivity σ_{ph} such that $\sigma_{ph} \gg \sigma_d$; high light sensitivity; high resolution; wide spectral response; and fast response. It is

important that the photoreceptor has a high dark resistivity in order that there is little voltage across the liquid crystal layer in the OFF-state. On the other hand, the dynamic range of the photoconductivity should be large such that most of drive voltage will be applied on the LC layer in the ON-state. The dark conductivity is given by

$$\sigma_d = \sigma_0 \exp\left(-\frac{E_g}{2k_BT}\right) \tag{2.12}$$

where k_B is Boltzmann's constant ($k_B = 1.38\times10^{-23}$ J/K, $k_BT = 0.026$eV at T = 300 K); Eg is the band gap (eV); and T is temperature (K).

The photoconductivity σ_{ph} is given by [33]

$$\sigma_{ph} = e\mu_n\tau_n\eta\frac{I(1-R)}{h\nu}\frac{(1-e^{-\alpha d})}{d} \tag{2.13}$$

where e is the electron charge; μ_n is the electrons' mobility; τ_n is the electrons' lifetime, which has different values at low light intensity and high light intensity; η is the quantum efficiency, which depends on temperature, photon energy and material. If the photon energy is high enough, η may be greater than unity;[34] I is the incident light intensity; R is the reflectance at the surface; hν is the photon energy; α is the absorption coefficient of the material; and d is the thickness of the photoreceptor layer.

A comparison of the characteristics for amorphous hydrogenated silicon (a-Si:H), crystalline silicon (c-Si) and cadmium sulfide (CdS) is given in Table 2.2.[33-35] The values in the Table are typical ones, which can vary in a large range due to different doping or preparation.

	E_g (eV)	σ_d $(\Omega\,cm)^{-1}$	σ_{ph}/σ_d	Time constant(μs)	μ_n (cm^2/V.s)
c-Si	1.1	10^{-6}	10^3~ 10^4	5	1350
a-Si:H	1.75	10^{-9}~ 10^{-11}	10^3~ 10^4	0.1	0.1~1
CdS	2.4	10^{-8}~ 10^{-10}	10^5	1000	300

Table 2.2. Typical values of the characteristics for amorphous hydrogenated silicon (a-Si:H), crystalline silicon (c-Si) and cadmium sulfide (CdS).

A wide range of types and forms of photoreceptor have been used in LCLVs. These include polycrystalline,[36] amorphous,[37,38] and single crystal[39]

photoconductors; amorphous[40,41] and crystalline photodiodes; and amorphous metal-insulator-semiconductor (MIS) structures.[42] In a photoconductor both electrical contacts are ohmic so that a carrier is injected at one contact for each carrier that is collected at the other. Photogenerated carriers drift with the electric field and contribute to the current until they recombine. In contrast, the photodiode has blocking contacts, under reverse bias no carriers are injected by the contacts. Consequently a deletion region with an approximately uniform electric field extends between the contacts. Photogenerated carriers drift with the electric field and are collected by their respective contacts: holes by the p-type contact and electrons by the n-type contact.[43]

The response time of a photoconductor is limited by the recombination time, the degree of carrier trapping, and the time required for carriers to drift through the device in an electric field. But the main factor is the recombination time. A photoconductor with long recombination time will show a memory effect, i.e. the actual value of the photoconductivity depends on the history of the photoconductor. So hysteresis is present: on the conductance curve the decrease in light intensity does not follow the same path as the previous increase in light intensity.[34] Table 2.2 gives the response time constant for some photoconductors. CdS has the longest time constant.

The response time of photodiodes depends on the transit time of carriers drifting across the depletion layer. Photodiodes are generally faster than photoconductors because the strong reverse field in the depletion region imparts a large velocity to the photogeneration carriers, thereby reducing transit time. Furthermore, photodiodes are not affected by many of the trapping effects associated with photoconductors.[44] The reverse bias gives a very high dark resistance as well.

Low-mobility photoconductors are attractive because they can be deposited as thin films and charge spreading is limited. These favor high resolution. The crystalline silicon photoreceptor needs a thicker layer (typical value is greater than 100μm) due to its low absorption coefficient. It also has a high mobility (see Table 2.2). These properties result in a low resolution. By using charge-confinement structures provided by p-n junction barriers, a resolution of 30 lp/mm was achieved.[45] Other crystals such as gallium arsenide (GaAs)[46] and bismuth silicon oxide ($Bi_{12}SiO_{20}$ or BSO)[47] have also been used as the photoreceptors, but both have much thicker layers: 0.5mm for GaAs and 2mm for BSO, and give poor resolution.

Of the polycrystalline semiconductors, CdS is particularly appropriate because the

light blocking layer can be easily formed in the same material system, e.g. CdTe.[36] A further advantage of CdS is the peaked spectral sensitivity in the green because a red read light can be used and the effects of read light breakthrough are minimized. However, the slow speed of response of CdS limits its more widespread use. One of the valves we have used, LCLV1, is based on sputtered cadmium sulfide CdS with a 19 μm layer of CdS. Hydrogenated amorphous silicon (a-Si:H) can also be prepared with a high dark resistivity in thin layers and has fast response. The other two valves which we have investigated, LCLV2 and LCLV3, use this material in a photoconductive layer. Both had much thinner photoconductor layers (about 2 μm). However, the reflector/light blocking layer cannot be made with the same isolation property as the CdS.

B. Reflector and light blocking layer

The reflector/light blocking layer is a critical part of the valve. Its function is to separate the photoreceptor from the read-out light and support efficient read-out. In many systems we require that the read and write beams are present on the device at the same time, that they have the same wavelength of light, and that the read illumination is several orders of magnitude greater than the write illumination. It is not efficient to make a good dielectric mirror because the performance of the valve is compromised by thick dielectric layers in between the photoreceptor and the liquid crystal. Because of the high-resistivity reflector/light blocking layer, there is a large voltage drop across it, which decreases the dynamic range of the photoconductor/reflector/light blocking layer structure.

LCLV1 has a 3 μm layer of CdTe light blocking layer and a 6 H/L pairs mirror on top of CdS. LCLV2 was commercial products made at GEC-Marconi, UK, had a dielectric mirror with no light blocking layer, we do not have the exact layer dimensions. LCLV3 was a commercial product of STC Technology, UK, and had 120 nm thick metal reflectors. The metal reflector was expected to isolate completely the photoreceptor from the read light because it is opaque. In order to achieve local voltage modulation it was pixellated on a 20 μm repeat spacing, so 25 line-pair resolution is available.

2.1.3 Alignment of LC and Operation Mode of LCLV

The role of the alignment is to produce single domain liquid crystals. The method for aligning the LC molecules on the bounding surfaces greatly affects the performance of LCLVs. For example, the nematic can be aligned either parallel or

perpendicular to the surface. Similarly, the smectic C phase of chiral molecules can be aligned with the layers perpendicular to the surfaces (bookshelf geometry) or vertically tilted to the surfaces (chevron structure). In each case the electro-optic response is quite different. The interaction between the external electric field and the dielectric polarization of LC molecules produces an electric torque, which rotates the molecules off the equilibrium state. The reorientation, which is also called deformation, at the same time produces a elastic torque which tends to force the molecules back the equilibrium state. There always exists a viscous torque as the molecules rotate. The three torques govern the molecules behavior under external electric field. The theoretical analysis is very complicated, so in this section we only qualitatively discuss three different alignments: homeotropic nematic, twisted nematic and smectic C* with bookshelf geometry, and corresponding operation mode: electrically controlled birefringence (ECB), hybrid field effect and surface stabilized bistability.

A. Homeotropic configuration of the nematic LC

The orientation of nematic LCs at surfaces is usually described by the tilt-bias angle defined as the angle made between the LC director and the plane of the surface. When the tilt angle is zero the orientation is "homogeneous" and when it is 90° it is "homeotropic" (see Fig.2.3(a)). The homeotropic alignment can be produced by judicious cleaning of the substrates, addition of surfactants to the liquid crystal, and deposition of surface coupling agents on the substrate.[48]

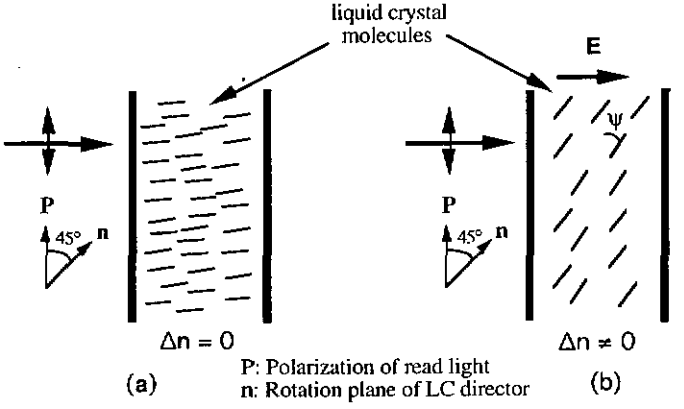

Fig. 2.3 Configuration of liquid crystal director in homeotropic alignment.; (a) OFF-state, (b) ON-state

The homeotropic configuration of the nematic is used with liquid crystals of negative dielectric anisotropy. In the absence of a electric field the molecules align nearly perpendicular to the surface (Fig.2.3(a)). The birefringence is essentially zero for light propagating along the optic axis (LC director). In the presence of an electric field applied normal to the surface, the liquid crystal director tends perpendicular to the field, i.e. parallel to the plane of the cell (Fig.2.3(b)). The equilibrium tilt angle is given by

$$\psi = \begin{cases} 0 & \text{for } V \le V_c \\ \frac{\pi}{2} - 2\tan^{-1}\exp\left(-\frac{V - V_c}{V_0}\right) & \text{for } V > V_c \end{cases} \qquad (2.14)$$

where V is the applied rms voltage, V_0 a constant which can be determined by measuring the voltage when the tilt angle is 50° and V_c a threshold voltage at which the tilting process begins,

$$V_c = \pi\left(\frac{K}{\Delta\varepsilon\varepsilon_0}\right)^{\frac{1}{2}}. \qquad (2.15)$$

The threshold voltage is about 2.5 v for $K = K_{33} = 7\times10^{-12}$(N); $\Delta\varepsilon = 1$; $\varepsilon_0 = 8.85\times10^{-12}$. After field removal, the molecules relax back to their original ordering. In this case the LC layer behaves like a wave plate with variable birefringence. The magnitude of the birefringence depends on the electric field and is a maximum when the director cannot move further as the voltage is increased, i.e. it is almost fully perpendicular to the applied field. So the operating mode is called electrically controlled birefringence (ECB).[49] In order that the director rotates to a well-defined orientation within the plane and that it rotates smoothly, a pre-tilt of several degrees is usually imposed on the liquid crystal by the particular alignment treatment.

The retardation of the LC layer is given by

$$\Delta(\psi) = \frac{2\pi}{\lambda}[n_e(\psi) - n_o]\,2d, \qquad (2.16)$$

$$\frac{1}{n_e^2(\psi)} = \frac{\cos^2\psi}{n_o^2} + \frac{\sin^2\psi}{n_e^2}, \qquad (2.17)$$

where d is the thickness of the LC, λ is the wavelength of the light, n_e and n_o are the refractive indices for the "slow" and "fast" components, respectively, ψ is the tilt anglegiven by Eq. (2.14). If the LC layer is set in such a way that the rotation plane of the liquid crystal director is at 45° to the plane of polarization of the incident light beam, then a crossed analyzer will give a dark OFF state and a light

ON state. By properly choosing the liquid crystals (n_o, n_e) and d, one can obtain π of the maximum retardation and the maximum reflectance. The LCLV1 had this configuration.

B. Twisted configuration of the nematic LC

The configuration of twisted nematics, such as 90° or 45° twist, refers to the total twist angle of the liquid crystal director between the front and back surface of the cell. On each surface the LC molecules align homogeneously, i.e. the director is parallel to the surface. This homogenous alignment can be obtained, e.g. by putting a polymer on the glass surface and then rubbing the polymer with a cloth in one direction, or by use of oblique vacuum depositions of very thin films of silicon monoxide and other materials onto the surface.[50] It turns out that the alignment layer forces the liquid crystal molecules to lie parallel to the cell walls with their optical axes along the alignment direction. Then we can arrange the cell plates so that the two alignment directions are at an angle to each other. The molecules between the two surfaces will, according to the continuum theory,[30] continuously and uniformly twist from one surface to another. If the plates are turned 45° with respect to each other, then we obtain 45° twist (see Fig. 2.4(a)). The 90° twist is commonly used in transmission cells, and the 45° twist is used in reflective devices, such as the Hughes LCLV[36] and the LCLV2.

In order to describe the orientation of molecules clearly, we define two angles: twist angle describes the rotation in the plane which is parallel to the electrodes plane, and tilt angle describes the rotation in the plane which is perpendicular to electrodes plane. In the absence of a electric field the tilt angle for all molecules is zero, but the twist angle of a molecule depends on its position across the layer, e.g. it is 0° on the front cell wall and 45° on the back. The twisted LC layer acts as an optically active medium which is able to rotate the polarization of a read light which passes through it. The incident light with polarization along the front alignment direction is guided by the molecules and its polarization rotates till the back plane, i.e. 45°. Then the light is reflected by the dielectric mirror and emerges with the same polarization. Therefore, there will be a dark OFF-state if we put a crossed analyzer in the reflected beam.

Nematics with positive dielectric anisotropy are used in the twisted configuration. When a electric field is applied across the liquid crystal, the helical arrangement disappears. The LC molecules tend to be perpendicular to the electrodes, i.e. tilt angle no longer zero. If all molecules were rotated to the

perpendicular alignment (tilt angle 90°), the polarization of the light would be unaffected by the liquid crystals and we would have a dark ON-state as well. However not all the molecules tilt by the same angle since the molecules on the cell walls are strongly constrained by the alignment layers. Actually only the molecules in the center of the cell tilt 90° to align with the applied electric field while the molecules on the cell walls keep along the alignment directions (tilt angle is still zero). The rest which are in the region near each wall of the cell tilt between 0° and 90°. In this orientation of the molecules, the optical birefringence appears. We call such regions birefringent regions. Obviously, there are two kinds of region near the front and back wall, respectively. But we will show that usually only one region is effective after we have discussed the twist angle (Fig. 2.4(b)).

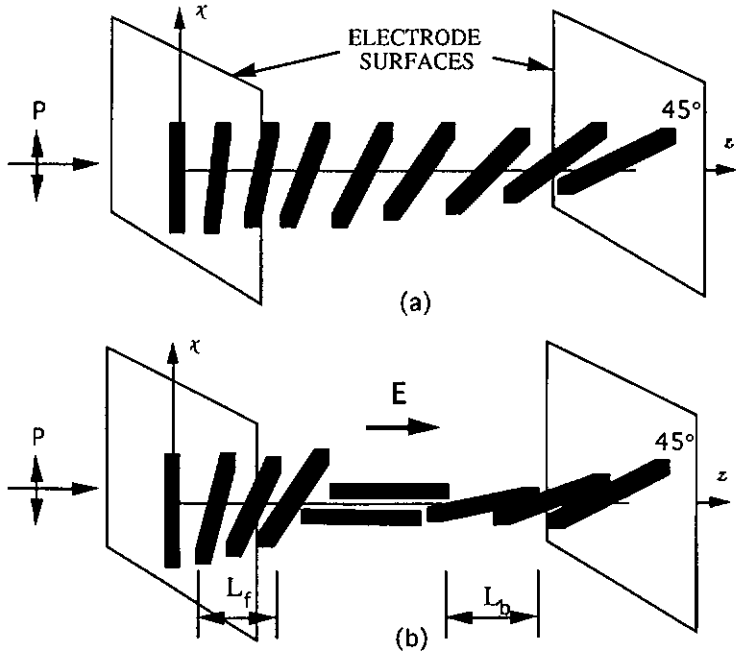

Fig. 2.4 Configuration of liquid crystal director in twisted alignment.; (a) OFF-state, (b) ON-state , Lf is the thickness of the front birefringent region., Lb is of the back birefringent region.

The twist of the molecules is transmitted from layer to layer by means of long range intermolecular alignment forces that are inherent in the liquid crystal. Generally speaking, as the tilt angle of the molecules increases (towards the perpendicular), the transmittance of the twist, from layer to layer, becomes less

effective. If any layer has molecules aligned perpendicular to the electrodes, the transmittance of the twist by that layer goes to zero. This has the effect of cutting the entire twist helix into two separate parts. It turns out that upon application of an electric field, half the molecules in the layer adopt the alignment direction associated with the front electrode (twist angle is zero), and the other half adopt the alignment direction associated with the back electrode (twist angle is 45°).[36]

When the polarization of the incident light is parallel to the front alignment direction, the front birefringent region no longer appears birefringence, but the back birefringent region will produce a retardation

$$\Delta = \frac{4\pi}{\lambda} \int_{L_b} [n_e(\psi) - n_o] dz, \tag{2.18}$$

$$\psi = f(V, z), \tag{2.19}$$

where L_b is the thickness of the back birefringent region, and ψ is the tilt angle. Because of the nonlinear distribution of the tilt angle (Eq. (2.19)), it has not been possible to determine an explicit expression for Δ. When $\Delta = \pi$ the LC layer acts as a half wave plate which rotates the incident polarization through 90°, so a crossed analyzer will give a bright ON-state. If the incident polarization is set parallel to the back alignment direction (45°), then the front birefringent region will affects the polarization. The operation mode in the twisted nematic configuration is called hybrid field mode since it uses the optical activity effect in the OFF-state and the optical birefringence effect in the ON-state.

There is a simplified model[25] in which the tilt angle is supposed to be same for all molecules under a given electric field, and the twist structure keeps unchanged. Under these approximation the Eqs. (2.14), (2.15) and (2.17) can be used for twisted nematics as well, with $K = K_{11} + (K_{33} - 2K_{22})/4$.

The twisted nematic assures a better dark OFF-state and fast response compared with the homeotropic nematic. But it is difficult to obtain a linear polarization output due to the nonuniform birefringence and the uncontrollable thickness of the birefringent region, which results in a less efficient ON-state. In the homeotropic nematic, however, the thickness of LC layer is well defined and the rotation of the molecules is nearly uniform since the alignment force in the homeotropic is much weaker than in the twisted configuration. So a high efficiency linearly polarized output can be obtained in the homeotropic configuration.

C. Surface stabilized configuration of ferroelectric LC (SSFLC)

The chiral smectic C phase has ferroelectric properties (see Section 2.1.1) and the spontaneous polarization in each layer is parallel to the layer plane and normal to the LC director. In the bulk FLC the LC director precesses in a helix from layer to layer (see Fig. 2.5(a)). All possible orientations of the director form a cone. The polarization direction accordingly rotates from layer to layer as well. The spatial average of the polarization is zero, and therefore bulk FLCs cannot exhibit ferroelectric domains.

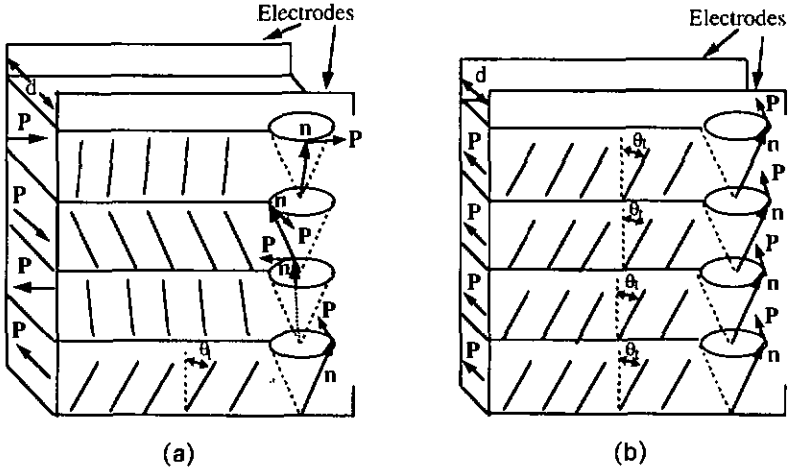

Fig. 2.5 Configuration of liquid crystal director in smectic C (a) Helical structure in bulk FLC; (b) Bookshelf structure in surface stabilized FLC.*

The surface stabilized ferroelectric liquid crystal (SSFLC) is a concept employing geometry and surface interaction to suppress the helix in the bulk FLC and produce two stabilized polarization orientations. The key to the SSFLC is using a very thin LC cell gap, usually less than two micrometers. As long as the cell thickness is less than the pitch of the helix, the strong surface forces align the molecules parallel to the substrate and the helix is unwound. The molecules are then arranged in the so-called 'bookshelf' geometry as shown in Fig. 2.5(b). The double constraint from cone and surfaces ensures two, and only two, directions of **n** at angles $\pm\theta_t$ with respect to the layer normal. However, these molecular directions are connected to opposite electric polarization directions that are perpendicular to the electrode plane. Application of an electric field **E** produces a torque through a first-order interaction with **P**, which switches the orientation of the FLC between these two stable states. In Fig. 2.5(b) one polarity of **E** results in **P**

pointing into the paper, and n at angle $+\theta_t$, reversing E rotates n to $-\theta_t$ with P pointing out of the paper.

Conventional techniques for aligning nematics also may be useful for ferroelectric smectic LC. This can be achieved if the LC material possesses a phase sequence of isotropic to cholesteric (nematic) to smectic A to smectic C*. It has been shown that the alignment obtained in the nematic phase is preserved when the material is cooled into the smectic phase.[31] However, one undesirable outcome often observed for most aligning agents is that the layers are not perpendicular to the cell walls, but tilted to the walls, forming a chevron structure. This geometry reduces the reorientational angle, and hence the contrast, and also can have effects on the bistable nature of the device. The chevron structure can be electrically reoriented to the bookshelf geometry.[51]

Unlike nematic LC where the electric field changes the birefringence of the LC layer, in SSFLC where δn is a constant the electric field does not change the birefringence, but rotates the optic axis. We call this operating mode the electrically switched optic axis (ESOA). The switching speed can be as fast as 20~30μs.[23] Typical values for the material birefringence δn range from 0.1 to 0.2. When the thickness of the LC cell is $d = \lambda/(4\delta n)$, a 180° phase shift occurs between the ordinary and the extraordinary eigenmodes of propagation, and the FLCLV operates as a switchable halfwave plate. An intensity modulator is made by placing the device between crossed polarizers. When the LC optic axis n is aligned with the incident polarizer, no rotation of polarization occurs, and the light is extinguished by the output analyzer. Reversing the sign of E rotates the optic axis by $2\theta_t$, resulting in a rotation of incident linearly polarized light by $4\theta_t$, and causing light to be transmitted by the output analyzer. By properly choosing the material, the tilt angle can be 45° ($2\theta_t = 45°$), therefore, the polarization between ON- and OFF-state rotates 90°. In practice, as we shall see, this ideal is difficult to attain. Moreover, the electrical address scheme precludes very fast electro-optic switching because the capacitance of the valve has to be charged and discharged during each cycle.

2.2 DRIVE SCHEMES AND THE EFFECTS ON THE OUTPUT OF LCLVs

When we discussed the function of the photoreceptor and the operation of the liquid crystal in the last section, we always supposed that there had been a proper

electric field, which was able to transfer the signal from the write side to the read side, across the photoreceptor and the LC. In this section we discuss the electric field for different configurations and operating modes. In order to avoid the electrolytic degradation of liquid crystals, a LCLV should be driven by a low frequency AC voltage instead of DC voltage.[30] In the case of a FLC, a balanced DC pulses should used such that the net DC voltage is zero.

2.2.1 Effects of the Drive Waveform on the Nematic LCLVs

The square waves were chosen to drive drive the nematic valves. Note that in the nematics there is no spontaneous polarization but an induced polarization, so the response of LC molecules to the electric field is quadratic. This means that the molecules respond only to the rms voltage, no matter what the direction of the field. The AC component on the read-out light appears when the frequency is below a critical frequency. The minimum frequency of the waveform is that at which the LC molecules begin to follow the amplitude rather than the rms of the waveform and the reflected light begins to exhibit a modulation at the drive frequency (usually about 500 Hz). There is a interest in working close to the minimum frequency because increasing the frequency reduces the sensitivity of the valve. We worked at 450 Hz with LCLV1 and at 1 kHz with LCLV2. The amplitude is set at the highest voltage which still gives a good dark state.

2.2.2 Effects of the Drive Waveform on the Smectic LCLVs

Because of its inherent bistable states, a FLCLV must be driven by using a bipolar pulse train (see Fig.2.6). A pulse of one polarity SETS the spatial distribution of director orientation according to the image incident on the write side, and a pulse of opposite polarity ERASES that distribution.

In Fig. 2.6, the positive pulse in the drive waveform corresponds to the ERASE pulse which switches the valve off and the negative pulse corresponds to the SET pulse which enables the write light to switch the valve on. For a FLCLV the drive waveform not only supports a bipolar electric field but also is a clock. The reading and writing operations need to be synchronized with the state of the clock. For examples; the FLCLV is absolutely switched off no matter whether there is a write beam when the ERASE pulse comes and only switched on when the SET pulse comes. Therefore the reading during $T_+ + T_+^D$ is always zero, and the writing is valid only during T_-. The reading may be called synchronous, when it takes place in the period of $T_-+T_+^D$, or integrated, when it takes place during the whole

duration of the waveform (Fig. 2.6).

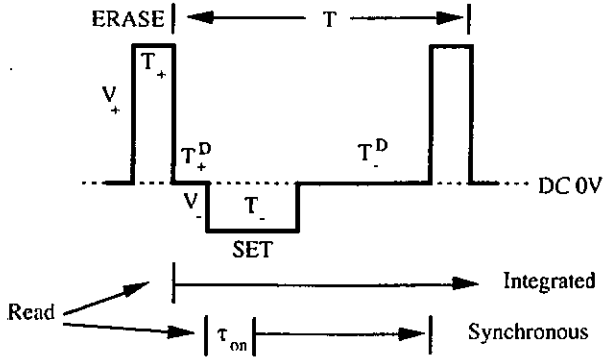

Fig. 2.6 Bipolar drive waveform for FLCLV.

There are several methods for synchronous reading. When the ferroelectric LC is in the bookstack geometry and therefore bistable, the FLCLV can be read in both SET pulse T_- and the delay T^D after SET pulse because the write-in image is stored and unaffected until the ERASE pulse comes. It is common to read during T^D where no voltage is applied to the valve.[52,53] This is advantageous where the light blocking layer is imperfect, because the effects of read light breakthrough on the operation of the valve are negligible, so the gain can be realized easily (see Section 2.3.2). However, read and write operations must be temporally separated, and this is not possible in all of the systems in which the FLCLV will be used as a real time threshold and feedback element, i.e. the reading and writing must take place in the same period T_-. If the state of the valve is read continuously over several driving periods, i.e. integrated reading, the results obtained will be far from optimum. The read-out efficiency of integrated mode is lower than of synchronous mode.

FLC's respond to the area of the drive pulse. The width of the pulse should be greater than its response time, and the amplitude is set at the highest voltage which still gives a good dark state and highest efficiency. However, the balanced DC waveforms are not so easy to obtain. For the valves using a photoconductor, the current-voltage characteristic is almost symmetric though there always exist some weak junction effects between the layers. The balanced DC waveforms may either enable both the ON- and OFF-state or none of them without any write light. Introducing an ERASE light may overcome the difficulty,[53] but increases the system complexity.

We chose an asymmetric bipolar waveform at 90 Hz cycle frequency (Fig. 2.6). The parameters of the drive waveform are: V_+ = 22.2V; V_- = 3.6V; T_+ = 655 μs; T_- = 3.2 ms; T^D = 6.65 ms; and the total period of the waveform is 11 ms. The disadvantage of this waveform is that the net voltage across the LC is not completely DC balanced. The latter may give rise to electrolytic degradation of the LC in the long term, although no such effects have been observed.

2.3 CHARACTERISTIC PARAMETERS OF LCLV

The operating principles and drive conditions of the LCLVs have been described in the last two sections. However, few real devices can operate according to the theoretical model, and few devices really have the versatility to meet all requirements for different applications. Therefore, how to characterize the LCLVs from a neural network system point of view is of concern in this section.

The performance of a LCLV is represented by a set of characteristic parameters. How to choose the parameters depends on the application. There exist some parameters which are widely used to characterize LCLVs, such as resolution, sensitivity, response speed and contrast.[1,24,45,54] However people often concentrate on one or a few performance characteristics at the expense of others. Performance numbers are critically dependent on measurement conditions, but the conditions are often not given in the literature or are not consistently related to actual device application. In order to avoid this imprecision, we define a set of parameters which are important to our application, before giving the experimental characterization results in the next chapter.

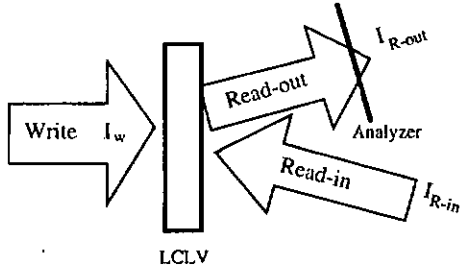

Fig. 2.7 Schematic of reading and writing a LCLV.

Before discussing the characteristic parameters we clarify some terminology which will be frequently used in the following discussions. As shown in Fig. 2.7,

there are three light beams related to reading and writing a LCLV: write light represented by its intensity I_W; read-in light represented by its intensity $I_{R\text{-}in}$ and polarization orientation; read-out light represented by its intensity $I_{R\text{-}out}$ and polarization. Usually the read-in light is linearly polarized with fixed polarization orientation and constant intensity. The read-out light is the reflection of the read-in light, but its polarization state has been modulated. The intensity modulation can be obtained behind the analyzer, however, the read-out intensity $I_{R\text{-}out}$ should exclude the absorption in the analyzer because the latter can vary according to the type selected.

2.3.1 Read-out Efficiency

The read-out efficiency η is defined as the ratio of read-out light intensity $I_{R\text{-}out}$ to read-in light intensity $I_{R\text{-}in}$.

$$\eta = \frac{I_{R\text{-}out}}{I_{R\text{-}in}} \tag{2.20}$$

Obviously the read-out efficiency is a function of write light intensity since the read-out intensity depends on the write light. Therefore $\eta \sim I_W$ curve can be used to represent the transfer characteristic instead of $I_{R\text{-}out} \sim I_W$ curve. In this way the transfer curve is more informative and comparable than other expressions.[24,54] The maximum read-out efficiency η_{max} directly indicates the power loss due to the LCLV in the system. So it must be considered in designing an optical system involving the LCLVs.

There are many factors which affect the maximum read-out efficiency. Some of them relate to the fabrication of the valve, such as the reflectance of the mirror and the thickness of the liquid crystal layer. These factors, which we call internal factors, set a limit to the η_{max}. For different valves there may be a large difference in the maximum read-out efficiency. However, to obtain the maximum efficiency, we have to optimize the external factors, such as the drive waveform. This is understandable because all the operations of the LCLV are directly dependent on the drive voltage. For the FLCLV the read-out efficiency is also related with the reading operation.

As discussed in Section 2.2.2, there are two ways to read the FLCLV: synchronous reading or integrated reading (see Fig. 2.6). When the rise time of the valve is much less than the SET time ($\tau_{on} << T_-$) and the reading is synchronous, the read-out efficiency can be maximum (η_{max}). However the integrated reading is effective only when the reading lasts at least one cycle time (T). The integrated

read-out efficiency (η_i) is

$$\eta_i = \eta_{max} \frac{T_- - \tau_{on} + T_-^D}{T}. \tag{2.21}$$

Although the result above is based on the optically addressed ferroelectric liquid crystal light modulator, the conclusion is also applicable to the electrically addressed FLC devices. This effect should also be considered in optical system design whenever a ferroelectric liquid crystal light valve is involved.

2.3.2 Effective Gain

The gain means the amplifying ability of a LCLV, which is usually defined as the ratio of the maximum read-in light intensity, which does not affect the transfer characteristic, to the minimum write light intensity which switches the valve on. This definition has some drawbacks, because if the read-out efficiency is very low there is no amplification available, even though the read-in light may be very strong.

Here we redefine the gain taking account of the read-out efficiency. We name it 'effective gain' (G_v), which is defined as the ratio of the read-out light intensity $I_{R\text{-}out}$ to the write light intensity $I_w(90\%)$ which switches the valve to 90% of the full ON-state.

$$G_v = \frac{I_{R\text{-}out}}{I_w(90\%)}. \tag{2.22}$$

According to Eq. (2.10), Eq. (2.12) becomes

$$G_v = \frac{\eta I_{R\text{-}in}}{I_w(90\%)}. \tag{2.23}$$

The maximum effective gain G_{eff}^{max} is obtained when both read-out efficiency and read-in light intensity reach their maximum value.

$$G_{eff}^{max} = \frac{\eta^{max} I_{R\text{-}in}^{max}}{I_w(90\%)}. \tag{2.24}$$

The effective gain is the usable amplifying power of a valve. $G_{eff}^{max} \leq 1$ means that there is no net gain.

With an ideal light blocking layer, write light at the threshold intensity would be capable of activating the liquid crystal layer and modulating a read beam of infinite intensity giving an LCLV with infinitely high gain. However this is not possible in real devices, because the performance of the valve is compromised by

thick dielectric layers in between the photoreceptor and the liquid crystal. In a LCLV a small percentage of read light passes through the mirror and affects the photoconductor. We fix an acceptable limit of breakthrough when the LCLV reaches 10 percent of its full ON-state due to the read-in light intensity. This defines a maximum read-in intensity $I_{R\text{-}in}^{max}$ for the valve.

For FLCLV there are two kinds of reading which result in different restrictions on the maximum read-in light intensity: one is the reading during the SET pulse T_-, called dynamic reading, and another is the reading during T_-^D, called static reading. In dynamic reading the maximum read-in light intensity $t_{R\text{-}in}^{max}$ is restricted by the breakthrough light which affects the photoconductor. In static reading there is no drive voltage across the device, so the read-in light intensity may be very high. In this case the maximum read-in light intensity $I_{R\text{-}in}^{max}$ is only limited by the characteristics of the FLC materials.

2.3.3 Spatial Uniformity

A good uniformity is very important but is not often available. Each parameter of the LCLV may vary according to the position on the valve. All parameters should be measured on a small area of each LCLV, because the optical performance is not homogeneous across the whole aperture of the FLCLV. We try to quantitatively evaluate the uniformity by using a uniformity area. For any characteristic parameter the uniformity area is defined as an area where the variation of the parameter's value is less than ±10 percent.

2.3.4 Response Speed

The response speed of the silicon-based photoreceptor is much faster than that of the liquid crystals.[45] The expressions for both rise and decay times of the nematic LC are[55]

$$\tau_r = \frac{\gamma}{\Delta\varepsilon\varepsilon_0 E^2 - K(\pi/d)^2} \tag{2.25}$$

$$\tau_d = \frac{d^2\gamma}{K\pi^2} \tag{2.26}$$

where γ = viscosity, $\Delta\varepsilon$ = dielectric anisotropy, E = electric field, K = effective elastic constant ($K \doteq K_{33}$ for homeotropic nematics and $K = K_{11} + (K_{33} - 2K_{22})/4$ for twisted nematics), d = the cell thickness. The rise time and decay time are 1.3 ms and 7 ms, respectively for a homeotropic nematic LC layer with the following

specifications: $K_{11} = 7.1\times10^{-12}$ N; $K_{22} = 5.9\times10^{-12}$ N; $K_{33} = 13.7\times10^{-12}$ N; d = 2.8 μm; $\Delta\varepsilon = 1$; $\gamma = 0.12$; V = 10 V (E = V/d); $\varepsilon_0 = 8.85\times10^{-12}$ As/Vm.

The switching speed of the FLC device can be written as[23]

$$\tau = \frac{\gamma}{P \bullet E}, \tag{2.27}$$

where γ = viscosity, P = material macroscopic polarization, E = electric field. Numerically τ = 100 μs for P = 10 nC/cm^2 and E = 10 V/μm. As observed from Eqs. (2.25) and (2.27), the rise times are decreased with increasing the electric field, and therefore are dependent on the write light intensity.

The response speed of the valve using a cadmium sulfide photoconductor is dependent on both the LC and the photoreceptor. In this case, the speed, particularly the decay time is much slower than that of the silicon-based valve due to the large band gap of the CdS (2.4eV) resulting in a long detrapping time of the photocharge. The rise time also decreases with increasing write light intensity.

When the photoreceptor is a photoconductor, the speed of the LCLV is also limited by the RC time constant of the photoreceptor/liquid crystal combination. Referring to Fig. 2.2b, the RC-time is given by

$$\tau_{RC} = \frac{C_{bm} + C_L + C_p}{1/R_L + 1/R_p}. \tag{2.28}$$

For example, consider the following typical values: C_{bm} = 1.5 nF; R_L = 2.2 MΩ; C_L = 1.5 nF; R_p = 20 GΩ (dark); C_p = 2.5 nF; then the RC time is about 12 ms.

2.3.5 Other Parameters

There are other parameters widely used in the characterization, such as spectral response, sensitivity, contrast ratio, and resolution. The meaning of each parameter is obvious, but here we make a few remarks.

The sensitivity is represented by the minimum write light intensity which switches the valve on to 90% of full on-state. For different wavelengths the sensitivity is different, and the spectral response curve describes this relation. The contrast ratio should be given together with the maximum read-out efficiency because the contrast ratio can be made very high by improving the dark OFF-state at the expense of the read-out efficiency. In our neural network system the resolution requirement is as low as 1 lp/mm, so it is less of concern.

2.4 MATHEMATICAL TECHNIQUES FOR ANALYZING THE BEHAVIOR OF THE LCLV

It is impossible to characterize some properties, such as the transfer characteristic and the polarization state of the read-out by single numeric parameters, so usually they are given by experimental curves. In order to quantitatively describe and compare these properties, this section gives two mathematical techniques for analyzing and modeling the LCLVs' behavior. The mathematical modeling is particularly important in simulating the neural network system involving LCLVs.

2.4.1 The Transfer Characteristic and Curve Fitting by a Sigmoid Function

The sigmoid (S-shaped) function is a bounded, monotonic, nondecreasing function

$$s(x) = -w_0 + \frac{w_1}{1 + \exp[-w_2 - x/w_3]} \tag{2.29}$$

where the coefficients (w_0, w_1, w_2, w_3) which control the behavior of this function can be any real numbers. The function reaches the upper bound when $x \gg w_3$ and lower bound when $x \ll w_3$, and provides a graded, nonlinear response within a specified range (see Fig. 2.8).

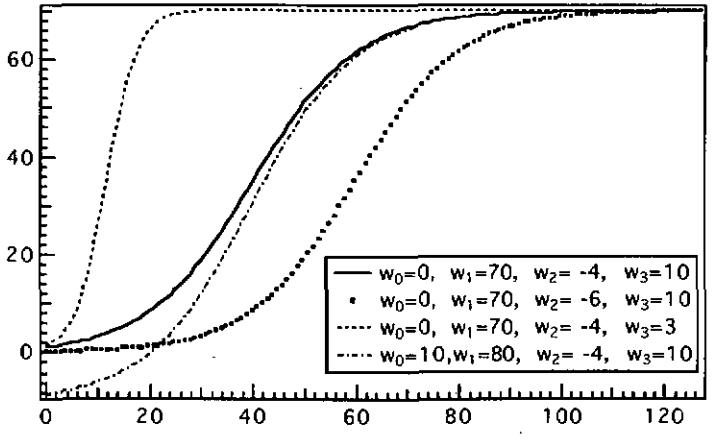

Fig. 2.8 Sigmoid curves for some typical parameters.

The w_3 quantifies the slope of the nonlinear response, the smaller the w_3 the steeper is the curve. The w_2 quantifies the translation of the curve along the x-axis. Decreasing w_2 results in the curve's moving in the +x direction. The w_0 quantifies the translation of the curve along the y-axis. Decreasing w_0 results in the curve's moving in the +y direction. The w_1 quantifies the height of the curve between the lower and the upper bounds.

The transfer characteristic of a valve represented by a transfer curve gives the relation between read-out light intensity and write light intensity. A typical transfer curve for LCLV3 is given in Fig. 2.9 (dotted line). We notice that there are some similarities between the shapes of the transfer curve and the sigmoid function. Therefore we used the sigmoid function to fit the transfer curve, and obtained a satisfactory result (the full line in Fig. 2.9).

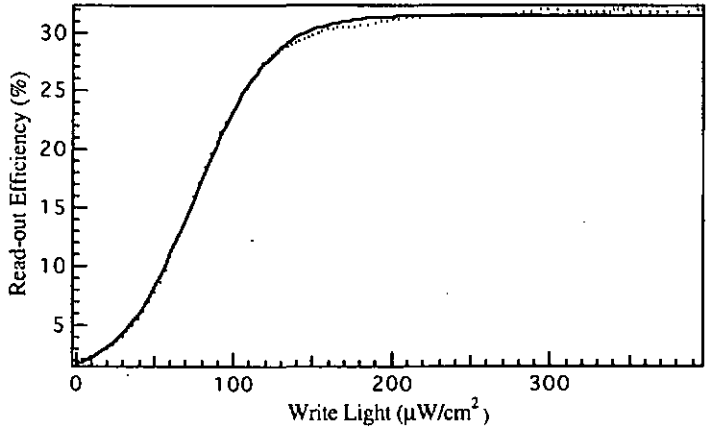

Fig. 2.9 Efficiency curve (dotted line) of LCLV3 for integrated reading and fitting curve(full line) .

There are four coefficients (w_0,w_1,w_2,w_3) to be fitted to Eq. (2.29). The best coefficients are such that the difference between the experimental data and the data produced by inserting the coefficients into the sigmoid function is minimized. There are many different algorithms and software available which can be used to solve this optimization problem. We did the curve fitting by Igor[56] (a graphing and data analysis software) on Macintosh.[56] Igor combines the advantages of the curve fitting and the graphing capacities which facilitate choosing the initial coefficients.

The results of the curve fitting are presented in Table 2.3. From the LCLV point of

view, w_2 quantifies the stability of the dark state. The more negative w_2 is, the longer the dark state remains as the write light intensity is increased. The w_3 quantifies the sharpness of the threshold. Therefore we can quantitatively describe and compare different transfer curves. The threshold is steeper for LCLV1, and LCLV3 has the longer dark state.

Valve	w_0	w_1	w_2	w_3
LCLV1	28.236±1.71	97.661±1.77	-0.93357±0.0534	11.549±0.195
LCLV2	82.688±12.8	118.01±12.8	0.81604±0.152	162.64±4.18
LCLV3	-0.45832±0.163	31.021±0.18	-3.2039±0.0567	23.494±0.327

Table 2.3 Curve fitting parameters for the three LCLVs.

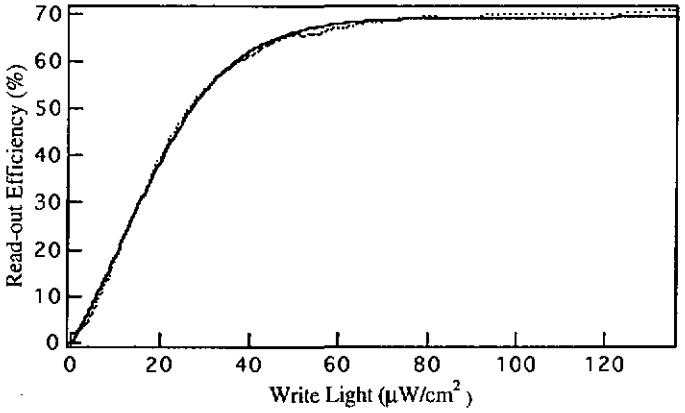

Fig. 2.10 Efficiency curve (dotted line) for LCLV1 and fitting curve (full line) using one sigmoid.

Valve		w_0	w_1	w_2	w_3
LCLV1	$x \leq 16$	0.95183±0.225	38.783±0.781	-2.767±0.0578	3.6218±0.0993
	$x > 16$	28.236±1.71	97.661±1.77	-0.93357±0.0534	11.549±0.195
LCLV2	$x \leq 80$	0.49296±0.151	16.026±0.47	-2.8047±0.0978	22.843±0.948
	$x > 80$	82.688±12.8	118.01±12.8	0.81604±0.152	162.64±4.18

Table 2.4 Two sigmoid curve fitting parameters for LCLV1 and LCLV2.

The sigmoid function has a symmetric S shape. However the experimental transfer curves usually are asymmetric with a short dark OFF-state and long bright ON-state. It is difficult to fit the whole transfer curve by one sigmoid function. In Fig. 2.10 the fitting matched the transfer curve well on most of points, but drifted off in the lower part of the curve. In this case we may divide the transfer curve into two parts, and fit the two parts separately. We refit the transfer curve by two sigmoid functions, one for the OFF-state, the other for the ON-state, and obtain a perfect result (see Fig. 2.11).

$$S(x) = \begin{cases} -0.95183 + \dfrac{38.783}{1 + \exp\{2.767 - x/3.6218\}} & \text{for } x \le 16 \\ -28.236 + \dfrac{97.661}{1 + \exp\{0.93357 - x/11.549\}} & \text{for } x > 16 \end{cases}$$

The two sigmoid fitting parameters for LCLV1 and LCLV2 are presented in Table 2.4.

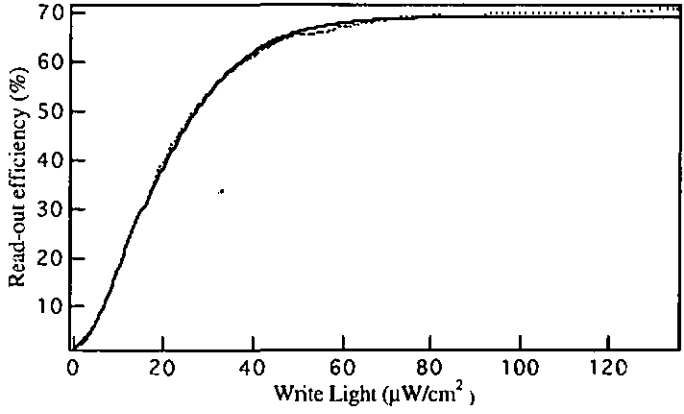

Fig. 2.10 Efficiency curve (dotted line) for LCLV1 and fitting curve (full line) using two sigmoids.

2.4.2 The Polarization Characteristic

A. Analysis of homeotropic nematic and ferroelectric LCLV by Jones calculus

Both LCLV1 and LCLV3 may be considered as wave plates which convert the polarization state of the incident light to another polarization state depending on the retardation and orientation of the plate. We can analyze the polarization characteristic of the LCLVs by using the Jones matrix calculus.[57] The coordinates

are defined as follows (Fig. 2.12). The f and s axes are the "fast" and "slow" axes of liquid crystal. The x and y axes are fixed laboratory axes, and the x-y plane is parallel to the s-f plane. The z axis is the propagation direction of the light beam. There may be a tilt angle θ between the z and the optic axis s. The Jones matrix of the LC layer in the s-f coordinate system is given by

$$\mathbf{J}^{sf} = e^{-i\phi}\begin{bmatrix} e^{-i\Delta(\psi)/2} & 0 \\ 0 & e^{i\Delta(\psi)/2} \end{bmatrix} \tag{2.30}$$

where $\Delta(\psi)$ is the phase retardation given by Eq. (2.16). ϕ is the absolute phase change which has no effect on the polarization state. Therefore we will neglect the phase factor $e^{-i\phi}$ in Eq. (2.30) hereafter.

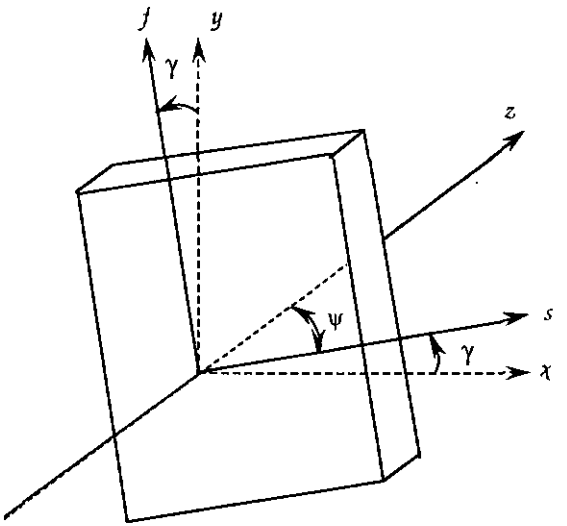

Fig. 2.12 Liquid crystal cell with rotation angle γ.

The Jones matrix in Eq. (2.30) can be transformed to the x-y coordinate system by

$$\mathbf{J}^{xy} = \mathbf{R}(-\gamma)\,\mathbf{J}^{sf}\,\mathbf{R}(\gamma) \tag{2.31}$$

where $R(\gamma)$ is the rotation matrix:

$$\mathbf{R}(\gamma) = \begin{bmatrix} \cos\gamma & \sin\gamma \\ -\sin\gamma & \cos\gamma \end{bmatrix} \tag{2.32}$$

$$\mathbf{J}^{\Psi} = \begin{bmatrix} \cos\frac{\Delta(\psi)}{2} - i\sin\frac{\Delta(\psi)}{2}\cos 2\gamma & -i\sin\frac{\Delta(\psi)}{2}\sin 2\gamma \\ -i\sin\frac{\Delta(\psi)}{2}\sin 2\gamma & \cos\frac{\Delta(\psi)}{2} + i\sin\frac{\Delta(\psi)}{2}\cos 2\gamma \end{bmatrix} \quad (2.33)$$

The Eq. (2.33) describes a generic polarization state for both LCLV1 and LCLV3. For LCLV1 the tilt angle ψ depends on the electric field strength or write light intensity, therefore, the retardation $\Delta(\psi)$ varies with the electric field while γ stays unchanged. For LCLV3, however, the rotation angle γ changes with the electric field while the Δ is a constant.

The LCLV1 is usually used at $\gamma = 45°$. In the ideal case, when the LC is in the OFF-state, $\theta = 0$ and the birefringence $[n_e(\psi) - n_o]$ vanishes according to Eqs. (2.16) and (2.17). The LC is isotropic, and the Jones matrix is

$$\mathbf{J}_{\mathbf{off}}^{\Psi} = \begin{bmatrix} 1 & 0 \\ 0 & 1 \end{bmatrix}. \quad (2.34)$$

When the valve is in the ON-state, the Jones matrix is

$$\mathbf{J}_{\mathbf{on}}^{\Psi} = \begin{bmatrix} \cos\frac{\Delta(\psi)}{2} & -i\sin\frac{\Delta(\psi)}{2} \\ -i\sin\frac{\Delta(\psi)}{2} & \cos\frac{\Delta(\psi)}{2} \end{bmatrix}. \quad (2.35)$$

The LCLV3 is usually used at $\psi = 90°$. When the valve is in the OFF-state, $\gamma = 0°$, and the Jones matrix is

$$\mathbf{J}_{\mathbf{off}}^{\Psi} = \begin{bmatrix} \cos\frac{\Delta(90°)}{2} - i\sin\frac{\Delta(90°)}{2} & 0 \\ 0 & \cos\frac{\Delta(90°)}{2} + i\sin\frac{\Delta(90°)}{2} \end{bmatrix}. \quad (2.36)$$

When the LCLV3 is in the ON-state, the Jones matrix is

$$\mathbf{J}_{\mathbf{on}}^{\Psi} = \begin{bmatrix} \cos\frac{\Delta(90°)}{2} - i\sin\frac{\Delta(90°)}{2}\cos 2\gamma & -i\sin\frac{\Delta(90°)}{2}\sin 2\gamma \\ -i\sin\frac{\Delta(90°)}{2}\sin 2\gamma & \cos\frac{\Delta(90°)}{2} + i\sin\frac{\Delta(90°)}{2}\cos 2\gamma \end{bmatrix}. \quad (2.37)$$

Provided that the read-in light is linearly polarized along the x axis, the Jones vector is

$$\mathbf{I}_{\text{R-in}} = \begin{bmatrix} 1 \\ 0 \end{bmatrix}. \tag{2.38}$$

Then the read-out light reflected from the valve in the OFF-state is

$$\mathbf{I}_{\text{R-out}} = \mathbf{J}_{\text{off}}^{xy}\mathbf{I}_{\text{R-in}}. \tag{2.39}$$

It can be seen that the read-out light has always the same linear polarization as the read-in for LCLV3 (diagonal Jones matrix), however, for LCLV1 the read-out is linearly polarized only if the retardation $\Delta = 0$, i.e. $\psi = 0$. In a real device the tilt angle in the OFF-state never can be zero because a pre-tilt of the LC molecules of about 5° is necessary to ensure that the molecules rotate to a given direction. This pre-tilt angle results a non-zero retardation, therefore spoils the OFF-state of LCLV1. For example, consider a LC layer 2.5 μm thick with $n_e = 1.583$ and $n_o = 1.491$. According to Eqs. (2.16) and (2.17), $n_e(5°) = 1.4916$ and $\Delta(5°) = 2°$.

The read-out light reflected from the valve in the ON-state is

$$\mathbf{I}_{\text{R-out}} = \mathbf{J}_{\text{on}}^{xy}\mathbf{I}_{\text{R-in}}. \tag{2.40}$$

The read-out light generally is elliptically polarized. When the retardation $\Delta(\psi)$ for LCLV1 or $\Delta(90°)$ for LCLV3 is equal to π, the read-out is linearly polarized. The polarization is along y axis for LCLV1 and at 2γ with respect to x for LCLV3.

B. Analysis of LCLV2 (twisted nematic) by Jones calculus

The twisted nematic LC in the OFF-state can be considered as a stack of identical wave plates, each of which has a different orientation. The optic axes gradually rotate around the normal of the LC cell. The overall Jones matrix can be obtained by multiplying together all the matrices associated with these plates.

Firstly, we show that a transmissive twisted LC layer acts as a polarization rotator. Let Δ be the retardation of the LC layer when it is untwisted, and α be the total twist angle. Then

$$\Delta = \frac{2\pi}{\lambda}[n_e - n_o]d, \tag{2.41}$$

where d is the thickness of the LC layer. The LC layer may be divided into N equally thick plates. Each plate has a retardation of Δ/N. The plates are oriented at angles α/N, $2\alpha/N$, $3\alpha/N$, ..., $(N-1)\alpha/N$. The overall Jones matrix for these N plates is given by

$$\mathbf{J}_N^{xy} = \prod_{m=1}^{N} \mathbf{R}(m\alpha/N)\,\mathbf{J}^{sf}\mathbf{R}(-m\alpha/N) \tag{2.42}$$

$$\mathbf{J}^{sf} = \begin{bmatrix} e^{-i\Delta/2N} & 0 \\ 0 & e^{i\Delta/2N} \end{bmatrix}, \tag{2.43}$$

where **R** is the rotation matrix defined in Eq. (2.32). By using the following identity for the rotation matrix:

$$\mathbf{R}(\rho_1)\,\mathbf{R}(\rho_2) = \mathbf{R}(\rho_1 + \rho_2), \tag{2.44}$$

Eq. (2.42) can be written

$$\mathbf{J}_N^{xy} = \mathbf{R}(\alpha)\left[\mathbf{J}^{sf}\mathbf{R}\left(\frac{-\alpha}{N}\right)\right]^N. \tag{2.45}$$

Using Eqs. (2.32) and (2.43), we obtain

$$\mathbf{J}_N^{xy} = \mathbf{R}(\alpha)\begin{bmatrix} \cos\frac{\alpha}{N}e^{-i\Delta/2N} & -\sin\frac{\alpha}{N}e^{-i\Delta/2N} \\ \sin\frac{\alpha}{N}e^{i\Delta/2N} & \cos\frac{\alpha}{N}e^{i\Delta/2N} \end{bmatrix}^N. \tag{2.46}$$

Eq. (2.46) can be further simplified and in the limit when N tends to infinite ($N\to\infty$), becomes[58]

$$\mathbf{J}_N^{xy} = \mathbf{R}(\alpha)\begin{bmatrix} \cos\beta - i\frac{\Delta\sin\beta}{2\beta} & -\alpha\frac{\sin\beta}{\beta} \\ \alpha\frac{\sin\beta}{\beta} & \cos\beta + i\frac{\Delta\sin\beta}{2\beta} \end{bmatrix} \tag{2.47}$$

$$\beta = \left[\alpha^2 + \left(\frac{\Delta}{2}\right)^2\right]^{\frac{1}{2}}. \tag{2.48}$$

In the real devices the retardation Δ is much larger than the twist angle α. If we assume $\Delta \gg \alpha$, the Eq. (2.47) becomes

$$\mathbf{J}_N^{xy} = \mathbf{R}(\alpha)\begin{bmatrix} e^{-i\Delta/2} & 0 \\ 0 & e^{i\Delta/2} \end{bmatrix}. \tag{2.49}$$

It can be seen that the operation of the Jones matrix on polarization vector is to rotate the vector by an angle α except a phase shift. If the incident light is linearly

polarized along x axis at the input plane, the polarization vector will follow the rotation of the optic axes and remain the linear polarization. This is called adiabatic following.

An LCLV which operates in a reflective mode can be equivalently unfolded in the form of a cascade of two identical transmissive cells with mirror-symmetric structure. By use of Eq. (2.47), the Jones matrix for a twisted nematic reflective LCLV is

$$\mathbf{J}^{xy} = (\mathbf{M}\,\mathbf{R}(-\alpha)\,\mathbf{J}_N^{xy}\,\mathbf{R}(\alpha)\,\mathbf{M}\,)\,\mathbf{J}_N^{xy}$$

$$= \begin{bmatrix} \left(\frac{\alpha}{\beta}\right)^2 + \left(\frac{\Delta}{2\beta}\right)^2 \cos 2\beta - i\frac{\Delta \sin 2\beta}{2\beta} & i\frac{\alpha\Delta}{2\beta^2}(1 - \cos 2\beta) \\ i\frac{\alpha\Delta}{2\beta^2}(1 - \cos 2\beta) & \left(\frac{\alpha}{\beta}\right)^2 + \left(\frac{\Delta}{2\beta}\right)^2 \cos 2\beta - i\frac{\Delta \sin 2\beta}{2\beta} \end{bmatrix}, \tag{2.50}$$

where $\mathbf{M}$ is the mirror transformation matrix defined by

$$\mathbf{M} = \begin{bmatrix} -1 & 0 \\ 0 & 1 \end{bmatrix}. \tag{2.51}$$

The following condition is valid for the OFF-state

$$\Delta \gg \alpha, \quad \beta \approx \frac{\Delta}{2}. \tag{2.52}$$

By using Eq. (2.52) to simplify Eq. (2.50), we obtained the Jones matrix for the OFF-state

$$\mathbf{J}_{off}^{xy} = \begin{bmatrix} e^{-i\Delta/2} & 0 \\ 0 & e^{i\Delta/2} \end{bmatrix}. \tag{2.53}$$

It can be seen that the read-out light in the OFF-state is linear if the read-in light is linearly polarized along x or y axis.

Using a simplified model[25] the Eq. (2.41) can be used for ON-state as well, but with $\Delta(\psi)$ instead of Δ.

$$\Delta(\psi) = \frac{2\pi}{\lambda}[n_e(\psi) - n_o]d, \tag{2.54}$$

where $n_e(\psi)$ is defined in Eq. (2.17). In the ON-state the Eq. (2.52) is no longer valid because the retardation decreases with increasing the electric field.

Therefore, the read-out light will be elliptically polarized even if the read-in is linearly polarized.

C. Analysis of the polarization output of an LCLV by complex number representation

From the discussion above we found that the generic polarization output of LCLV in the ON-state is elliptical as shown in Fig. 2.13. How the elliptical state is described and what is the relation between the ellipse and the retardation and orientation of the LCLV are matters of concern. An elliptical polarization can be completely described by the orientation angle θ and the ellipticity angle ε defined by

$$\tan\varepsilon = \pm \frac{b}{a}, \tag{2.55}$$

where the positive and negative correspond to right-hand and left-hand elliptical polarization, respectively.

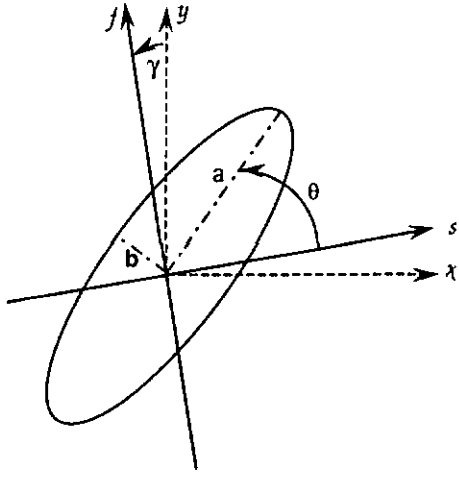

Fig. 2.13 Coordinate system and elliptical output in the ON-state.

We assume that the read-in light is linearly polarized along the x axis. In order to derive the dependence of the output ellipse on the retardation and orientation of LC, we use the Cartesian complex-plane[59] to express the polarization state of the read-out light. In this representation, the elliptical light is described by a complex variable χ which is defined as

$$\chi = \frac{E_f}{E_s} = \tan\gamma\, e^{i\Delta}, \tag{2.56}$$

where E_s and E_f are the two components of Jones vector in the principal coordinate s-f for the same ellipse. γ is the angle shown in Fig. 2.13. Δ is the retardation between the s and f axes.

On the other hand, the complex variable χ can be expressed in terms of the ellipticity angle ε and the orientation angle θ as

$$\chi = \frac{\tan\theta + i\tan\varepsilon}{1 - i\tan\theta\tan\varepsilon}, \tag{2.57}$$

From Eq. (2.57) we obtained the following equations

$$\tan 2\theta = \frac{2\,\mathrm{Re}(\chi)}{1 - |\chi|} \tag{2.58}$$

$$\sin 2\varepsilon = \frac{2\,\mathrm{Im}(\chi)}{1 + |\chi|}, \tag{2.59}$$

By using Eq. (2.56), Eqs. (2.58) and (2.59) become

$$\tan 2\theta = \tan 2\gamma \cos\Delta \tag{2.60}$$

$$\sin 2\varepsilon = \sin 2\gamma \sin\Delta\,. \tag{2.61}$$

This corresponds to an elliptical polarization oriented at θ, with semi-major and semi-minor axes a and b (Fig. 2.13).

The importance of Eqs. (2.60) and (2.61) are that the characteristics of the LC layer can be deduced from macroscopic measurements, and that a sensitivity analysis can be carried out in order to identify fabrication tolerances. In the case of LCLV3 (FLCLV), for example, γ and $(\theta + \gamma)$ can be easily measured, then, Eq. (2.60) together with Eq. (2.16) will give the LC cell thickness d. The value of the ellipticity can be calculated from Eq. (2.61). The calculations using these equations will be given in Section 3.6.

3

EXPERIMENTAL CHARACTERIZATION OF LCLVS

This chapter is the experimental part relating to the characterization of LCLVs. We have investigated experimentally three different types of LCLVs: based on twisted nematic, homeotropic nematic and ferroelectric (smectic C*) liquid crystals.[60-62] The characteristic parameters have been defined in the last chapter. In order to make the experimental results understandable and comparable, we also give the experimental procedure and conditions in detail. Finally, a comparison of three LCLVs is presented.

3.1 CALIBRATION CURVE

The calibration curve, which can be obtained by measuring the read-out intensity with respect to the drive voltage without write light, is an important reference for selection of the drive voltage.

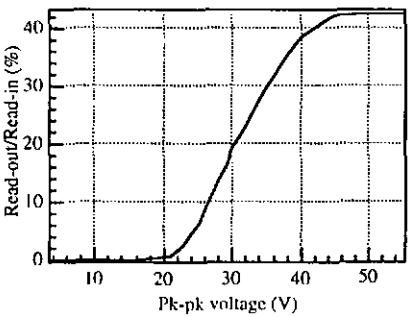

Fig. 3.1 Calibration curve for LCLV1

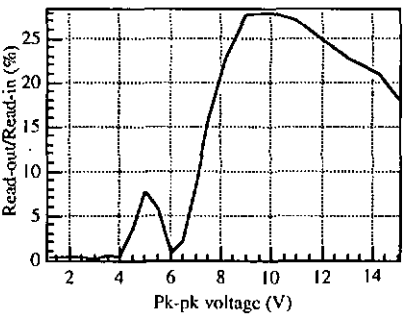

Fig. 3.2. Calibration curve for LCLV2 at 0°

For the homeotropic nematic LCLV1, the director was set at 45° to the incident polarization vector. The polarizer and analyzer were crossed. The drive frequency of the square wave was set at 450 Hz. Although the sensitivity increases with decreasing frequency, the AC component on the read-out light below 450 Hz is an

undesirable side effect. The calibration curve for LCLV1 is shown in Fig. 3.1. It can be seen that as the amplitude of the voltage is increased, there is a critical point below which there is a dark state, but above which the dark state begins to deteriorate. This point usually is selected as the drive voltage. In this case 21 V (pk-pk) is chosen.

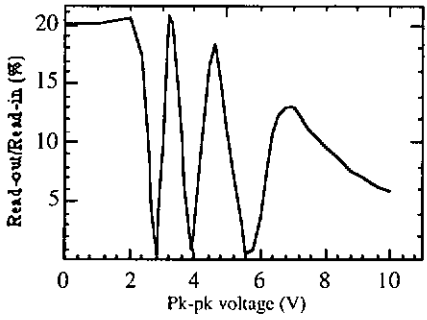

Fig. 3.3. Calibration curve for LCLV2 at 45°.

For the twisted nematic LCLV2, the director alignment on the front surface of the cell was set either parallel to (0°) or at 45° to the incident polarization vector. The drive frequency of the square wave was chosen to be 1 kHz. The calibration curves for LCLV2 in the 0° and 45° positions are given in Fig. 3.2 and Fig. 3.3, respectively, which are generally consistent with the results obtained by others[22,25]. We found from Fig. 3.2 that there are two voltages at about 4 V and 6 V, respectively, which give good dark state and can be chosen as the drive voltage. We chose 6 V because the read-out efficiency of the ON-state from this voltage is much higher than that for 4 V. For the 45° position, there is a choice of three operating voltages given by the three minima. However, in this orientation the dark state is not as robust as when the incident polarization is parallel to the LC director. Moreover, the ON-state does not saturate and the intensity of the reflected beam passes through a maximum and then falls off. Therefore, this configuration is not suitable for implementing thresholding.

For the smectic LCLV3, one of the director orientation was aligned with the incident polarization. The drive waveform was more complicated(see Fig. 2.7) than in the case of a nematic, because the smectic material must be driven into the two positions within each cycle. The width and height of the two pulses were optimized for good contrast and high read-out efficiency. The cycle frequency used was about 100 Hz, which is now the frequency at which the LCLV3 is refreshed. There is a range of operating voltage waveforms which produce good contrast, because a good waveform depends on the balance between the pulses rather than absolute heights. Figure 3.4 shows how a suitable waveform can be found.

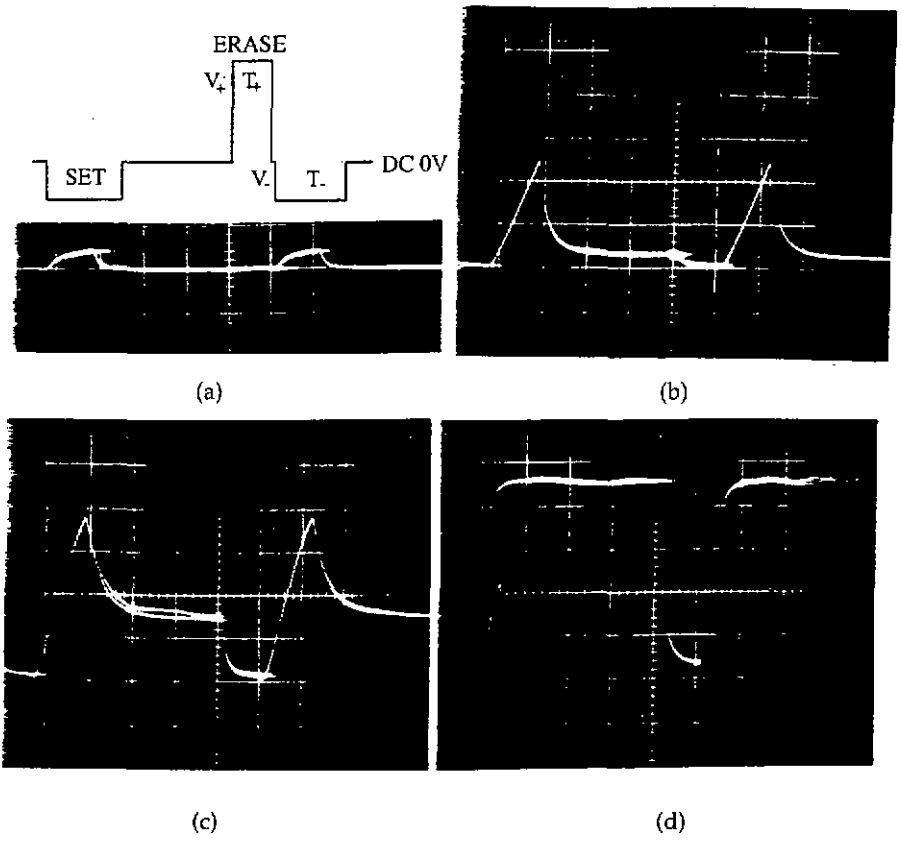

Fig. 3.4 *Dynamic response of LCLV3 to the drive pulses. (a) The upper bipolar pulse train shows the drive waveform. The lower trace shows the read-out intensity when the area of the SET is small without the ERASE. (b) The read-out for further increasing the SET and introducing the ERASE. (c) The read-out when the SET is below the threshold. (d) The bistable output when The SET is above the threshold.*

The write side of LCLV3 is illuminated with an appropriate intensity to ensure that the photoconductor is in the ON-state, and the read-out is monitored by using a detector and an oscilloscope. Starting with a negative (SET) pulse, increasing the height(V-) and width(T-), we can see that the read-out is increasing (Fig. 3.4 (a) and (b)). At the same time, the dark state is getting worse, so we have to introduce a positive (ERASE) pulse to maintain the dark state (Fig. 3.4 (b)). The read-out decays from the maxmum value (3.4(c)) because the amplitud of the SET pulse is below threshold. As further increasing the negative pulse over the threshold, we obtain a

stable saturated ON-state (Fig. 3.4 (d)). The threshold represented by the area of the SET pulse is 11.52 V-ms. The width of negative and positive pulses must be longer than the rise and decay time of LC, respectively. In order to get higher read-out efficiency in the integrated reading, we chose the ERASE pulse as narrow as possible and the SET pulse as wide as possible.

3.2 SPECTRAL SENSITIVITY

The spectral sensitivity of a LCLV depends on the characteristic of the photoconductor. The optical setup for measuring spectral sensitivity is shown in Fig. 3.5.

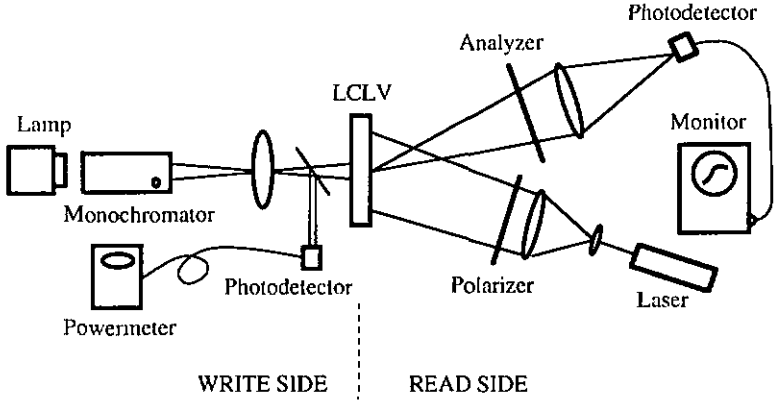

Fig. 3.5 The optical setup for measuring the spectral sensitivity

The write side was illuminated by a tungsten halogen lamp through a monochromator. A collimated Ar^+ laser (λ = 515 nm) beam was used as the read light for LCLV2 and LCLV3. For the LCLV1 a dye laser (λ = 555 nm) was used as the read light. We adjusted the write light intensity for each wavelength such that the read-out intensity just reaches 90% of full ON-state, then we measured the write light intensity from the powermeter. By changing the wavelength of the write light and measuring the write intensity, we obtained the spectral sensitivity curves for the three LCLVs as shown in Fig. 3.6. Because the spectral sensitivity of LCLV1 was very critical at the wavelength range from 550 nm to 590 nm, its spectral sensitivity curve in this spectral range was measured by use of a dye laser as the write light instead of white light with monochromator.

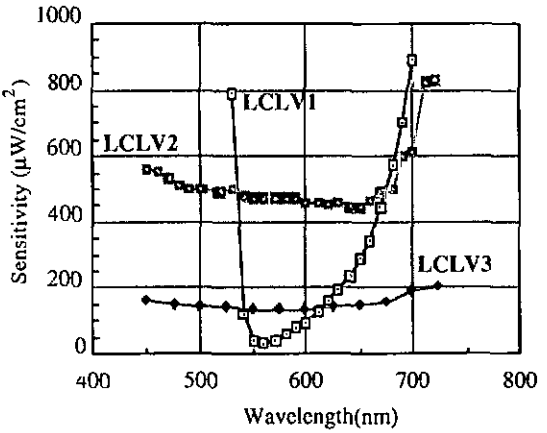

Fig. 3.6 The spectral sensitivity

From the curves we found the LCLV2 and LCLV3 have nearly uniform response to the wavelength from 450 nm to 650 nm, so we can use either Ar^+ laser or He-Ne laser as the write light for these valves. For LCLV1, however, the most sensitive spectral range is limited within 540~600 nm, therefore we can not use Ar^+ laser to write LCLV1. A dye laser can give moderate output power in this spectral range. The calibration curve and output power for Rhodamine 110 dye pumped by Ar^+ laser is given in Appendix 3.1.

3.3 EFFICIENCY CURVE

The dependence of the read-out light intensity on the write light intensity was measured by use of the setup illustrated in Fig. 3.7. The read-out and write light intensities were detected simultaneously when the write light intensity was changed. The signal from the detectors were fed to the computer through a DAS16 A/D interface board. All data acquisition and plotting were realized by means of two acquisition programs: DAS and DAS1.[63] The measured read-out light intensity was then normalized by the read-in light intensity and plotted as a function of the write light intensity. The ordinate in this plot is the read-out efficiency, therefore we call the curve as efficiency curve. The read-out light intensity was detected behind the analyzer and corrected for the absorption in the analyzer, which can vary according to the type of polarizer.

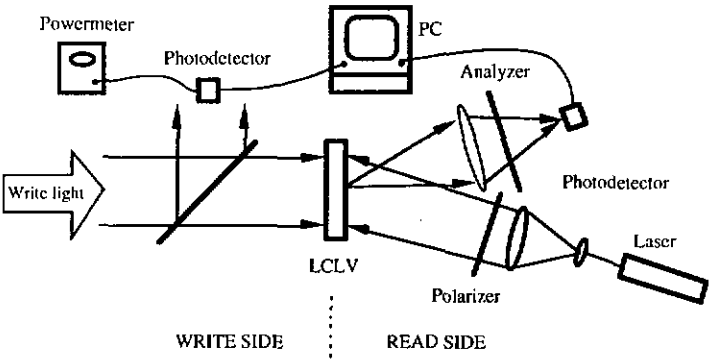

Fig. 3.7 Setup for measuring the efficiency curves

The efficiency curve for LCLV1 is given in Fig. 3.8. A dye laser (Rhodamine 110) at 555 nm was used as both read and write light. From the curve, the maximum read-out efficiency for LCLV1 is about 70%, which is constrained mainly by the imperfect dielectric mirror. We found that the read-out light did not saturate at high write light intensity but fell off when the read light wavelength was shorter than 555 nm (Fig. 3.9). This is because the LC layer produced π retardation in the ON-state at the wavelength 555 nm. Any wavelength shorter than 555 nm will result in the retardation of ON-state exceeding π. Therefore the efficiency curve falls off after passing through a maximum which corresponds to the π retardation.

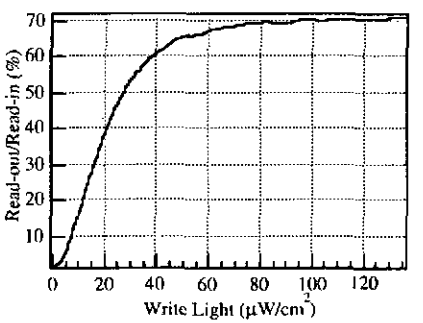

Fig. 3.8 Efficiency curve for LCLV1 at 555 nm.

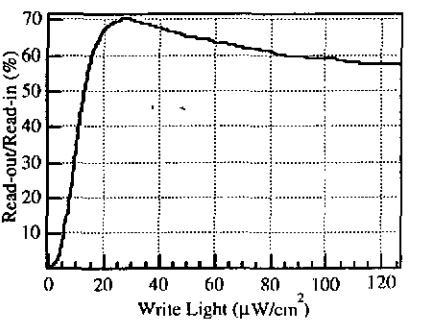

Fig. 3.9 Efficiency curve for LCLV1 at 547 nm.

The efficiency curve for LCLV2 is given in Fig. 3.10. Both the read and write light were at 515 nm. The maximum read-out efficiency for LCLV2 is about 36%. There are two main reasons for the low efficiency: One is the poor dielectric mirror whose reflectance is only 68% without the polarizer, analyzer and the drive voltage; Another is the twisted structure in which the linear polarization is hard to obtain.

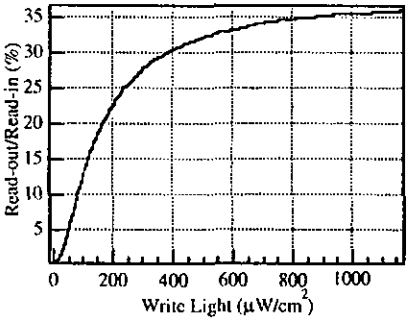

Fig. 3.10 Efficiency curve for LCLV2.

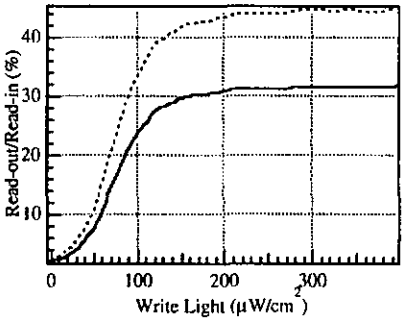

Fig. 3.11 Efficiency curve for LCLV3.

The efficiency curve for LCLV3 is given in Fig. 3.11, where the dash line is for the synchronous reading, and the solid line is for the integrated reading. The maximum read-out efficiencies for synchronous reading and integrated reading are about η_{max} = 45% and η_i = 32%, respectively, so η_i = 71% η_{max}. This result is close to the theoretical result η_i = 76% η_{max} from Eq.(2.11), when τ_{on} = 1.4 ms, τ_{off} = 0.6 ms (Section 3.7). The lower efficiency is mainly due to the gaps between the metal mirrors, which take up about 30% of the working area. We should keep in mind that the transfer curves are valid only for a certain read-in light intensity and for the given drive conditions (see Table 3.1).

	LCLV1	LCLV2	LCLV3
Waveform	Square wave	Square wave	see Fig. 2.7
Frequency	450 Hz	1 kHz	T1 = 655 μs T2 = 494 μs T3 = 3.2 ms T = 11 ms
Voltage	21 V (pk-pk)	6 V (pk-pk)	U1 = 4.44x5 V U2 = 0.72x5 V
Read-in light intensity (μW/cm²)	200 in Fig. 3.8 336 in Fig. 3.9	42	21

Table 3.1 Drive condition and read-in light intensity for measured efficiency curves.

The efficiency curve actually is a normalized transfer curve which indicates the relation between the read-out and write light intensity. Therefore from the efficiency curves we can evaluate the transfer characteristics of these valves. In the Section 2.4.1

we showed that the transfer characteristic of a light valve may be approximated by a sigmoid function and quantified by a set of parameters. It can be seen from the efficiency curves that the dark states are very short. This is because the drive voltage we chose is always as high as possible before the dark state deteriorates. In this way the valve is in a very sensitive state, any write light, even very weak, can result in a read-out and a very steep transfer characteristic. We are going to use the light valve as a threshold element in neural networks, so the steeper the curve the better it is. In other applications, where grey level is necessary, a flatter transfer curve may be preferable. By adjusting the drive voltage and frequency, the transfer characteristic can be changed, but usually the change is very limited. The Fig. 3.12 gives an example of linearization of the efficiency curve by reducing the drive voltage and increasing the frequency, V= 13 V (pk-pk), f= 800 Hz, read-in light = 212 $\mu W/cm^2$. In comparison with Fig. 3.8, we found that the transfer curve became quite linear, but at the expense of read-out efficiency. In this case the efficiency is only 20% although the write light reaches 640$\mu W/cm^2$. So this operating condition is not recommended.

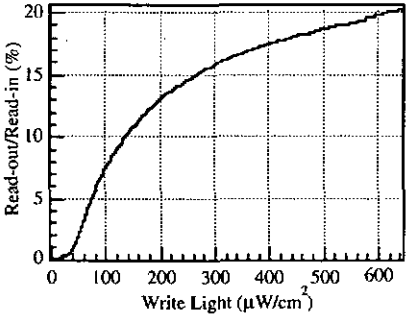

Fig. 3.12 Linearization of transfer curve for LCLV1 by change voltage and frequency.

From the efficiency curves, we may obtain the write sensitivity and the contrast ratio. The write sensitivities are 45 $\mu W/cm^2$ for LCLV1 at 555 nm, 514 $\mu W/cm^2$ for LCLV2 at 515 nm, 133 $\mu W/cm^2$ and 136$\mu W/cm^2$ for LCLV3 at 515 nm in integrated and synchronous reading, respectively. The contrast ratio C is defined as the ratio of the read-out light intensity $I_{R\text{-}out}$ in the ON state to the intensity in the OFF state

$$C = \frac{I_{R\text{-}out}(ON)}{I_{R\text{-}out}(OFF)} . \tag{3.1}$$

From the efficiency curves we obtained C = 41 for LCLV1, C = 50 for LCLV2, and C = 16 and 22 for LCLV3 in integrated and synchronous reading, respectively. These values are not the highest ones, we can get them higher by decreasing the drive voltage to improve the dark state (OFF-state). Fig. 3.13 gives an example. It can be

seen that the improvement of the dark state from 1.7% to 0.4% (see the small figure in Fig. 3.13) results in a high contrast ratio 140:1 though the maximum efficiency is down to 58%. So we should balance the efficiency and contrast ratio according to different applications.

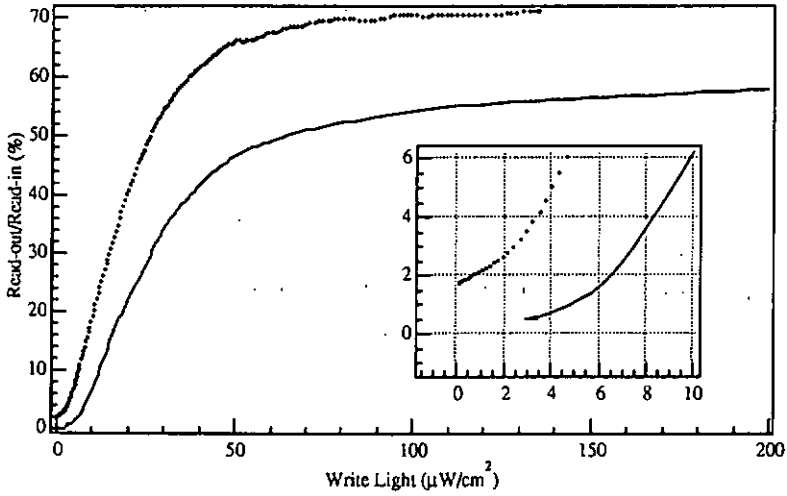

Fig. 3.13 Improvement of the contrast ratio for LCLV1 by decreasing the voltage. The markers line is the normal efficiency curve of LCLV1 copied from Fig. 3.8, and the solid line is the new curve obtained by decreasing the drive voltage to 19.5 V (pk-pk). The dark parts of the curves are enlarged and shown in the small figure from which it can be seen that the dark state is improved from 1.7% to 0.4%.

3.4 EFFECTIVE GAIN

To find the maximum effective gain, according to Eq. (2.24), we need to know the maximum read-in light intensity $I_{R\text{-}in}^{max}$. This can be known by measuring the efficiency curve for different read-in light intensities (see Fig. 3.15). We found that the effect of the breakthrough light is to displace the dark state vertically up the axis of read-out efficiency. Therefore, we built a setup shown in Fig. 3.14, to measure the effect of read-in light intensity on the read-out.

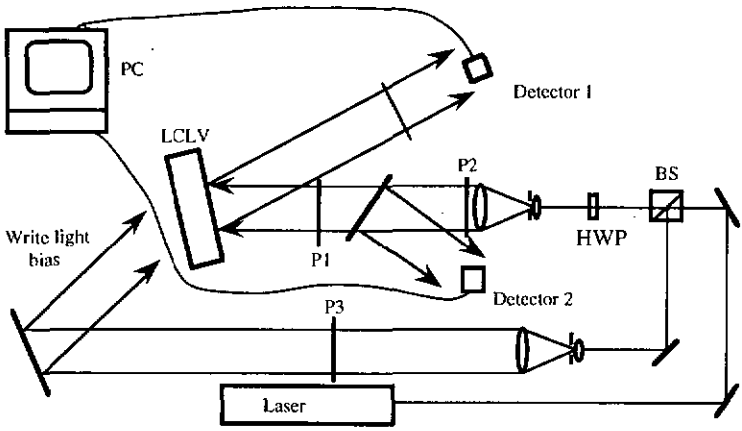

Fig. 3.14 Setup for measuring the read light's effects on the output, HWP: Half wave plate.

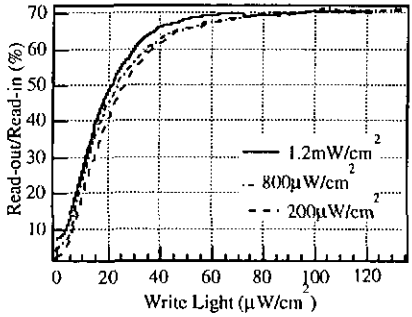

Fig. 3.15 Efficiency curve of LCLV1 for different read-in light intensity at 555 nm.

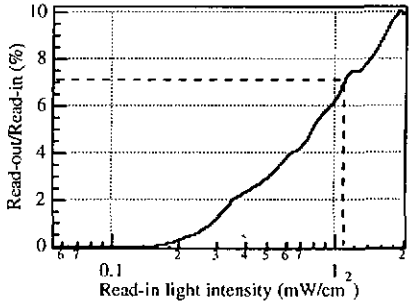

Fig. 3.16 The effect of read-in light on the read-out for LCLV1 at 555 nm.

The P1 and P2 are polarizers with fixed orientation. In order to simulate the working condition and decrease the resistance of the photoconductor layer, so as to get higher sensitivity in the measurement, we put a low intensity write light bias which was chosen according to the transfer curve such that the valve is still in the OFF state. The bias is 2 $\mu W/cm^2$ for LCLV1, 40 $\mu W/cm^2$ for LCLV2 and 30 $\mu W/cm^2$ for LCLV3. Rotating the half-wave plate (HWP) to change the read-in light intensity, we monitored the read-in and read-out intensities by means of two detectors, D1 and D2, respectively. The ratio of intensities at D1 and D2 should be a constant with increasing read-in light intensity, when there is no breakthrough light. However, if there is any read light breaking through the light blocking layer, the intensity at D1 will increase more quickly than that at D2 because that breakthrough light is

equivalent to a write light. Therefore the ratio of intensities will depend on the read-in light intensity.

Figures 3.16 and 3.17 are the measurements for LCLV1 and LCLV2, respectively. Fig. 3.18 is the measurement for LCLV3 using synchronous reading. The ordinates in the curves have been changed to the ratio of read-out to read-in light intensity, so that we can compare these curves with the transfer curves.

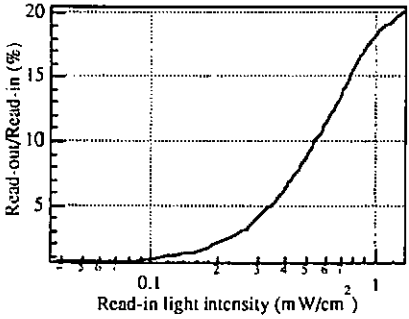

Fig. 3.17 The effect of read-in light on the read-out for LCLV2.

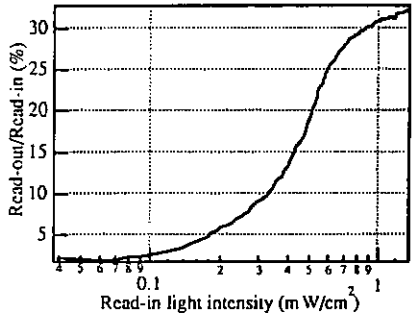

Fig. 3.18 The effect of read-in light on the read-out for LCLV3.

It can be seen from Fig. 3.16 that as the efficiency reaches 7%, which is the 10% of its maximum efficiency (see Fig. 3.8), the corresponding read-in light is about 1mW/cm^2, which is defined as the maximum read-in light intensity. The maximum effective gain G_{eff}^{max} of LCLV1, according to Eq. (2.24), is 17. From Fig. 3.17 and Fig. 3.18 the maximum read-in light intensity for LCLV2 and LCLV3 can be determined to be 300 μW/cm^2 and 180 μW/cm^2, respectively. The maximum effective gain G_{eff}^{max} is 0.21 for LCLV2 and 0.59 for LCLV3.

Comparing the three valves, we find that LCLV1 has the potential of amplification due to its good light blocking layer and relatively high efficiency. In LCLV2 the effect of breakthrough light is severe because there is no light blocking layer. In LCLV3 a pixellated metal mirror was used instead of the dielectric mirror and light blocking layer. Unfortunately, there exist many transparent gaps among the pixels. The sizes were experimentally determined to be 14 μm square pixels with 3 μm gaps. Fig. 3.9 is a magnified image of the pixels and the gaps, which was taken by using a laser beam to illuminate the read side of LCLV3 and using a objective lens to obtain the image from the write side. The breakthrough light due to these gaps is so intense that LCLV3 is fully switched on when the read-in light intensity was over 1 mW/cm^2. In the case of LCLV2 and LCLV3, there is no gain at all.

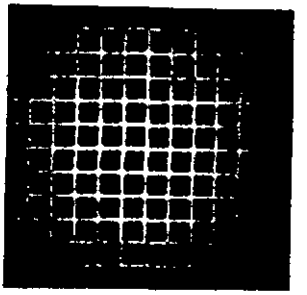

Fig. 3.19 Image of the pixellated metal mirror taken through a objective lens from the write side of LCLV3 which was illuminated by a laser beam. The black squares are the pixels, and the bright lines are the gaps.

3.5 SPATIAL UNIFORMITY

All characteristic parameters are position-dependent, i.e. the performance is not homogeneous on the whole working aperture of the LCLV. We measured the uniformity of the ON- and the OFF-state. The setup for the measurement is shown in Fig. 3.20.

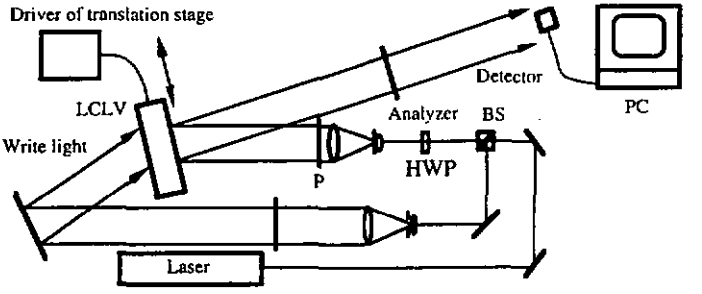

Fig. 3.20 Setup for measuring the uniformity

The LCLV was mounted on a translation stage which was moved at constant speed while a collimated beam read the LCLV. Then the read-out intensities for ON- and OFF-states were measured. The diameter of the detector was 1.5 mm. The results are given in Figs. 3.21-3.23. If we assume that the non-uniformity is isotropic (to a first approximation), then we can obtain the uniformity area from these curves. The uniformity areas are about 4 cm^2 for LCLV1, 1.5 cm^2 for LCLV2 and 3.2 cm^2 for LCLV3. The LCLV2 and LCLV3 have more uniform OFF-states than LCLV1, but the

latter has the more uniform ON-state. Usually we characterize each valve on its center, that means the result is probably not the best one. From Fig. 3.22, e.g., it can be seen that the read-out efficiency is very low at the center, but it is nearly doubled at the edge of the valve. Fig. 3.24 gives two different transfer curves of LCLV2 corresponding to two different positions on the valve.

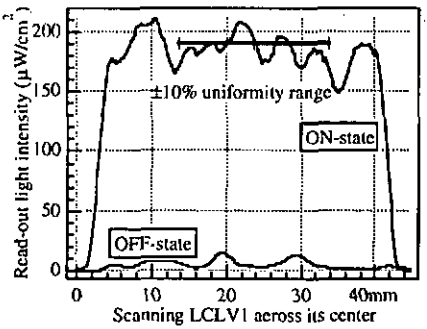

Fig. 3.21 ON- and OFF-state reflectivity as a function of position on LCLV1.

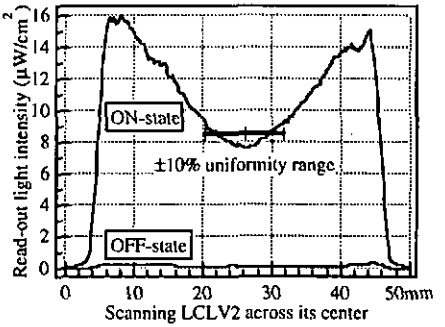

Fig. 3.22 ON- and OFF-state reflectivity as a function of position on LCLV2.

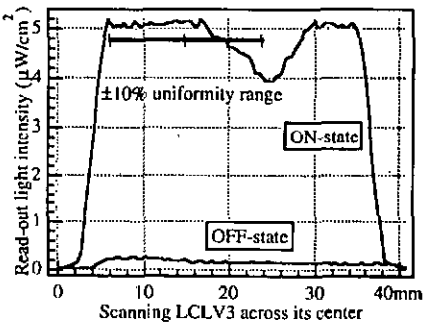

Fig. 3.23 ON- & OFF-state reflectivity as a function of position on LCLV3.

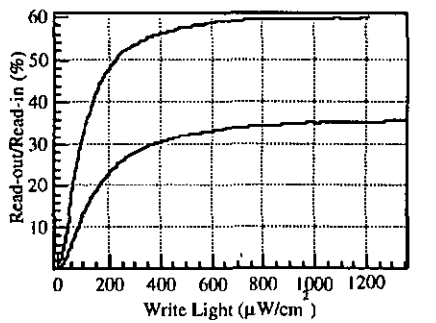

Fig. 3.24 Transfer curves for two different positions on LCLV2.

The uniformity of a valve mainly depends on the alignment which should make the liquid crystal a single domain, i.e. all molecules are (on the average) aligned along one common direction. If there is any defect in the alignment, the LC will have many domains, namely, multi-domains. The molecules in different domains have different responses to the electric field and modulate the read light in different ways. Therefore the read light through different domains will change their polarization state differently. The intensity distributions over different domains were photographed behind the analyzer by using a camera instead of the detector in Fig.

3.20. The results for LCLV2 are shown in Fig. 3.25. It can be seen that without the write light there was an uniform domain in the center, which gave a good dark state, while there existed other domains around, which formed the fringes (Fig. 3.25(a)). The uniform domain was getting bright (ON-state) with increasing the intensity of the write light (Fig. 3.25(b), (c) and (d)). However, other areas had different or even no response to the write light.

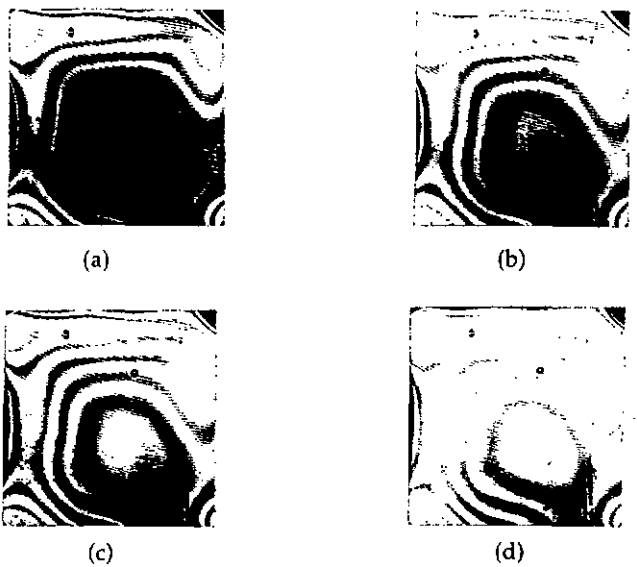

Fig. 3.25 Nonuniformity of LCLV2 resulted from the multi-domains. (a) Without write light there existed a uniform domain in the center, while other domains around; (b) With write light intensity 150 $\mu W/cm^2$ the uniform domain was getting bright (ON-state); (c) With write light intensity 340 $\mu W/cm^2$; (d) With write light intensity 450 $\mu W/cm^2$ the uniform domain was full-ON, however, other domain had different or even no response to the write light.

3.6 POLARIZATION OUTPUT

The ideal light valve should be a light-activated half wave plate, which rotates the linear read-in light through an angle and gives a linear read-out. However, the read-out light from a real device is usually elliptical. The experimental setup for measuring the polarization properties of the LCLV is shown in Fig. 3.26.

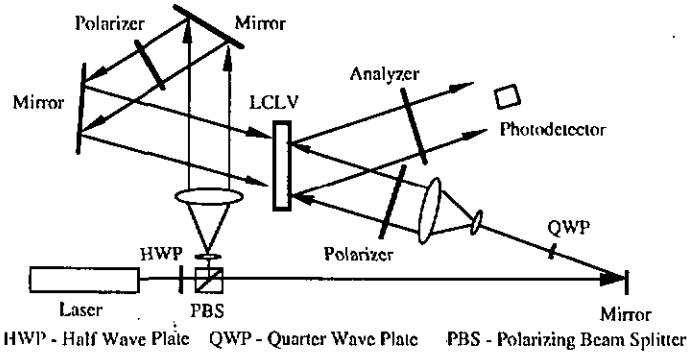

Fig. 3.26. Experimental setup for measuring state of polarization

For LCLV1, the director (optic axis) rotates in the same plane as the propagation vector of the light beam. The angle between the rotation plane and the incident polarization vector is set at 45°. The write light intensity changes the retardation of the liquid crystal layer. Therefore, the ellipticity angle ε of the read-out light changes with the write light intensity. However, the orientation angle θ does not change, i.e. the ellipse is always regular in the principal coordinate. The retardation versus write intensity was measured by the insertion of a Soleil-Babinet compensator before the crossed analyzer in Fig. 3.26. The wavelength of the read light is 555 nm. The result is shown in Fig. 3.27, from which we find that a 180° retardation, i.e. a linear polarization with 90° rotation, can be achieved only for a specific write intensity. In the other cases the read-out light from LCLV1 is elliptically polarized.

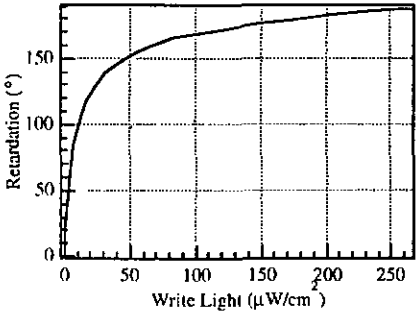

Fig. 3.27 Retardation of LCLV1 vs. write light intensity (λ = 555 nm).

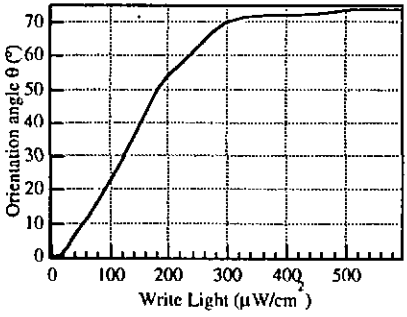

Fig. 3.28 The orientation angle of LCLV2 at 0° vs. write light intensity.

In the case of LCLV2, the read-out light is always elliptically polarized. The orientation angle of the ellipse θ (defined in 2.4.2C), which changes with the write intensity, was measured by keeping the azimuth of the incident polarization fixed

and rotating the analyzer to find the minimum output intensity, as a function of the write light intensity. The LC director on the front surface of the cell was set either parallel to (0°) or at 45° to the incident polarization vector. The orientation angle at 0° is shown in Fig. 3.28. The maximum angle is 74°. For the 45° position, there is a choice of three operating voltages given by the three minima (see Fig. 3.3). If we choose the first minimum, a rotation of 85° can be achieved upon increasing the write light intensity. From the second minimum a rotation of 70° can be achieved. From the third minimum, a rotation of 40° can be achieved.

For LCLV3, the read-out light is elliptically polarized as well. We set one of the director positions to be aligned with the incident polarization. The rotation angle of the director (γ) was measured by rotating the valve between a crossed polarizer/analyzer pair and recording the positions of the null-states when the valve is ON and OFF. We found $\gamma = 49°$. We measured the orientation of the ellipse by rotating the analyzer to find a minimum angle with increasing the write light intensity. In this way the measured angle is $(\theta + \gamma)$. The result is shown in Fig. 3.29. The maximum orientation angle is 82° with respect to the incident polarization.

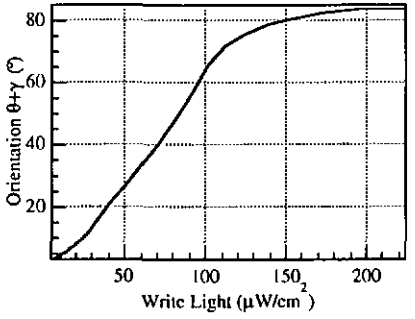

Fig. 3.29 Orientation of the ellipse for LCLV3 vs. write light intensity.

According to Eq. (2.50) and Eq. (2.20) for $\psi = 90°$, we found that the optical path difference $(n_e - n_o)\,2d = (m+1)\lambda/2 \pm \lambda/5$, with m integer. This could be accounted for by a birefringence $(n_e - n_o) = 0.18$ and a cell thickness $d = 1.86\ \mu m$. The cell thickness should be increased by 13% to 2.11 μm in order for the cell to function efficiently as a half wave plate. The value of the ellipticity can be calculated from Eq. (2.51) which gives $\varepsilon \approx 0.61$. We also converted the elliptical light into linear light by use of a Soleil-Babinet compensator. The compensated path difference is about 0.21λ, which confirms the independent measurement above. The thickness of the LC layer should be better controlled to reduce ellipticity. For a thickness of 5% below the ideal, the ellipticity is 0.3, and for 1% below, it is 0.1.

In the presence of the write light the read-out light from LCLV2 is generally elliptically polarized. We found, however, that for a given write intensity, LCLV2 had a specific orientation at which the read-out light maintained linear polarization, but the polarization was rotated by a certain angle with respect to that of the read-in light. The specific orientation changed with the write light intensity. This was measured by use of the same setup as shown in Fig. 3.26. For a given write light intensity we turned the polarizer (P1) and the analyzer (P2) iteratively to find the minimum read-out intensity, then measured the P1 and the P2. The corresponding read-in polarization was given by the orientation of P1 and the read-out polarization was at 90° with respect to the (minimum) position of P2. Continuously changing the write light intensity and measuring the P1 and P2, we obtained the read-in and read-out polarization as a function of the write light intensity shown in Fig. 3.30.

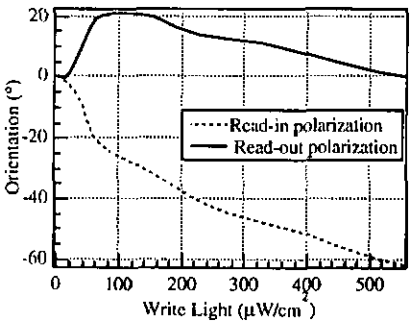

Fig. 3.30 Orientation of read-in and read-out polarization of LCLV2 for linearly polarized output.

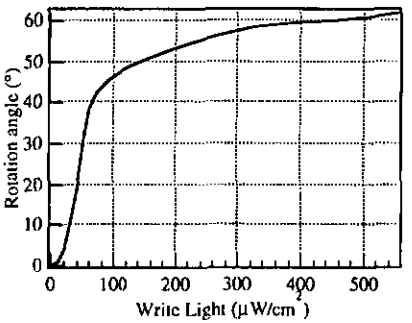

Fig. 3.31 Rotation angle between the read-in and out polarization of LCLV2 for linearly polarized output.

The rotation angle of the polarization orientation of read-out light with respect to that of read-in light was obtained as the difference of the two curves in Fig. 3.30 and shown in Fig. 3.31. LCLV1 and LCLV3 do not have this polarization rotation power.

3.7 RESPONSE SPEED AND RESOLUTION

To determine the response speed of LCLV1, the write side of the valve was periodically illuminated by using a shutter (UNIBLITZ, SD122) which was driven at 0.5 Hz using a function generator. The intensity of write light was chosen to be 72 $\mu W/cm^2$ higher than the write light for 90% of ON-state so as to fully switch on (saturate) the valve. The read-out light was detected by a photodetector, and the response time was measured from the oscilloscope. The rise time (τ_r) is from 10% to

90% of full ON-state, and the decay time (τ_d) is from 90% to 10% of full ON-state. The result is shown in Fig. 3.32, from which we get τ_r = 140 ms and τ_d = 680 ms. The slow response is mainly due to the cadmium sulfide photoconductor. We observed that the rise time was dependent on the write light intensity, the rise time decreased with increasing write light intensity. But the fall time remained nearly constant when the write light increased. This is consistent with the theoretical predictions in 2.3.4.

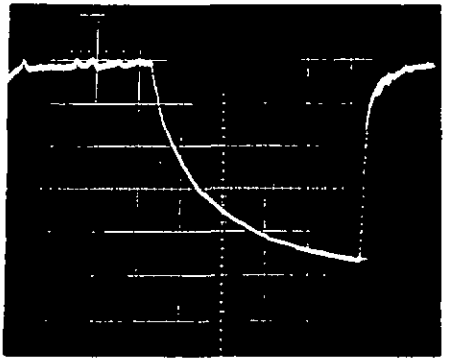

Fig. 3.32 Response time of LCLV1 (200 ms/div.).

The response time of LCLV2 was measured in a similar manner, the write light intensity was 1 mW/cm^2. The rise and decay times of LCLV2 are τ_r = 10 ms and τ_d = 14 ms, respectively (see Fig. 3.33).

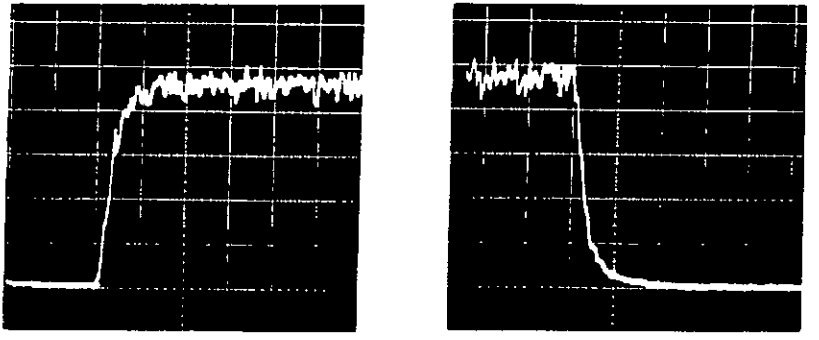

(a) (b)

Fig. 3.33 Response time of LCLV2. (a) rise time; (b) decay time (20 ms/div.).

The experimental arrangement for measuring the response time of LCLV3 was slightly different from that for LCLV1, because we must write the valve synchronously with the SET pulse and measure the rise time at the same time. We

used a high brightness LED (TOSHIBA,TLRA190P) which was directly driven by the SET pulse from the power supply of the valve, instead of the shutter. The response of the LED is much faster than that of valve, and the spectral range of 640-680 nm is within the spectral sensitive range of LCLV3. The average intensity of the LED was 480 $\mu W/cm^2$. The rise and decay times are τ_r = 1.4 ms and τ_d = 0.6 ms, respectively (see Fig. 3.34). This result is exactly the same as we got by using a constant write light because the response speed of amorphous silicon is much faster than that of the liquid crystal. So the response time we measured actually is nothing but the response of the liquid crystal to the drive waveform.

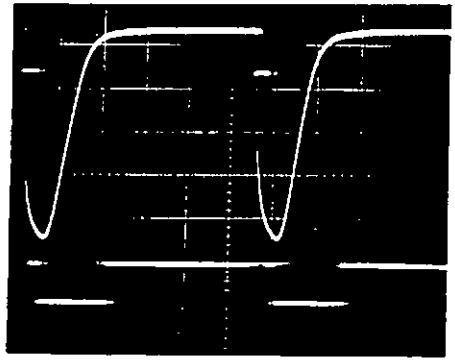

Fig. 3.34 Response time of LCLV3 (2ms/div.).

To determine the spatial resolution of a LCLV, a 1:1 image of a USAF test chart was projected onto the write side of the LCLV by using a tungsten halogen lamp. The input pattern was read out by a collimated laser beam from the read side. The resolution is 28 lp/mm for LCLV1, 12 lp/mm for LCLV2 and 14 lp/mm for LCLV3.

3.8 INVERTED OPERATION MODE AND DYNAMIC CHARACTERISTICS

All measurements and discussions above are based on an arrangement in which the polarizer and analyzer are crossed (see Fig. 3.7), thus the read-out light intensity is proportional to the write light intensity, i.e. the LCLV switches from the OFF-state to the ON-state with increasing write intensity. This is the normal operation mode or called positive mode. There is, however, another operation mode in which the polarizer and analyzer are parallel, and therefore the read-out light intensity are inversely proportional to the write light intensity, i.e. the LCLV is in ON-state when

there is no write light and switches to the OFF-state with increasing write intensity. This mode is called the inverted operation mode or negative mode. A transfer curve of LCLV1 for the inverted mode are shown in Fig. 3.35, which may be approximated by a negative sigmoid function. In the inverted mode the dynamic range is constrained by the dark state, therefore the minimum read-out efficiency η_{min} is of concern rather than the maximum η_{max} in the normal mode. The contrast ratio in the inverted mode may be much lower than that in the normal mode because of the worse dark state.

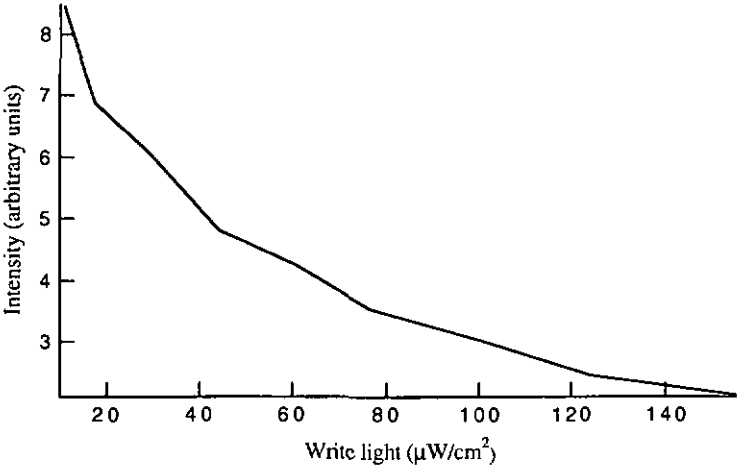

Fig. 3.35 A transfer curve of LCLV1 for the inverted mode.

The relation of the input (write light) and the output (read-out light) of a LCLV was described by the efficiency curve as discussed in Section 3.3. However the efficiency curve is valid only when the write light intensity changes very slowly, i.e. the rate of change of the write light intensity is much slower than the response speed of the LCLV. Each point on the efficiency curve indicates the equilibrium read-out intensity corresponding to the given write light intensity. Therefore the efficiency curve describes a static input/output relation. However, when the rate of change of the write light intensity is nearly equal to the response speed, the read-out light can never reach the equilibrium state. This happens in the free space optical feedback systems where the delay in the feedback path is negligible comparing with the response time of LCLV. In this case, we have to know the dynamic input/output relation which is a 3D surface

$$I_{R\text{-}out} = f(I_w, t) \tag{3.2}$$

This dynamic transfer function may be determined indirectly by measuring the response speed curves for different write light intensity, then synthesizing these curves. Fig. 3.36 gives the dynamic transfer characteristic of LCLV1.

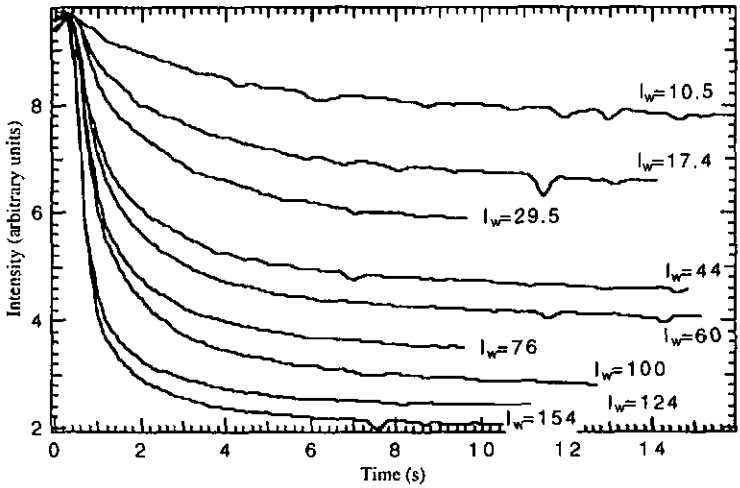

Fig. 3.36 Dynamic transfer characteristic of LCLV1 for the inverted mode (units of I_w: $\mu W/cm^2$).

3.9 COMPARISON AND DISCUSSION

The main characteristics of three types of liquid crystal light valves are summarized in Table 3.2. It can be seen that the LCLV1 has many advantages, such as high sensitivity, high efficiency, and the gain which is not obtainable for LCLV2 and LCLV3. However, slow response is the chief drawback of this valve, which is due to the cadmium sulfide photoconductor. Besides, its most sensitive spectral range covers neither He-Ne nor Ar^+ lasers wavelength, thus a dye laser has to be used with this valve. In contrast, LCLV3 has a wide uniform spectral range, fast response and unique bistability. The spatial nnnuniformity is a common and severe problem for the three valves. The LCLV2 and LCLV3 have more uniform OFF-states than the LCLV1, but the latter has the more uniform ON-state. The polarization states of the read-out light are always elliptically polarized for LCLV2 and LCLV3. A linearly polarized read-out with 90° rotation can be generated from LCLV1 for a specific write light intensity.

Device		LCLV1	LCLV2	LCLV3	MSLM
Spectral Sensitivity (nm)		540 ~ 600	450 ~ 650	450 ~ 650	300 ~ 650
Read-out Efficiency (max.)		70%	36%	45% (sync) 32% (integ)	4.6%
Write Sensitivity ($\mu W/cm^2$)		45 (at 555 nm)	514 (at 515 nm)	136 (sync) 133 (integ) (at 515 nm)	12 (at 515 nm)
Contrast Ratio		41 : 1	50 : 1	22 : 1 (sync) 16 : 1 (integ)	30 : 1
Max. Read-in Intensity		1 mW/cm^2	300 $\mu W/cm^2$	170 $\mu W/cm^2$	100 mW/cm^2
Effective Gain		17	0.21	0.56	383
Uniformity Area (cm^2)		4 (±10%)	1.5 (±10%)	3.2 (±10%)	0.5
Resolution (lp/mm)		28	12	14	<10
Response Time	rise	120	10	1.4	100
(ms)	decay	540	14	0.6	170

Table 3.2 Summary of the measured characteristics of the three LCLVs and the MSLM.

The nonuniformity and elliptically polarized read-out is related with the defects in the LC cell fabrication, such as bad alignment and inaccurate thickness. It should be noted that the optical path difference (OPD) in the twisted configuration (LCLV2) is not equal to, but a fraction of the thickness of the LC layer, and variable with write light intensity. It raises a question how to make the OPD correct so as to obtain a linearly polarized output in the twisted configuration. The gain is constrained only by the efficiency of the light blocking layer. When the light blocking layer is imperfect, the write sensitivity has an effect on the gain as well. The spectral sensitivity of amorphous silicon (a-Si:H) photoconductor seems superior to the cadmium sulfide because the Ar^+ laser can be used. However, it was reported that the sensitivity peak of the cadmium sulfide photoconductor could be moved to 520 nm by baking the evaporated film in Argon gas.[64] The twisted configuration (LCLV2) gives better dark state, and thus higher contrast ratio. Clearly there is much room for improving the performance of these basic devices. For the time being, however, device manufacturers and researchers are turning their interest towards

Smart SLMs,[65] so that there is an inevitable hiatus in the availability of improved devices.

The device performance may be improved to some extent by using supplementary optical systems or devices. In the case of LCLV2 the gain may be realized by using the image intensifiers on the write side of the LCLVs. The image intensifier is able to amplify the write light up to 10^4 times.[66] If we can produce a structured illumination to match each metal pixel in LCLV3, the gain will be available. The nonuniformity could be solved in principle by irradiating the write side with a supplementary array of individually tuned bias beams. However these compensation will increase the system complexity and there are a lot of technical details to be solved in practice. There is a fundamental difference between the ferroelectric LCLV and nematic LCLV. The input and output in the nematic LCLV are continuous functions of time. However, in smectic LCLV both input and output are discrete with time, i.e. the read-out is regularly set to be 'zero' (OFF-state) even if the valve is in full ON-state.

Finally we make a comparison of LCLV with another type of optically addressed spatial light modulator called microchannel spatial light modulator (MSLM).[68] The MSLM consists essentially of a photocathode, microchannel plate (MCP), and electrooptic crystal in a vacuum sealed tube. The characteristics of a MSLM fabricated by Hamamatsu Photonics is also given in Table 3.2. We find that the maximum read-out efficiency of MSLM is only 4.6% which is much lower than that of LCLV. This low efficiency means that the read-out light is elliptically polarized, therefore it is not suitable for using in inverted mode. The advantage of MSLM is that high gain may be realized by using a powerful read-in light which can be as strong as 100 mW/cm^2. There are some similarities between the MSLM and LCLV3, e.g. both operate in step with the electric drive waveform, both need an erase phase in each read/write cycle, both have memory capability. However, the frame rate for MSLM is only 4 Hz, in comparison with 90 Hz for LCLV3. The drive voltage for MSLM is very high, the half-wavelength voltage is 2 kV.

APPENDIX 3.1 CALIBRATION OF DYE LASER

We used a Coherent CR-599 dye laser pumped by an Ar^+ laser with all lines. The dye was Rhodamine 110 from Radiant Dyes Laser Accessories GmbH, Germany. The calibration curve is given in Fig. A3.1. The output power as a function of wavelength

is shown in Fig. A3.2. The concentration of the dye directly affected the output power. We dissolved one gram of dye in 100 ml of methanol and added 1554 ml of ethylene glycol. The pressure of the dye in the pump system is 40 psi (2.75 bar).

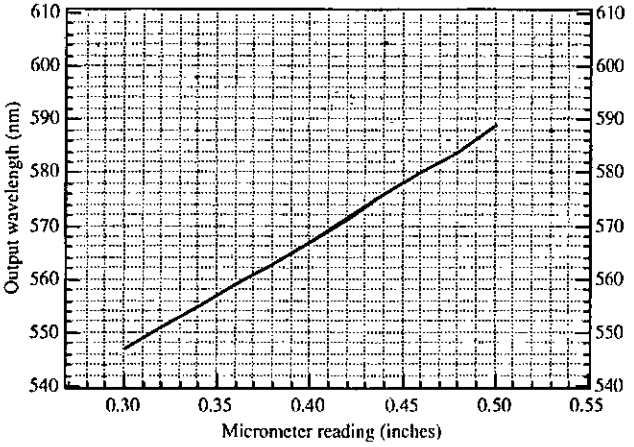

Fig. A3.1 Dye laser calibration curve for Rhodamine 110.

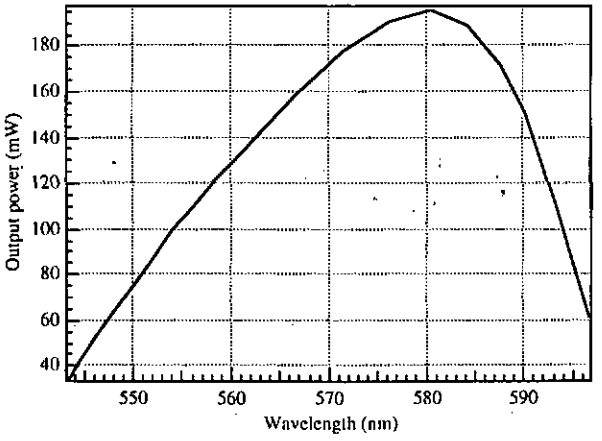

Fig. A3.2 Output power of the dye laser as a function of wavelength.

4

APPLICATION OF LCLV TO OPTICAL NEURAL NETWORKS

This chapter deals with the application of the LCLVs to optical neural networks (ONN). Our intention is to concentrate on the effects of the LCLV on the ONN behavior, rather than the models and theory of the neural network. We chose the Hopfield type models because these models have been well studied and have been optically realized by many groups in different ways. Section 1 presents the Hopfield neural network model (H-model) and two modified H-models which could be implemented using optics. Section 2 discusses the basic principles of ONN design and gives the parameters of the ONN. Section 3 gives the experimental results of the optical implementations of the two neural network models. Section 4 analyses the experimental results and gives the explanations of the system's behavior. Section 5 briefly discusses the limitations of the ONN and the requirements for the LCLV from a system point of view.

4.1 HOPFIELD TYPE MODELS FOR OPTICAL NEURAL NETWORKS

4.1.1 Hopfield Model

The Hopfield neural network model[12] (H-model) was the first model implemented using optics.[15] In H-model each neuron has two states, the OFF state $N_i = 0$ and the ON state $N_i = 1$ ($i = 1, 2, \ldots\ldots M$). The instantaneous state of the system is specified by listing the M values of N_i, so it is represented by a binary word of M bits.

The architecture of the H-model is such that all neurons are located in one layer, i.e. all neurons act as both input and output, and each neuron is connected with all of the other neurons.

The interconnection between neuron i and neuron j has a weight of T_{ij} which can be calculated for S memory patterns according to

$$T_{ij} = \begin{cases} \sum_{s=1}^{S} (2N_i^{(s)} - 1)(2N_j^{(s)} - 1) & \text{if } i \neq j \\ 0 & \text{if } i = j \end{cases}, \tag{4.1}$$

For excitatory interconnections, T_{ij} is positive, and it is negative for inhibitory ones. The information is stored in a distributed manner across the weight matrix, which is sometimes referred to as Hebbian storage.

Each neuron is updated according to the following dynamics

$$N_i = f(U_i) \tag{4.2}$$

$$U_i = \sum_{j=1}^{M} T_{ij} N_j - \theta_i + I_i , \tag{4.3}$$

where U_i is the activation potential of the i-th neuron; M is the total number of neurons; T_{ij} is the weight of the interconnection between the i-th neuron and the j-th neuron; θ_i and I_i are, respectively, the threshold level and external input to the i-th neuron, and $f(x)$ is a step function which represents the nonlinear input-output characteristic of the neuron i.

$$f(x) = \begin{cases} 0 & \text{for } x < 0 \\ 1 & \text{for } x \geq 0 \end{cases}, \tag{4.4}$$

The physical meaning of Eqs. (4.2) and (4.3) is a nonlinear thresholding and feedback system which is depicted schematically in Fig. 4.1. The first term of Eq. (4.3) represents the sum of the inputs to neuron i from all of other neurons.

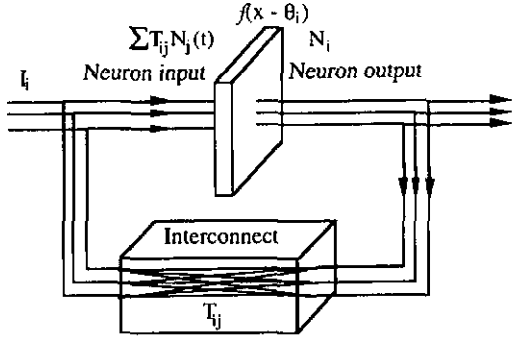

Fig. 4.1 A nonlinear thresholding and feedback system.

It has been shown[12, 69] that when T_{ij} is symmetric, one can define an energy function E for the neural system by

$$E = -\frac{1}{2}\sum_{i=1}^{M} U_i N_j = -\frac{1}{2}\sum_{i=1}^{M}\sum_{j=1}^{M} T_{ij} N_i N_j + \frac{1}{2}\sum_{i=1}^{M}(\theta_i - I_i)N_j \qquad (4.5)$$

For any threshold level θ_i and given input I_i, the energy of the system will be a decreasing function of the neuron state or a constant. This means that the network always evolves towards a steady state of local or global energy minimum. The descent to an energy minimum takes place by the dynamic process described by Eqs. (4.2) and (4.3) regardless of whether the state update of the neurons is synchronous or asynchronous.[70] The asynchrony, which means that updating the state of each neuron is independent of updating other neurons, is a natural property for all analogue neural systems because there are always propagation delays, nonuniformities of the devices and noise. In the case of digital neural systems which use switching threshold devices or computer feedback, one can choose either the asynchrony or synchrony.

The energy landscape can be modified in accordance with Eq. (4.5) by changing the interconnection weight T_{ij} and/or the threshold level θ_i and/or the external input I_i. Local minima in an energy landscape or steady states (attractors) in phase-space can be fixed by forming T_{ij} in accordance with Eq. (4.1). Therefore the H-model can function as the content-addressable memory, i.e. from an initial state of partial information about a memory, a final stable state with all the information of the memory can be found.

There are three major aspects to consider in order to build a neural network system based on the H-model: huge interconnections; bipolar grey scale weights; and thresholding. A system of M neurons requires MxM interconnections. Optical techniques due to inherent parallelism offer an effective means for the implementation of the huge interconnections. The thresholding can be performed by any device with nonlinear transfer characteristic, e.g. the LCLV which is of concern in this thesis. According to Eq. (4.1) the individual weights of the interconnection matrix may be positive, negative, or zero , and range from -S to +S with (2S+1) grey levels. The bipolar weight matrix means that there must be subtraction as well as addition in the implementation of Eq. (4.3). The bipolar interconnection weights and the subtraction, however, are somewhat difficult to be handled in optical systems. Therefore the first optical neural network[15] adopted an optoelectronic hybrid system, i.e. used two independent optical channels to process the positive and negative interconnections separately, and used the electric feedback to do the

subtraction and the thresholding. In order to exploit all-optical neural networks, some modified H-models have been proposed. For example, the weight matrix in Eq. (4.1) can be modified by simply adding a constant so that all its elements become positive. However, this results in a dynamic threshold,[16,71] thus increasing the system complexity.

4.1.2 Modified Hopfield Models

There do exist some modified H-models which use unipolar interconnections and do not need subtraction, thus are suitable to all-optical implementation. Here we briefly describe two modified H-models, namely, the inhibitory model and the inverted model.

A. Inhibitory model

The inhibitory model proposed by Shariv et al.[18] is based on some simulation results which show that the performance of the H-model is essentially unchanged by discarding all the positive interconnections. Therefore the interconnection matrix of the inhibitory model is obtained by simply cutting out all the positive weights from the matrix of the H-model, and only using the inhibitory interconnections of the H-model. The modified weight matrix is defined as

$$T'_{ij} = \begin{cases} |T_{ij}| & \text{if } T_{ij} \le 0 \\ 0 & \text{otherwise} \end{cases} \tag{4.6}$$

where T_{ij} is defined by Eq. (4.1), and T'_{ij} is a nonnegative matrix. The dynamic rule is redefined as

$$N_i = g_i(U_i) \tag{4.7}$$

$$U_i = \sum_{j=1}^{M} T''_{ij} N_j - \theta_i + I_i , \tag{4.8}$$

where T''_{ij} is the normalized weight matrix

$$T''_{ij} = \frac{T'_{ij}}{\sum_{j=1}^{M} T'_{ij}} , \tag{4.9}$$

g(x) is a new nonlinear function defined by

$$g_i(x) = 1 - f_i(x) \tag{4.10}$$

where $f_i(x)$ is defined by Eq. (4.4). It can be seen that the neurons in this model have the inverse response to that associated with the H-model, i.e. the neuron turns to the OFF-state when the activation potential of the neuron is high. The inhibitory model ensures that all the connections are positive, thus the subtraction is not required. The threshold value is a fixed positive number for each neuron. The disadvantage of this model is the low feedback efficiency because on average 50% of the feedback which corresponds to the positive interconnections, will be blocked. In order to maintain a sufficient feedback efficiency, the number of 1 in the stored patterns should be restrained. In practice we choose stored patterns in which half the neurons are 1 and the other half are 0. The effects of the low efficiency on the system design will be discussed later.

B. Inverted model

The inverted model[72] is based on the inhibitory model above, but uses a binary interconnection matrix instead of the grey level matrix. The binary matrix is calculated according to

$$T_{ij} = \begin{cases} \prod_{s=1}^{S} (1 - N_i^{(s)} N_j^{(s)}) & \text{if } i \neq j \\ 0 & \text{if } i = j \end{cases}, \qquad (4.11)$$

where $N_i^{(s)} = \{0, 1\}$ are the S stored patterns. Note that $T_{ij} = 0$ if , for at least one stored pattern, $N_i^{(s)}$ and $N_j^{(s)}$ are both 1, otherwise $T_{ij} = 1$. The inverted model follows the same dynamic rules Eqs. (4.7) and (4.8) as the inhibitory model does. Obviously according to Eq. (4.11), the number of non-zero elements in the matrix will decrease with increasing the stored patterns and the number of one in each pattern. Therefore the inverted model also suffers from low feedback efficiency.

4.1.3 Hopfield Continuous Model

The original H-model is based on binary neurons, and the nonlinear response of the neurons is the step function described by Eq. (4.4). The nonlinear characteristic of LCLV, however, is a sigmoid function (see section 2.4.1), i.e. the optical neurons may have any value between zero and a maximum. On the other hand, the all-optical feedback is continuous in time rather than discrete iterations. Therefore the continuous H-model[73] should be introduced to describe the all-optical neural network system.

Let the output variable N_i for neuron i have the range $N_i \in [0,1]$, u_i be the action potential of the i-th neuron, and $g_i(u_i)$ be a sigmoid-type continuous and monotone function of the instantaneous input u_i to neuron i, called the gain function. Then, the dynamics of the neural system follows the differential equation

$$\frac{du_i}{dt} = \sum_{j=1}^{M} T_{ij} N_j - \alpha_i u_i + I_i , \tag{4.12}$$

$$N_j = g_i(u_i), \tag{4.13}$$

where T_{ij} is the weight of the interconnection between the i-th neuron and the j-th neuron defined by Eq. (4.1), α_i is a constant indicating the decay time of i-th neuron, I_i is the external input to the i-th neuron.

It has been shown[73] that when the interconnection matrix is symmetric and the nonlinear function $g_i(u_i)$ is steep enough, then the continuous model has similar attractor dynamics to the discretized model. Therefore the continuous model can be used in associative memory as well. However, when the $g_i(u_i)$ is less steep the continuous model has fewer stable states than the discretized model with the same interconnection matrix. The system always converges to a unique point attractor provided that[74]

$$\sum_{i=1}^{M}\sum_{j=1}^{M} T_{ij}^2 < 1/(\max_i |g_i'|)^2 \tag{4.14}$$

where g_i' is the differentiation of $g_i(u_i)$, T_{ij} is the interconnection between i and j neuron.

4.2 OPTICAL NEURAL NETWORK SYSTEM USING LCLVs

We have discussed the 'software'— the ONN models. In this section the hardware implementation of these models is of concern. The nonlinear threshold device in our system will be the LCLV which has been dealt with in the last two chapters. In the following we will discuss the basic principles and optical techniques first, which may be applied to general all-optical feedback systems such as the one shown in Fig. 4.1. Then we describe in detail the ONN system, which was realized in our lab, and finally discuss the nonuniformity in the system.

4.2.1 Basic Principles and Optical Techniques

A. Optical neurons

In our ONN systems, the neurons are produced by the phase gratings and the LCLV as shown in Fig. 4.2. A laser beam illuminates a pair of crossed phase gratings and generates a spot array of approximately equal intensity at the read side of the LCLV.[75] Each spot represents a neuron. The states of the neuron are characterized by the valve's read-out intensity behind the polarizer, which, depending on the input, can take any value between the full ON- and OFF-states. Therefore this optical neuron is really continuous. The spot size D and spot spacing Δx are given by

$$D = \frac{2\lambda f_0}{A\sqrt{2\pi}} \tag{4.15}$$

$$\Delta x = \frac{\lambda f_0}{d_1}, \tag{4.16}$$

where λ is the laser wavelength, f_0 is the focal length of the lens, $A/\sqrt{\pi}$ is the half width of the laser beam, and d_1 is the period of the diffraction gratings.

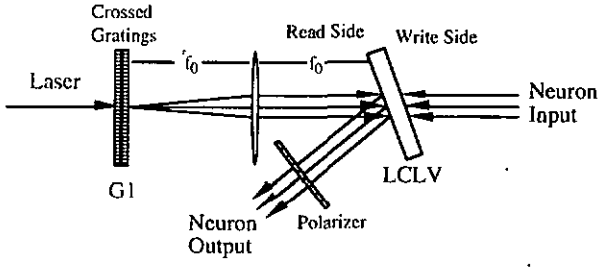

Fig. 4.2 Schematic of optical neuron array.

B. Interconnections and mask

The weighted interconnections in ONN can be divided into a fan-out/fan-in system and a photographic mask, since the interconnections are fixed without learning. The fan-out/fan-in system is illustrated in Fig. 4.3.

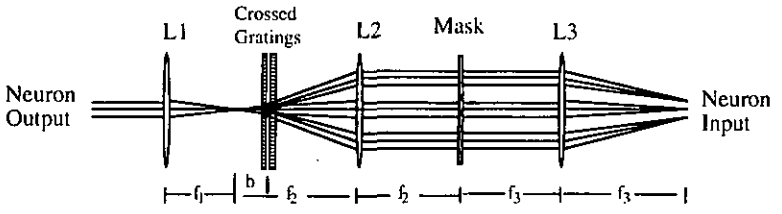

Fig. 4.3 Schematic of fan-out/fan-in system and the interconnection mask.

The fan-out of the neuron output array is produced using a second pair of crossed diffraction gratings. To ensure that these fan-out do not overlap at the mask plane, the focal length f_1 and the period of the second diffraction gratings d_2 must chosen so that

$$\frac{\lambda}{d_2} \geq \sqrt{M}\,\frac{\Delta x}{f_1}, \tag{4.17}$$

where λ is the wavelength, M is the number of neurons, and Δx is the separation of the neurons given in Eq. (4.16).

Therefore M images of the neurons array are obtained at the mask plane, which enables us to add weight to every pixel of the interconnection. Then each image is focused by L3 onto the corresponding neuron input port, thus the full interconnections are completed. The separation of the fan-in spot array is given by[19]

$$\Delta X = \frac{f_3}{f_2}\frac{\lambda b}{d_2}, \tag{4.18}$$

where f_2 and f_3 are the focal length of L2 and L3, respectively, d_2 is the period of the second diffraction gratings, b is the displacement of the gratings from the front focal plane (FFP) of L2. The separation of the fan-in spots must match that of the neurons, i.e. $\Delta X = \Delta x$. Actually each fan-in spot is just a image of the light spot at the FFP of L2. Usually it is necessary to put an aperture at the FFP of L2 in order to obtain the fan-in spots with proper size and clear edge.

The weights may be introduced from the mask plane, in principle, by any optical device or component which can modulate the transmittance of every pixel independently. We chose the photographic mask simply because it has low loss. The maximum transmittance of the mask can be 87%, in contrast to 35% for LCD (Epson EG-Y84320AT), and only 10% for LCTV (Epson Vidio Projector VPJ-2000). Two masks for inhibitory and inverted model, respectively, were fabricated by using milimask plates. The printout patterns of these masks are given in Fig. 4.4 and Fig.

4.5. Two memory patterns, the letters "T" and "L", were encoded in the masks according to Eq. (4.9) and (4.11), respectively. The mask for inhibitory model has three grey levels at which the transmittances are 100%, 50%, and 33%, respectively.

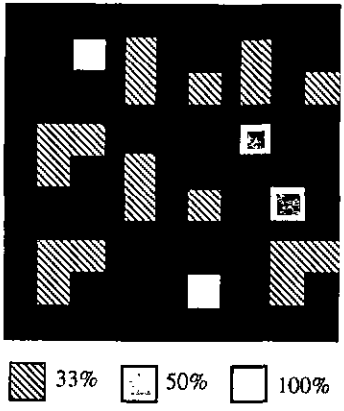

Fig. 4.4 Mask for inhibitory model.

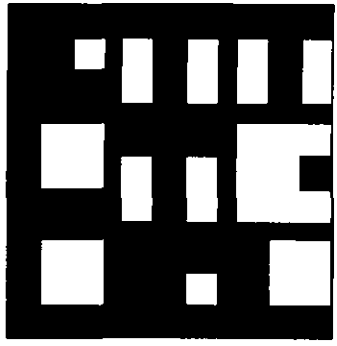

Fig. 4.5. Mask for inverted model.

For convenience of the following discussions, we number the neurons and the interconnection weights as shown in Fig. 4.6(a) and (b), respectively.

N1	N2	N3
N4	N5	N6
N7	N8	N9

(a)

$T_{1,1}$	$T_{1,2}$	$T_{1,3}$	$T_{2,1}$	$T_{2,2}$	$T_{2,3}$	$T_{3,1}$	$T_{3,2}$	$T_{3,3}$
$T_{1,4}$	$T_{1,5}$	$T_{1,6}$	$T_{2,4}$	$T_{2,5}$	$T_{2,6}$	$T_{3,4}$	$T_{3,5}$	$T_{3,6}$
$T_{1,7}$	$T_{1,8}$	$T_{1,9}$	$T_{2,7}$	$T_{2,8}$	$T_{2,9}$	$T_{3,7}$	$T_{3,8}$	$T_{3,9}$
$T_{4,1}$	$T_{4,2}$	$T_{4,3}$	$T_{5,1}$	$T_{5,2}$	$T_{5,3}$	$T_{6,1}$	$T_{6,2}$	$T_{6,3}$
$T_{4,4}$	$T_{4,5}$	$T_{4,6}$	$T_{5,4}$	$T_{5,5}$	$T_{5,6}$	$T_{6,4}$	$T_{6,5}$	$T_{6,6}$
$T_{4,7}$	$T_{4,8}$	$T_{4,9}$	$T_{5,7}$	$T_{5,8}$	$T_{5,9}$	$T_{6,7}$	$T_{6,8}$	$T_{6,9}$
$T_{7,1}$	$T_{7,2}$	$T_{7,3}$	$T_{8,1}$	$T_{8,2}$	$T_{8,3}$	$T_{9,1}$	$T_{9,2}$	$T_{9,3}$
$T_{7,4}$	$T_{7,5}$	$T_{7,6}$	$T_{8,4}$	$T_{8,5}$	$T_{8,6}$	$T_{9,4}$	$T_{9,5}$	$T_{9,6}$
$T_{7,7}$	$T_{7,8}$	$T_{7,9}$	$T_{8,7}$	$T_{8,8}$	$T_{8,9}$	$T_{9,7}$	$T_{9,8}$	$T_{9,9}$

(b)

Fig. 4.6 Spatial positions of neurons (a) and interconnection weights (b).

C. Feedback loop and system loss

Combining the optical neurons (shown in Fig. 4.2) with the fan-out/fan-in system (shown in Fig. 4.3), we obtain a loop in which the output of each neuron is, through the weighted interconnections, fed back to other neurons' inputs (the write side of the LCLV) as shown in Fig. 4.1. The function of the LCLV is to sum all inputs to each

neuron and then make a nonlinear transform. However, to make the loop work, the feedback intensity must be able to switch the LCLV on, i.e. the following inequality should be fulfilled,

$$\alpha_s \, \alpha_m \, I_{R\text{-}out} \geq I_w(90\%), \tag{4.19}$$

where $I_{R\text{-}out}$ and $I_w(90\%)$ are the read-out light intensity and the sensitivity of the LCLV, respectively, defined in Section 2.3.2. α_s, $\alpha_m \in (0, 1)$, are the loss coefficients due to the optical system and the neural model (different connection matrix), respectively. By using Eq. (2.22), the Eq. (4.19) becomes

$$\alpha_s \, \alpha_m \, G_v \geq 1, \tag{4.20}$$

where G_v is the effective gain of the LCLV. For a given LCLV, the effective gain is fixed, therefore how to reduce the losses becomes crucial. That is why we used photographic masks rather than LC devices. The neural model loss comes from the zero interconnections, for example, the mask of the H-model for the letters "T" and "L" has 55% of the pixels zero, while the one of inhibitory model has 73%. For the mask with grey levels, even the non-zero pixels cause some losses as well. The system loss is mainly due to the fan-out gratings and the polarizers. The diffraction efficiency of the crossed gratings is only 36%. The maximum transmittance of the polarizer is about 65%. Since α_s and α_m are always less than 1, any LCLV which can be used in the feedback system should have an effective gain greater than 1. From this point of view, only LCLV1 has the potential to be used in the system (see Table 3.2).

4.2.2 Experimental System

Based on the discussion above we designed and implemented the all-optical feedback neural network system illustrated in Fig. 4.7. The laser beam illuminates the grating G1 to produce a 3x3 light spot array on the read side of the LCLV. The polarization of P1 was fixed in the vertical direction. The intensity of each spot can be adjusted by rotating the half waveplate (HWP) so as to keep it below the maximum read-in intensity(given in Table 3.2). The P2 was set parallel to P1 such that the nonlinear transfer function of each neuron was a graded NOR function (inverted operating model) which was required by the inhibitory and inverted model. L3 and L4 are extra lenses for maintenance of spatial invariance of the feedback spots array. The He-Ne laser and G3 yield a 3x3 light array which illuminates the input mask as the initial input. The focal length of L8 and L9 should be chosen properly so as to match the initial input array with the neuron array. The objective lens and L7 are used for adjusting the spot size of the input. The states of

the neurons were measured by the CCD camera connected with the PC and the monitor. The main parameters are given in Table 4.1.

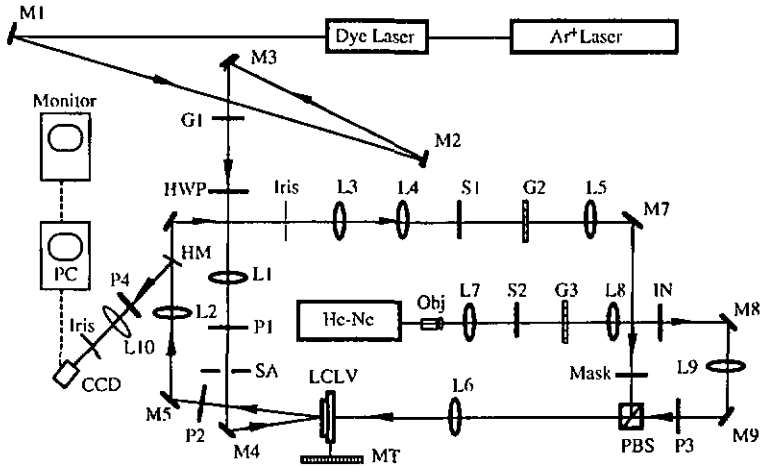

Fig. 4.7 All-optical feedback neural network system. M1-M9: mirrors; L1-L10: lenses; P1-P4: polarizers; HWP: half wave plate; SA: square aperture; S1, S2: shutters; G1-G3: gratings; PBS: polarization beam splitter; IN: initial input mask; Obj: objective lens; HM: half mirror; MT: micro translation stage.

L1, L2, L5, L6	Focal length f = 385 mm; Aperture diameter ϕ = 60 mm
L3, L4,	Focal length f = 100 mm; Aperture diameter ϕ = 30 mm
L9	Focal length f = 100 mm; Aperture diameter ϕ = 50 mm
L8	Focal length f = 120 mm; Aperture diameter ϕ = 50 mm
L7	Focal length f = 40 mm; Aperture diameter ϕ = 17 mm
Obj	Magnification: 4:1; Numerical aperture: 0.10
G1	Grating period d_1 = 64 μm
G2	Grating period d_2 = 20 μm
G3	Grating period d_3 = 77 μm

Table 4.1 The main parameters for the system.

To run the system we first closed the shutter S1 and opened S2 to introduce a initial pattern through the input mask IN. As soon as the system stabilized on the initial state, we closed S2 and at the same time opened S1. Then the system ran according to its dynamics. Note that the system is a continuous time one, i.e. any neuron's state is a continuous function of time. Therefore, the reading and writing in the LCLV should be done continuously. This excludes any possibility to use the clock operating devices such as the ferroelectric vale (LCLV3) and MSLM[20] in the system.

4.2.3 Spatial Nonuniformities in the ONN System

The main difficulties in setting up the ONN system were how to obtain the best spatial uniformity. Ideally all neurons should have the same ON- and OFF-state, and the response characteristics of the neurons should be the same as well. However, the nonuniformities in hardware realizations are inevitable. Our goal was to minimize the nonuniformities.

A. Uniformity of the neurons

The uniformity of the neurons depend on both gratings G1 and LCLV, as shown in Fig. 4.2. The intensity distribution of the diffraction orders of the gratings are very sensitive to the position where the laser beam strikes. The diffraction intensity was monitored when the gratings were moved so as to find the best position. The normalized intensities of the light spots from G1 is given in Fig. 4.8. It can be seen that the maximum nonuniformity is about ±7%. The diffraction efficiency of the crossed gratings at this position is relatively low, only 17%.

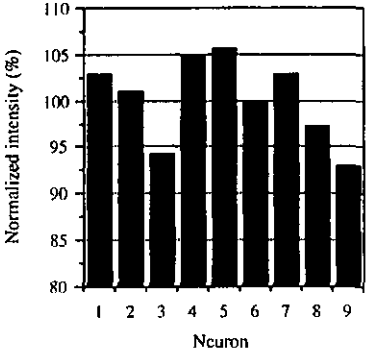

Fig. 4.8 Uniformity of the diffraction orders of G1.

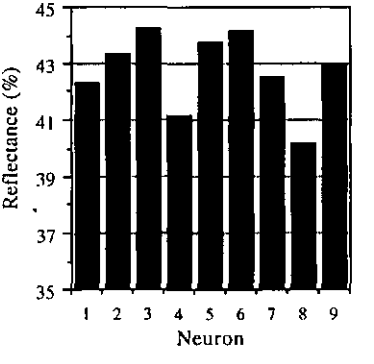

Fig. 4.9 Uniformity of the LCLV's reflectance in ON-state.

The reflectance of the LCLV was also spatially nonuniform as discussed in Chapter 3, therefore it should be possible to generally minimize the nonuniformity of the neurons' output by properly choose the working area on the LCLV. The reflectance of the LCLV in the ON-state is shown in Fig. 4.9, in which the absorption of the polarizer P2 was included. The uniformity of the neurons' outputs which is the combination of Fig. 4.8 and 4.9, are shown in Fig. 4.10. Comparing the Fig. 4.10 with Fig. 4.8 we found that the nonuniformity are still maintained at ±8% though some neurons changed their intensities. The uniformity of the neurons in OFF-state was optimized such that the highest contrast ratio was obtained.

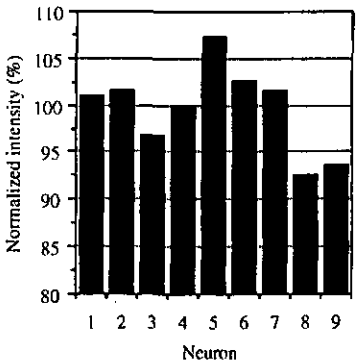

Fig. 4.10 Uniformity of the neurons' outputs in ON-state.

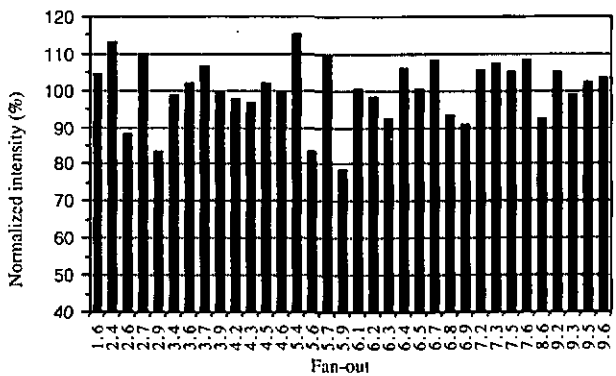

Fig. 4.11 Uniformity of the fan-outs at the mask plane.

B. Uniformity of the interconnections

The uniformity of the fan-out is related to the output of the neurons and the second grating pair G2. Note that more than half the fan-outs will be blocked by the mask, therefore only the usable fan-outs were measured and shown in Fig. 4.11. We found

that the uniformity was getting worse. Because G2 was located off the focal plane, actually each neuron was diffracted by different position of the gratings, thus uniform fan-out was hardly available.

The mask also introduced some nonuniformities, particularly the mask for the inhibitory model because there should be three grey levels, 33%, 50%, and 100%, on the mask as shown in Fig. 4.4. However it is not so easy to precisely control the grey levels in the fabrication. The transmittance of two inhibitory masks are given in Fig. 4.12. It can be seen that most of the pixels with 33% transmission deviate from the correct value.

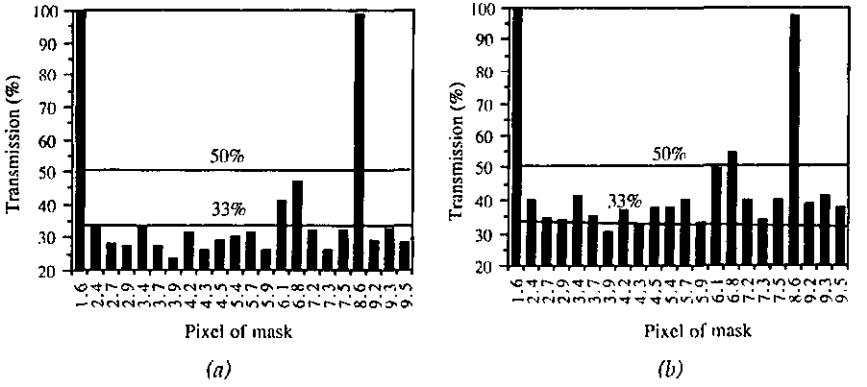

Fig. 4.12 Transmittance of the inhibitory Mask1 (a) and Mask2 (b). The theoretical grey level are 100% for pixels 1.6 and 8.6, 50% for pixels 6.1 and 6.8, and 33% for others.

Actually the strength of each interconnection depends on the combination of fan-out intensity with the transmittance of the corresponding pixel on the mask. Therefore the transmittance of each pixel on the mask should be chosen such that the normalized transmission intensity behind the mask is in accord with the theoretical grey level. To achieve the adjustable transmittance we first made a binary mask, then put it in the system, the transmittance of each pixel was adjusted by pasting a polarization sheet in a different orientation. In this way most of the nonuniformities due to the two gratings and the LCLV were compensated, and a quite uniform fan-in was obtained. The uniformities of the fan-in using the fixed Mask2 and using the adjustable Mask3 are shown in Fig. 4.13 (a) and (b), respectively. Comparing the two figures, we found that the uniformity has been greatly improved by the adjustable mask.

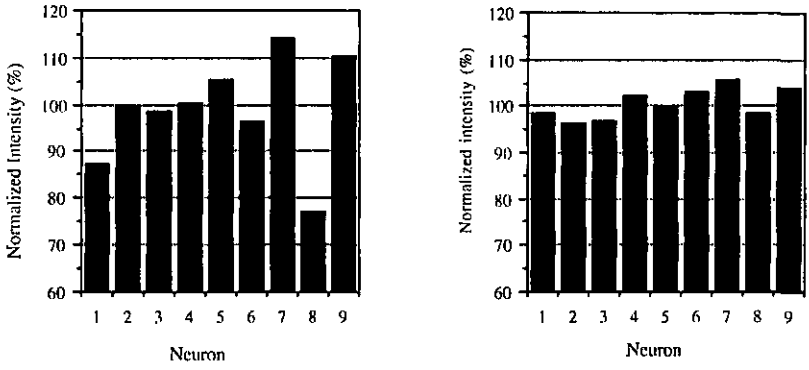

(a) *(b)*

Fig. 4.13 Uniformity of the fan-in for the fixed Mask2 (a) and the adjustable Mask3 (b).

C. Uniformity of the dynamic response

The response speed and the sensitivity of the LCLV are also spatially nonuniform. The response time for each neuron was measured. Note that the rise time of each neuron decreases with increasing the write intensity, but the switch-on energy which is defined as the product of the rise time and the write intensity, is a constant. Therefore, the switch-on energy was used as the measure of the uniformity of the dynamic response and shown in Fig. 4.14

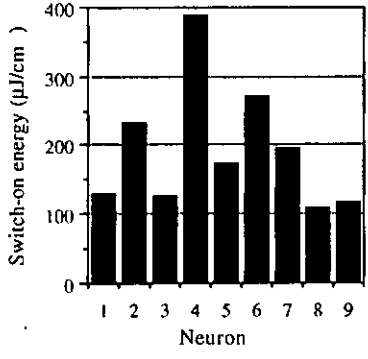

Fig. 4.14 Uniformity of the switch-on energy.

It can be seen that the maximum nonuniformity of the switch-on energy is about ±60%, which is much larger than that of neurons and of interconnections. Some

neurons need very high energy to switch on, e.g. the switch-on energy of neuron 4 is about four times higher than that of neurons 8 and 9. Therefore, this nonuniformity severely influenced the dynamic behavior of the system.

4.3 DYNAMIC BEHAVIOR OF THE ONN SYSTEM

The all-optical feedback network shown in Fig. 4.7 has been used to experimentally realized the inhibitory and inverted models. The only difference between the two models is in the interconnection matrix, therefore we need only to change the mask accordingly. The memory patterns stored in the masks are the letters "T" and "L". The experimental results fall roughly into two categories no matter which neural model: Fast converging to one stable state and Slowly evolving to a regular oscillation. Therefore in the following we give the experimental results in accordance with its properties rather than the type of the model.

4.3.1 One Stable State

Let us begin with the inhibitory model(using Mask2). First the system was set at the initial state with an input pattern "L" (Fig. 4.15(a)), and the read-in intensity was 1 mW/cm^2. Once the feedback was opened the network converged immediately to the stable state (Fig. 4.15(b)).

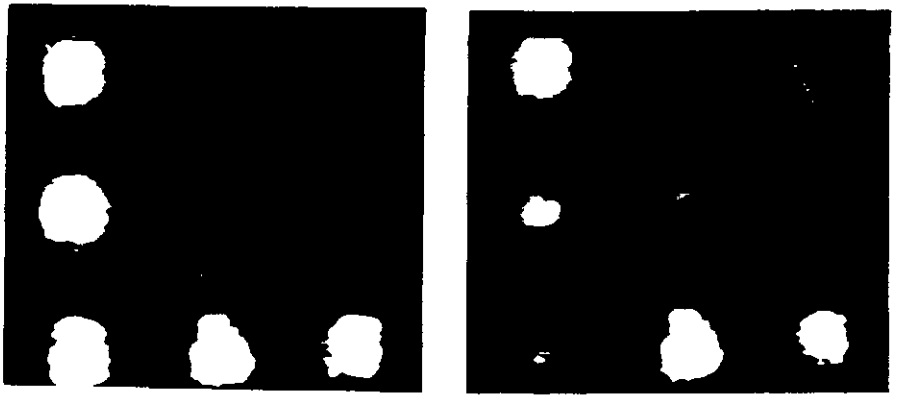

(a) *(b)*

Fig. 4.15 An initial input "L"(a) and the final stable state (b).

Actually this stable state was independent of the initial state, i.e. the system always converged to the state even if there was no initial pattern. To test the stability of the state we changed the read-in intensity up to ± 25% by rotating the half wave plate shown in Fig. 4.7 and found that the stable state is not sensitive to the changes though the contrast of the neurons changed.

The nonuniformities have a great influence upon the stable state. For example, when the LCLV was moved at slow speed (0.14 mm/s) by a micro-translation stage, we found that the state was changed accordingly. Figure 4.16 shows two more stable states corresponding to the movement of 3 mm and 6 mm, respectively.

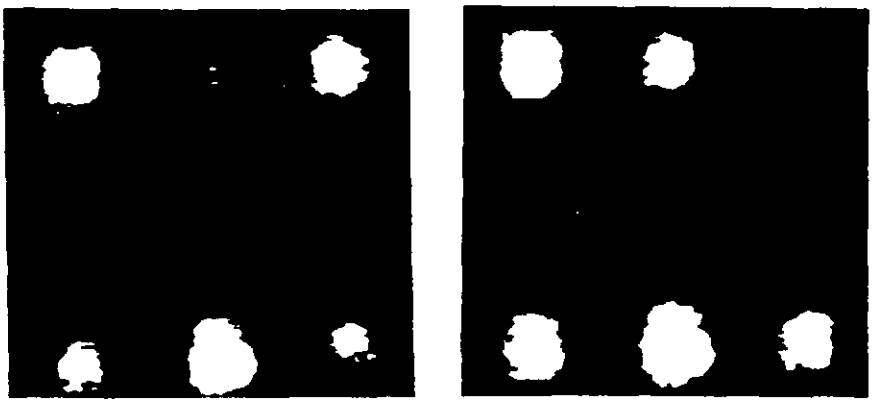

(a) *(b)*

Fig. 4.16 The stable states after the movement of 3mm (a) and 6mm (b).

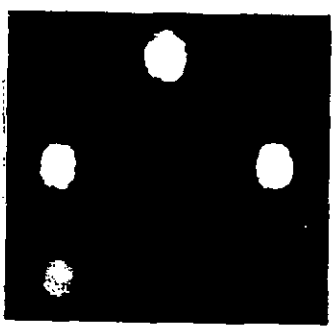

Fig. 4.17 Stable state for adjustable mask,.

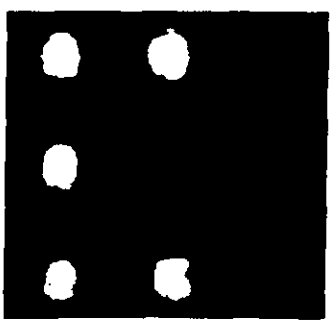

Fig. 4.18 Stable state for adjustable mask, by reducing the intensity of N6.

To minimize the nonuniformity the adjustable mask (Mask3) was used instead of the fixed mask (Mask2). We run the system again after carefully adjusting the mask so as to obtain the best uniform fan-in. However the system still stabilized on one state

shown in Fig. 4.17, regardless of the initial input. If we reduced the output intensity of the sixth neuron N6 by inserting a transparency, then we got another state shown in Fig. 4.18. This change of state can be understood easily from the mask (Fig. 4.4). Because N1 and N8 are only connected to the N6, a weaker N6 will allow N1 and N8 to be on. In turn, N1 and N8 force N6 off.

We also tried the inverted model and obtained similar results, i.e. always one stable state. It is quite clear that the one stable state is not due to the nonuniformities in the intensities of the neurons. There must be an inside dynamics in the system, which dominates the evolution. It was noticed that the dynamic responses of the neurons are spatially nonuniform as well, and these nonuniformities must be compensated during the operation of the system. This resulted in a new result — Oscillation!

4.3.2 Oscillation

The initial motivation of adjusting the weights was to correct the nonuniform dynamic responses of the neurons. To explain the idea, first we analyze the relation between the neurons in the inhibitory model. From the mask (Fig. 4.4), we find that the neurons can be divided into two independent groups (Group A and Group B) as shown in Fig. 4.19(a) and (b).

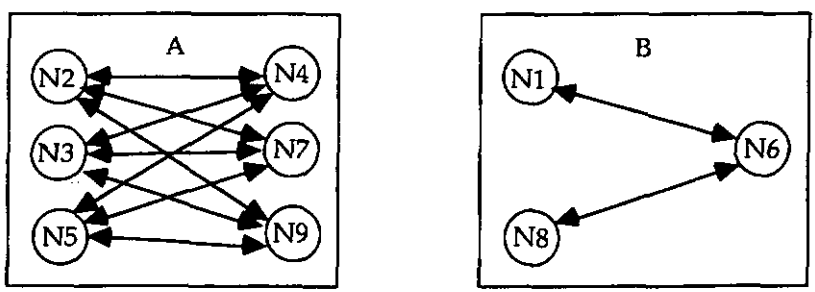

Fig. 4.19 The relations between the neurons in the inhibitory model.

The interconnections indicated by arrow lines are inhibitory (negative weights), also called "frustrated" or "competitive", i.e. each neuron excludes another neuron from having the same state by means of the connection. Therefore, there will be competition between the two sides in each group after opening the feedback loop. Suppose the left-sides in both group A and B won the competition, then the neuron N1, N2, N3, N5, and N8 keep ON-state while others turned off. This gives a steady

state " T" (see Fig. 4.6(a)). If the right-side won in group A while the left-side won in the group B, then the steady state is "L".

In the experiment with the adjustable mask, the intensity of the fan-in is nearly uniform, however the response is quite different for different neurons as shown in Fig. 4.14. We found that N3 and N9 were extremely sensitive and respond to the input very fast. As soon as the feedback was opened, they turned immediately off. In contrast, N4 and N6 had a high threshold and slow response, thus they were always on. Therefore the competition and evolution of the states were fully dominated by a few neurons which can be called dominators. As a result we obtained a strange steady state as shown in Fig. 4.17. Any dominator can be frustrated by changing the inhibitory strength to it, e.g. increasing the strength to N6 and decreasing the strength to N9, a memory state "L" was retrieved (Fig. 4.20). However there was still one stable state. We believe that if we increase the strength to N4 and decrease the strength to N3 such that their response speed are comparable with that of others, then we eliminate all dominators and make all neurons equal. In this case, the memory patterns "T" and "L" have equal opportunity to win the competition, the direction of the evolution will be dependent on the initial input. Essentially the way to modify the weights here is coincident with Hebb's idea.[70,76]

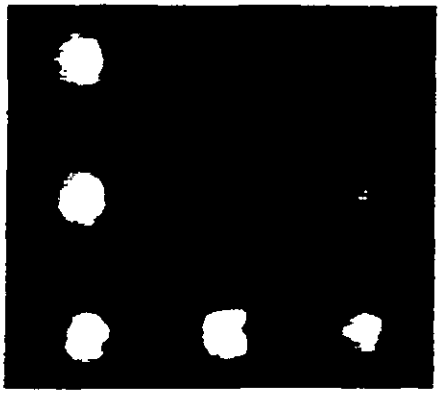

Fig. 4.20 A steady state evolved from Fig. 4.17 by changing some weight strength.

Following the idea above, we tried to modify the interconnection weights while the system was running. When we were changing the weights to N3 and N4, we observed that the switching speed of N3 slows down and that of N4 speeds up. The evolution also slowed down, though it still converged to "L". The longest evolution took 20 seconds. Therefore we could see the interesting dynamics. After further optimizing the weights, we gave the system a initial input "T", and found that it very

slowly evolved to "L", but it did not stop on "L", surprisingly, the "T" came back again! The system entered a regular oscillation state. Fig. 4.21 gives the intensities of the neurons in Group A as a function of time for initial pattern "T". In order to simplify the discussion without losing generality, we keep the intensities of the neurons in Group B constant, i.e. N1 and N8 are always ON while N6 is OFF.

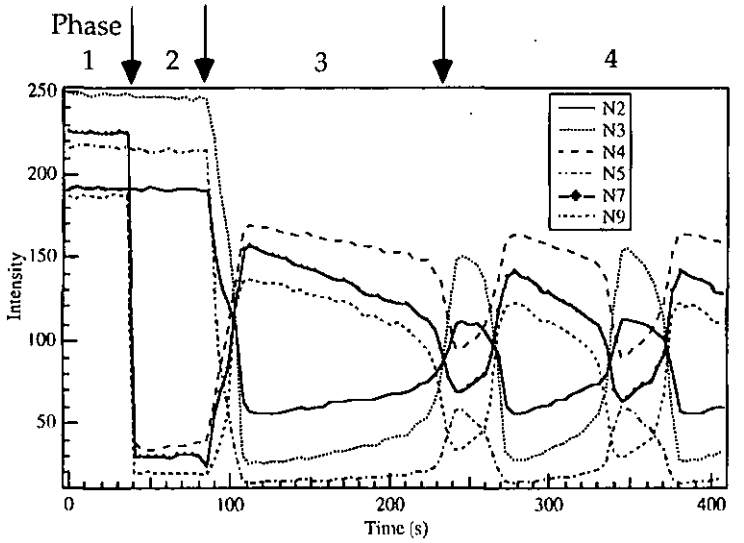

Fig. 4.21 Dynamics of the inhibitory NN for initial pattern "T".

It can be seen from the figure that the system goes through four phases: In the first phase, the feedback loop was closed and without initial input, therefore all neurons were ON though the intensities were not uniform. In the second phase , the feedback loop was still closed, but the system was set at the initial pattern "T". As soon as the feedback loop was opened, the system underwent a period of transition, the third phase. The length of the transition took 2~4 minutes depending on the initial input. At the beginning, all neurons tend to its opposite states, and then gradually evolved into the fourth phase: regular oscillation. The cycle time is about 100 seconds. We found that the dynamic range (amplitude) of each neuron in the oscillation became smaller than the initial state. If we decrease the intensity of the read-in light below a value of 700 $\mu W/cm^2$, the oscillation stops and all neurons are ON. In this case, the effective gain of the system is less than one, therefore the system can not work normally.

4.4 ANALYSES AND DISCUSSIONS

In this section an interpretation of the experimental results is given.

4.4.1 The Response Time of the Neuron and the Oscillation

First we define two time delays in the ONN. The propagation time is the time for transmission of the signal from one neuron to another. The response time is the delay time of the output behind the input of a neuron. Comparing our ONN system with Hopfield's electric NN system (H-system),[73] we found that there is a fundamental difference in the propagation and response time. In the H-system the connection weights are realized by the use of resistors, which are also the main source of the propagation time. The neuron's response time depends on the nonlinear amplifier. Hopfield assumed that the amplifiers are fast compared with the characteristic RC time of the network, therefore the response time was negligible. Based on this hypothesis, he concluded that under symmetric interconnections the system will converge to stable states and cannot oscillate or display chaotic behavior. However, in our ONN the signals between the neurons are transmitted by light in free space, the propagation time can be as short as 10 ns (suppose the optical path about 3 m). In contrast, the response time of the neuron (LCLV) is much longer, typically 120 ms. Therefore in our ONN Hopfield's assumption breaks down. It was this difference that resulted in the instability of the system. Actually our ONN system is a typical complex dynamic system which may have fixed attractors, oscillation attractors, and chaotic attractors.[77] Theoretical analyses and explanation of the system's dynamics are beyond the scope of the thesis. In the following we make a comparison between our ONN and a electronic analog neural network to understand why the oscillation happened.

Marcus reported a study on the oscillatory attractors in an electronic analog neural network.[78] His system was quite similar to Hopfield's system, but included a controllable CCD (charge coupled device) analog time delay in each neuron. He found that a network which is stable with no delay can have basins for oscillatory attractors when time delay is present. He obtained following conclusions:

(1)It is the ratio of response time to propagation time which is important for stability, the basin size of an oscillatory attractor increases with the ratio. The studies were based on a range for the ratio for oscillation between 0.48 and 0.61.

(2)The negative connections are a necessary condition for sustained oscillation. In a fully connected frustrated network there may exist both oscillation attractors and fixed attractors. The larger the frustrated network, the more easily it oscillates. For a given value of response/propagation time ratio, the size of the oscillatory basin increases with the number of the frustrated connections.

(3)The oscillatory modes can be eliminated by diluting the interconnection matrix.

Our ONN system may be equivalent to a diluted frustrated network. The ratio of response/propagation time in the system is as high as 10^7, thus oscillation is probable. Moreover, since all the connections in both the inhibitory and inverted model are negative, the oscillation mode will be further encouraged. The interconnection matrix in the inhibitory and inverted models is diluted due to discarding the positive connections. However it is not enough to balance the effects of the slow response and the negative weights. From these analyses it seems that the oscillation should be the inevitable and the only result in our system, but actually, as we described in the last section, the oscillation was not so easy to obtain. There must be other conditions which are necessary to either produce oscillation or maintain a stable state. We noted that in Marcus' system every neuron has the same response delay, but in our system each neuron has a different response time due to the nonuniformity. It is this nonuniform response which effectively prevents the oscillation. In our experiment the fan-in intensity to each neuron had to be adjusted so as to minimize the difference between the neurons. This procedure can be compared to the phase match, i.e. making all neurons have nearly the same response time. There must be a acceptable range for the response time since it is impossible to get it exactly the same for all neurons in the experimental system.

The cycle time of our system is much longer than that of Marcus' system. The difference is probably due to the existence of positive interconnections in his system, which can accelerate the evolution.

4.4.2 The Gain, the Transfer Characteristic and the One Steady State

Our experimental system only gave one steady state. This indicates that there is only a global minimum rather than local minima in the system. The nonuniformity, of course, may result in spurious attractors, but should not eliminate the local minimum. Actually the one steady state comes from the combination effects of the low gain in the ONN system and the less steep transfer characteristic. Hopfield analyzed the effects of the gain function on the local mimima and concluded that

when the steepness decreased below a critical value, there would be only one minimum.[73] There are other discussions about the gain curve and the discrimination capability of the neural system.[66,79] But all these analyses are qualitative. Next we give a quantitative analysis by use of Eq. (4.14).

The gain function $g_i(u_i)$ in our system is defined by

$$g_i(u_i) = \alpha_s \alpha_m G_v \tag{4.21}$$

where α_s α_m are constants (see Eq. 4.19); G_v is the effective gain of the LCLV, given in Eq. (2.23).

$$G_v = \frac{\eta I_{R\text{-}in}}{I_w(90\%)}. \tag{2.23}$$

Therefore, the gain function will have the same form as the transfer curve represented by S(x) in Eq. (2.29).

$$S(x) = -w_0 + \frac{w_1}{1 + \exp\{-w_2 - x/w_3\}} \tag{2.29}$$

The differentiation are given by

$$g_i' = \frac{w_1}{w_3} \frac{\exp\{-w_2 - u_i/w_3\}}{1 + \exp\{-w_2 - u_i/w_3\}}, \tag{4.22}$$

$$(\max_i |g_i'|)^2 = \left|\frac{w_1}{4w_3}\right|^2 \tag{4.23}$$

where the coefficients w_1, w_2, w_3, w_4 can be obtained by fitting the gain curve, but we are interested in only w_1 which quantifies the maximum gain, and w_3 which quantifies the steepness of the curve. Note that the maximum gain in the system loop is about one, i.e. it is just able to maintain the operation. The coefficients for the LCLV1 are shown in Table 4.2.

Valve	w_0	w_1	w_2	w_3
LCLV1	0.3989	1.3788	-0.93255	11.553

Table 4.2 Curve fitting coefficients for the gain curve of LCLV1.

By using Eq. (4.23), we obtain the following numerical value

$$1/(\max_i |g_i'|)^2 = 1123. \tag{4.24}$$

On the other hand, the sum of the normalized interconnection strength can be obtained by measuring the intensity behind the mask, then dividing by the threshold intensity $I_w(90\%)$. The measured value is 718, i.e.

$$\sum_{i=1}^{M}\sum_{j=1}^{M} T_{ij}^2 = 718. \tag{4.25}$$

Therefore our ONN system satisfied the inequality Eq. 4.14. This means that there is only one stable state.

$$\sum_{i=1}^{M}\sum_{j=1}^{M} T_{ij}^2 < 1/(\max_i |g_i'|)^2 . \tag{4.14}$$

The two parameters shown in Eqs. (4.24) and (4.25) are called the gain constant and the interconnection constant, respectively, which represent the system's gain and the interconnection strength of the model.

From Eq. (4.23) we found that it is the ratio of the gain to the slope which is important for associative memory. When the ratio decreases, i.e. low gain (high loss) or/and less sharp transfer curve, the number of the local minima decreases accordingly. There is a critical value of the ratio below that there exist only one global minimum in the system, therefore, the system loses the function as an associative memory. The critical value of the gain constant is given in Eq. 4.25. It is interesting to note that the critical value is related to the interconnection strength. The less the interconnections, the higher is the critical value. From this point of view, the inhibitory and inverted model have a disadvantage for realizing associative memory because the masks of the two models are diluted. The conclusion is based on the static transfer characteristic. If we consider the response delay in the neurons, the slope of the dynamic transfer curve is even lower. Therefore higher gain or more interconnections are necessary to obtain the multi-stable state. We believe that if we could find a new model with the interconnection constant greater than 1123, there would exist local minima in our system.

Many optimization problems can be defined by the minimization of the energy function of a neural network system. In these applications it is desired to design the system which has only one global minimum. This is just the advantage of our ONN, in which the global equilibrium can be easily obtained, and oscillation is effectively prevented by the nonuniform delay of response.

4.5 LIMITATIONS OF THE OPTICAL NEURAL NETWORK AND CHALLENGE TO LCLV

4.5.1 Limitations of the Optical Neural Network

The key hardware in the optical neural network (ONN) is the LCLV, therefore, the performance of the system was limited to a great extent by the LCLV. The first limitation is the low gain of the valve. The actual value of the gain sets a maximum gain for the system, so some compromises were made in the system design, e.g. using photographic mask instead of a LCD. The low gain also affected the dynamics of the system as shown in Eq. 4.23, and thus degraded the associative memory function. The second limitation is the graded transfer characteristic and the slow response time. We have seen that, in order to realize the associative memory a steeper transfer curve is better. The slow response time increases the possibility of oscillation. The third limitation is the nonuniformity which is the combined effect of the LCLV and the fan-out gratings. This nonuniformity is a fatal weakness in the system with fixed interconnections. The last limitation is the spectral sensitivity of the LCLV, which is out of the spectral range of the Ar^+ laser. A dye laser was used in the system, thus greatly increasing the system's complexity.

Another important component in the system is the fan-out grating, which has two aspects to be improved. One is the efficiency, which is currently 36% for two crossed 1D gratings. The other is the nonuniformity of the diffraction orders. There are also some high order diffractions between these main orders, which causes noise in the system. All these can be improved by using the continuous phase 2-D gratings.[80,81]

Besides the imperfections in hardware, the system architecture has some limitations. One is the limitation on the number of neurons due to limited aperture of the fan-in lens L6 (see Fig. 4.7). According to the calculations in Ref. 82, the maximum neuron array is 16x16 for the aperture of 60mm and neuron spacing of 150 μm. The other limitation is from the fixed interconnections (mask). The fixed mask which is made independently of the system can not adapt to the nonuniformity. Therefore the final strength of the interconnections may deviate from the correct values. As a result the system will stabilized on states which are not the memory states in the mask. To overcome this problem, a modifiable mask and a learning algorithm should be used. The difficulty in the alignments of the neurons and the mask will greatly increase with the number of the neurons. Therefore, the precise control of the alignment will be a big problem if the number of the neurons is further increased.

Some limitations come from the models of ONN. Both the inhibitory and inverted model only use frustrated connections, which result in very high loss. On the other hand, the all negative connections make the system susceptible to oscillation. So the two models are not ideal ones for optical implementation. White et al. proposed a modified H-model.[83] Since it is based on a transformation of the variables rather than the modification of the dynamic rule, this model is more general than the inhibitory and inverted ones. However, to implement the model two separated interconnection channels are essential, thus the system will be more complex.

4.5.2 Challenge to LCLV

What are the basic requirements for the LCLV which is suitable for the optical neural network? First of all, effective gain is a must. An effective gain of 100 is necessary if we want to use the LCD as the mask instead of photographic plate. This requires that the LCLV should have high sensitivity, high read-out efficiency and a good light blocking layer. There has to be a compromise since the improvement of the light blocking layer will decrease the dynamic range of the LCLV, and therefore decrease the sensitivity. This is the big shortcoming for the LCLV. The transfer characteristic of LCLV should be steep so as to realize the associative memory. Fast response is another important parameter which has a great influence on the dynamics of the system. The nonuniformities of the reflectance and of the sensitivity across the working aperture should be minimized. To sum up, we hope to have a LCLV with fast response, better uniformity, high sensitivity, high efficiency, and high gain.

Although further device engineering could improve the performance of LCLV, the smart advance spatial light modulator (SASLM)[65] seems more promising to fulfil the above requirements. In SASLM the modulator and detector are pixellated. These pixels are connected by electronic circuits. In this way the read light can be very strong and there is no worry about the breakthrough. Therefore it is easy to obtain the high gain. More important is that the transfer characteristic can be controlled in the fabrication. The sensitivity (threshold) and the response time may be controlled or modified as well. This gives the SASLM a great flexibility to adapt different models of neuron networks and to compensate the nonuniformity electronically.

5

CONCLUSION

Liquid crystal light valve (LCLV) as a nonlinear thresholding and gain element plays a very important role in the optical neural networks (ONN). From the point of view of ONN system, a LCLV should be characterized by the parameters such as the effective gain, the spatial uniformity, the response speed, and the transfer characteristic represented by a sigmoid function. Of these parameters, the key is the effective gain. Building an ONN using a LCLV without effective gain is thus a dream. Even if the effective gain is greater than one, but not big enough to bear the loss of the system, it is still impossible to run the system. The effective gain which takes account of the sensitivity and the read-out efficiency, indicates the usability of a LCLV. Unfortunately, we have not found so far any supplier of LCLVs listing this parameter in their specifications. The spatial nonuniformity is a common and severe problem, which greatly increases the difficulty in implementing ONN. The nonuniformity of the reflectance can be corrected by using an adjustable mask. However the nonuniformity of the dynamic response (sensitivity and response speed) has to be compensated in the system by a learning procedure. The response speed greatly affects the dynamics of ONNs. Fast responding is advantageous to the realization of associative memories, and the alleviation of oscillations in the system. We have shown that using a sigmoid function to fit the transfer curve is an effective means of the characterization of LCLVs. The curve fitting can be used not only to compare the transfer characteristics of different LCLVs quantitatively, but also to analyze the effect of the LCLV on the dynamics of the system.

The characterization of three types of liquid crystal light valves has been performed. We found that the LCLV using amorphous hydrogenated silicon (a-Si:H) as the photoreceptor has a faster response speed and a wider spectral range than the one using cadmium sulfide (CdS), however the latter has better sensitivity. The twisted nematic configuration gives better contrast ratio, but has very low read-out efficiency. The ferroelectric liquid crystal light valve (FLCLV) has fast response and the potential to obtain the effective gain because of using metal mirrors instead of dielectric mirrors. However, the FLCLV cannot be directly used to replace the nematic one in ONN because of its clock operation mode, i.e. alternatively reading

and writing. In order to use FLCLV in ONN, one has to append a temporary memory element, thus increasing the complexity of the system.

Optical neural networks (ONNs) possess not only the advantage of 3-D global interconnections, like the optoelectronic neural networks, but have also its own properties. The inherent peculiarity of ONNs lies in the fast communication speed between the neurons and the relatively slow response speed of each neuron. This results in a quite different behavior of ONNs compared to other neural network implementations. We have designed and built an ONN based on the Hopfield model. The ONN shows more complex and rich behavior, including oscillations. These complex behavior is well known in biological neural systems. This similarity signifies that the ONN with a simple structure may be used to study a very complex system. In contrast, these complex behavior has never been observed in the optoelectronic neural network (OENN) or in the hybrid simulator. This fact means at least that the ONN has different dynamics than the OENN or the hybrid simulator.

The dynamic behavior of the ONN depends on the parameters of the system and on the interconnections. The main parameters are the two ratios: the ratio of the response time to the propagation time and the ratio of the gain of the system to the slope of the transfer curve. The response speed of the ONN is limited by the LCLV, thus the time ratio is very high. The high time ratio increases the probability of oscillations. Using faster neurons is welcome, however, we should not hope for any dramatic change of the time ratio in the near future. Our experiments showed that the oscillations occur when all neurons have similar response speed. Fortunately, the nonuniformity of the LCLV can effectively prevent the oscillation. The ratio of the gain to the slop influences the system's capability for associative memory. Our ONN system gave only one stable state, and no other local minimum was observed. Therefore the system lost the function as an associative memory. This was because the ratio of the gain to the slop was below a critical value determined by the interconnection strength.

The interconnections depend on the neural network model. In our experiments we used the inhibitory model and the inverted model. The interconnections in the two models are all negative, which increases also the probability of oscillations. Moreover, because of the deletion of all positive interconnections, the feedback efficiency of the two models is very low. This is disadvantageous for the realization of an associative memory. Therefore the two models are not ideal ones for ONNs.

The performance of the ONN system can be further improved in many aspects. We believe that a new generation of spatial light modulators (SLMs) with high gain and

modifiable transfer characteristic, such as the Smart SLM, will greatly enhance its flexibility and capability. The fan-out gratings with high efficiency and good uniformity are available. The interconnection mask may be replaced by a LC modulator which can modified each pixel individually and give continuous grey levels.

Our research on the dynamics of ONN is just preliminary. What we have learned about ONNs is far from comprehensive. There is still much work to be done. The conditions for associative memory need to be proved experimentally. Although we have tried experimentally to compensate the nonuniformity of the dynamic response in the ONN, a mathematical model for this procedure has not been introduced yet. New models of neural networks suitable for ONN have to be developed. Finally, what can ONN do? We are still unable to answer this question. But how can you answer that question before you really understand Optical Neural Networks.

ACKNOWLEDGEMENTS

I would like to express my gratitude to Prof. R. Dändliker, the director of this thesis, who gave me the opportunity to come to Switzerland, and for his constant support, encouragement and guidance throughout these past years.

I would also like to thank Prof. A. Shah and Dr. H. White for their comments and their interest in reviewing my thesis as members of the jury.

I would like to thank Dr. N. Collings who took charge of the project related to this thesis, for his helpful discussions and the corrections related to this manuscript. I would especially like to thank Dr. Ken Weible for his many assistance. Not only has he given valuable advice on the research work, but he has always been present when I need help: searching apartment, dealing with police, and so on. Without his friendship I would really have hard times. Also, I would like to thank all colleagues and the secretarial staff in the institute for their assistance. Special thanks go to Drs. R. Thalmann, G. Pedrini, D. Prongué, and B. Acklin.

致谢

我衷心地感谢我的父母。他们不仅养育了我，而且全力支持和鼓励我走上科学之路。

我衷心地感谢自小学以来给予我指教和关心的老师们。

我衷心地感谢我的妻子晓英和女儿碧碧。在过去的十年间，她们以无私的奉献精神、纯真的爱和超人的忍耐力，承担了精神上和生活上的全部重负，使我得以先后完成硕士学位，考取博士研究生，出国学习，直到完成这个论文。如果没有她们始终如一的理解，支持和爱，这一切都是不可能的。

REFERENCES

1. A. D. Fisher, "Spatial light modulators: functional capabilities, applications, and devices," Int. J. Optoelectro. **5**, 125-167 (1990).
2. D. Casasent, "Coherent light valves," *Applied optics and optical engineering*, R. Kingslake (Ed.), Academic Press, New York, 143-200 (1979).
3. Special issue of Applied Optics on SLMs for optical information processing, Appl. Opt. **28**, 4715-4954 (1989).
4. Special issue of Applied Optics on SLMs for optical information processing, Appl. Opt. **31**, 3857-4072 (1992).
5. T. D. Beard, W. P. Bleha, and S. Y. Wong, "AC Liquid-crystal light valve," Appl. Phys. Lett. **22**, 90-92(1973).
6. G. Moddel, "Amorphous silicon for optically addressed spatial light modulators," *Amorphous and microcrystallinesemiconductor devices: optoelectronic devices*, J. Kanicki (Ed), (Artech House, Boston, 1991) pp369-412.
7. D. Jared and K. M. Johnson, "Optically addressed thresholding very large scale integration liquid crystal SLM," Opt. Lett. **16**, 967-969 (1991).
8. T. Drabik and M. A. Handschy, "Silicon VLSI/FLC technology for micropower optoelectronic computing devices," Appl. Opt. **29**, 5220-5223 (1990).
9. A. D. Fisher and J. N. Lee, "The current status of two-dimensional spatial light modulator technology," Proc. SPIE 634, 352-371 (1986).
10. C. Warde and A. D. Fisher, "Spatial light modulators: Applications and functional capabilities," in *Optical signal processing*, J. Horner, Ed., (Academic Press, San Diego, 1987).
11. F. J. Pineda, "Dynamics and architecture for neural computation," J. Complexity 4, 216-245 (1988).
12. J. J. Hopfield, "Neural networks and physical systems with emergent collective computational abilities," Proc. Natl. Acad. Sci. USA **79**, 2554-2558 (1982).
13. T. Kohonen, *Self-Organisation and Associative Memory*, (Springer-Verlag, Berlin, 1984).

14. G. A. Carpenter and S. Grossberg, "ART3: Hierarchical search using chemical transmitters in self-organizing pattern recognition architectures," Neural Network **3**, 153-176 (1990).

15. N. H. Farhat, D. Psaltis, A. Prata, and E. Paek, "Optical implementation of the Hopfield model," Appl. Opt., **24**, 1469-1475 (1985).

16. J.-S. Jang, S.-W. Jung, S.-Y. Lee, and S.-Y. Shin, "Optical implementation of the Hopfield model for two-dimensional associative memory," Opt. Lett. **13**, 248-250 (1988).

17. H. J. White, "Experimental results from an optical implementation of a simple neural network," SPIE **963**, Optical Computing' 88, 570-575 (1988).

18. I. Shariv and A. A. Friesem, "All-optical neural network with inhibitory neurons," Opt. Lett. **14**, 485-487 (1989).

19. K.-Y . Hsu, H.-Y. Li, and D. Psaltis, "Holographic implementation of a fully connected neural network", Proc. of IEEE **78**, 1637-1645 (1990).

20. L.-S. Lee, H. M. Stoll, and M. C. Tackitt, "Continuous-time optical neural network associative memory," Opt. Lett. **14**, 162-164 (1989).

21. T. Lu, X. Xu, S. Wu, and F. T. S. Yu, "Neural network model using interpattern association," Appl. Opt. **29**, 284-288 (1990).

22. C. Powles, B. Pollock, S. Reid, and M. Powell, "Enhancement of optically addressed liquid crystal SLM performance for specific applications by selection of input polarisation," Proc. SPIE **1151**, 507-521 (1990).

23. K M. Johnson and G. Moddel, "Motivations for using ferroelectric liquid crystal spatial light modulators in neurocomputing," Appl. Opt. , **28**, 4888 (1989).

24. T. D. Hudson, R. K. Worcester, and D. A. Gregory, "Performance characteristics of an optical addressed ferroelectric liquid-crystal spatial light modulator," Appl. Opt., **30**, 2867-2872 (1991).

25. Kanghua Lu and Bahaa E.A. Saleh, "Complex amplitude reflectance of the liquid crystal light valve", Appl. Opt. **30**, 2354-2362 (1991).

26. N. H. Farhat and M. Eldefrawy, "The bifurcating neuron: characterization and dynamics," in Photonics for Computers, Neural Networks, and Memories, W. J. Miceli, J. A. Neff, S. T. Kowel, Eds, Proc. SPIE **1773**, 23-35 (1992).

27. N. H. Farhat, "Chaotic neurons," in Adaptive Computing: Mathematics, Electronics, and Optics, Su-Shing Chen, H, J. Caufield, Eds, Proc. SPIE **CR55**, (1994).

28. Special issue of IEEE transactions on circuits and systems on Chaos in Nonlinear Electronic Circuits, IEEE Trans. Circuits and systems **40**, No.11 (1993).

29. Birendra Bahadur, *Liquid crystals: applications and uses*, Vol.1, World Scientific, (1990).

30. P. G. de Gennes, *The physics of liquid crystals*, Clarendon, Oxford (1975).

31. J. S. Patel and J. W. Goodby, "Properties and applications of ferroelectric liquid crystals," Opt. Eng. **26**, 373(1987).

32. S. Chandrasekhar, *Liquid crystals*, Cambridge University Press (1992).

33. A. Shah, *Matériaux électroniques amorphes*, Vol.2, Institute de Microtechnique, Université de Neuchâtel (1992)

34. P. Ciureanu and S. Middelhoek, *Thin film resistive sensors*, chapter 2, IOP publishing Ltd (1992).

35. Ben G. Streetman, *Solid state electronic devices*, Prentice-Hall, Inc., Englewood cliffs, NJ 07632 (1980).

36. W. P. Bleha, L. T. Lipton, E. Wiener-Avnear, J. Grinberg, P. G. Reif, David Casasent, H. B. Brown and B. V. Markevitch, "Application of the liquid crystal light valve to real-time optical data processing," Opt. Eng. **17**, 371-384 (1978).

37. L. Samuelson, H. Wieder, C. R. Guarnieri, J. Chevallier, and A. Onton, "Fast photoconductor coupled liquid-crystal light valve," Appl. Phys. Lett. 34(7), 450-452 (1979).

38. P. R. Ashley and J. H. Davis, "Amorphous silicon photoconductor in a liquid crystal spatial light modulator," Appl. Opt. **26**, 241-246 (1987).

39. K. Sayyah, M. S. Welkowsky, P. G. Reif, and N. W. Goodwin, "High performance single crystal silicon liquid crystal light valve with good image uniformity," Appl. Opt. **28**, 4748-4756 (1989).

40. I. Abdulhalim, G. G. Moddel, and K. M. Johson, "High-speed analog spatial light modulator using a hydrogennated amorphous silicon photosensor and an electroclinic liquid crystal," Appl. Phys. Lett. 55(16), 1603-1605 (1989).

41. G. Moddel, K. M. Johson, W. Li, and R. A. Rice, "High-speed binary optically addressed spatial light modulator," Appl. Phys.Lett. 55(6), 537-539 (1989).

42. T. Horikawa, S. Tahata, S. Kaho, T. Masumi, N. Mikami, K. Takahashi, M. Nunoshita, H. Nakajima and K. Nishi, "Ferroelectric liquid crystal light valve using SiO_2/a-Si:H Photodiode," Mat. Res. Soc. Symp. Proc., **219**, 203-208 (1991).

43. P. R. Barbier and G. Moddel, "Hydrogenated amorphous silicon photodiodes for optical addressing of spatial light modulators, Appl. Opt. **31**, 3898-3907 (1992).

44. Bahaa E. A. Saleh and Malvin C. Teich, *Fundamentals of photonics*, John Wiley & Sons, Inc., 1991.

45. U. Efron, J. Grinberg, P. O. Braatz, M. J. Little, P. G. Reif, and R. N. Schwartz, "The silicon liquid crystal light valve," J. Appl. Phys. **57**(4), 1356-1368 (1985).

46. D. Armitage, J. 1. Thackara, and W. D. Eades, "Photoaddressed liquid crystal spatial light modulators," Appl. Opt. **28**, 4763-4771 (1989).

47. P.Aubourg, J. P. Huignard, M. Hareng, and R. A. Mullen, "Liquid crystal light valve using bulk monocrystalline $Bi_{12}SiO_{20}$ as the photoconductive material," Appl.Opt. **21**, 3706-3712 (1982).

48. W. E. Haas, "Liquid crystal display research: the first fifteen years," Mol. Crys. & Liq. Crys. **94**, 1-31(1983).

49. R. A. Soref and M. J. Rafuse, "Electrically Controlled Birefringence of thin nematic films," J. Appl. Phys. **43**, 2029-2037 (1972).

50. M. Nakamura and M. Ura, "Alignment of nematic liquid crystals on ruled grating surface," J. Appl. Phys. **52**, 210-218 (1985).

51. W. J. A. M. Hartmann and A. M. M. Luyckx-Smolders, "The bistability of the surface-stabilized ferroelectric liquid-crystal effect in electrically reoriented chevron structures," J. Appl. Phys. **67**, 1253-1261 (1990).

52. J. L. de Bougrenet de la Tocnaye and J. R. Brocklehurst, "Parallel access read/write memory using an optically addressed ferroelectric spatial light modulator", Appl. Opt. **30**, 179-180 (1991).

53. S. Fukushima, T. Kurokawa, and M. Ohno, "Ferroelectric liquid-crystal spatial light modulator achieving bipolar image operation and cascadability", Appl. Opt. **31**, 6859-6868 (1992).

54. D. Casasent, "Performance evaluation of spatial light modulators," Appl. Opt., **18**, 2445-2453 (1979).

55. E. Jakeman and E. P. Paynes, "Electro-optic response times in liquid crystals," Phys. Lett., **39A**, 69-70 (1972).

56. Igor is copyrighted program of WaveMetrics. Macintosh is trademark of Apple computer, Inc..

57. R. C. Jones, "New calculus for the treatment of optical systems," J. Opt. Soc. Am. **31**, 488-493 (1941).

58. A. Yariv and P. Yeh, *Optical Waves in Crystals*, Chapter 5, John Wiley & Sons, Inc., (1984).

59. R. M. A. Azzam and N. M. Bashara, *Ellipsometry and polarized light*, (North-Holland Physics Publishing, 1987).

60. The nematic LCLV is a valve fabricated in 1983 for our institute by ASULAB S.A. in Neuchâtel, Switzerland.

61. Marconi Research Centre *Techbrief* No M342, 'Amorphous Silicon Nematic Spatial Light Modulator'.

62. D. Williams, et al., 1988, 'An amorphous silicon/chiral smectic spatial light modulator', J.Phys. D, **21**, S156-S159.

63. W. Xue and B. Acklin, Data acquisition programs using DAS16G/F board, Users Guide.

64. Y. Sakai and H. Okimura, "Properties of photoconductive CdS evaporated films", Jap. J. Appl. Phys. **3**, 144-149 (1964).

65. IEEE LEOS Topical Meeting on Smart Pixels (Santa Barbara, August 10-12, 1992).

66. K. Hsu and D. Psaltis, "Invariance and discrimination properties of the optical associative loop", Proc. IEEE conf. Neur. Networks, II, 359-402 (San Diego, July 1988).

67. A. W. Lohmann, Array illuminators and complexity theory, Opt. Comm., Vol.89, 167-172 (1992).

68 T. Hara, Y. Ooi, Y. Suzuki and M. H. Wu, Transfer characteristics of the microchannel spatial light modulator, Appl. Opt., **28**, No. 22, 4781-4786 (1989).

69. S. V. B. Aiyer, M. Niranjan, and F. Fallside, "A theoretical investigation into the performance of the Hopfield model," IEEE Trans. Neural Net., **1**, No.2, 204-215 (1990).

70. R. Serra and G. Zanarini, *Complex systems and cognitive processes*, Springer-Verlag (1990).

71. N. H. Farhat, S. Miyahara, and K. S. Lee, "Optical analog of two-dimensional neural networks and their application in recognition of radar targets," in *Neural Networks for Computing*, J. Denkar, Ed., (American Institute of Physics, New York, 1986), pp146-152.

72. I. Shariv, T. Grossman, E. Domany and A. A. Friesem, "All-optical implementation of the inverted neural network model," *Optics in Complex*

Systems, F. Lanzl, H.-J. Preuss, G. Weight, Editors, Proc. SPIE 1319, 194-195 (1990).

73. J. J. Hopfield, "Neurons with graded response have collective computational properties like those of two-state neurons," Proc. Natl. Acad. Sci. USA, 81, 3088-3092 (1984).

74. A. F. Atiya, "Learning on general network," Proceeding of IEEE Conference on Neural Information Processing Systems, (D. Z. Anderson, ed.) Denver, CO, Nov.8-12, pp22-30 (1987).

75. F. B. McCormick, "Generation of large spot array from a single laser beam by multiple imaging with binary phase gratings," Opt. Eng. 28, 299-304 (1989).

76. D. O. Hebb, *The organization of behavior*, (Wiley, New York, 1949).

77. R. L. Ingraham, *A survey of nonlinear dynamics*, (World Scientific, Singapore, 1990).

78. C. M. Marcus and R. M. Westervelt, "Basins of attraction for electronic neural networks", Proceeding of IEEE Conference on Neural Information Processing Systems, (D. Z. Anderson, ed.) Denver, CO, Nov.8-12, pp524-533 (1987).

79. N. Collings and W. Xue, "Characterization of optically addressed SLMs for recurrent optical neural networks", Int. J. Opt. Compt. 2, 97-107 (1991).

80. H. P. Herzig, D. Prongué, and R. Dändliker, "Design and fabrication of highly efficient fan-out elements," jpn. J. Appl. Phys. 29, L1307-L1309 (1990).

81. A. Vasara et al., "Binary surface-relief gratings for array illumination in digital optics", Appl. Opt. 31, 3320-3336 (1992).

82. K. J. Weible, *Experimental investigation of optical neural networks and learning systems*, PhD Thesis, University of Neuchâtel, Neuchâtel, November 1993.

83. H. J. White, N. B. Aldridge, and I. Lindsay, "Digital and analogue holographic associative memories," Opt. Eng. 27, 30-37 (1988).

BIOGRAPHY

Wei Xue was born in Harbin, China, in 1956. He received his BS and MS degree from Harbin Institute of Technology in 1982 and 1984, respectively. From 1985 to 1989 he was an assistant and lecture in the Department of Applied Physics at Harbin Institute of Technology. He was a Ph.D. student in Harbin Institute of Technology during 1986-1989. He went to Switzerland and jointed Institute of Microtechnology, University of Neuchâtel, as an assistant in 1989. He received a Ph.D. degree in applied optics from University of Neuchâtel in 1994. His research interests include liquid crystal light modulators, optical information processing systems, holography, and dynamics of complex systems.

Part of the results in this thesis have been or will be published as regular papers in international journals or presented at conferences.

Publications:

1. N. Collings, W. Xue and G. Pedrini, "The Efficiency of Liquid Crystal Light Valves as Polarization Rotators", *Optics for Computers: Architectures and Technologies*, Guy J. Lebreton, Editor, Proc. SPIE 1505, 12-19(1991).
2. N. Collings and W. Xue, "Characterization of Optically Addressed SLM's for Recurrent Optical Neural Networks", Int. J. Optical Computing, 2, 97-107(1991).
3. W. Xue, N. Collings, and K.J.Weible "The Performance Characteristics of a Ferroelectric Liquid Crystal Light Valve with Pixellated Metal Reflector", Optical Computing & Processing, Vol.2, No.2, 107-114(1992).
4. N. Collings and W. Xue, "Liquid crystal light valves (LCLV) as thresholding elements in neural networks: basic device requirements", Appl. Opt. 33, to be published in May, (1994).

Conference papers:

5. W. Xue and N. Collings, "Polarization Behavior of a Ferroelectric Liquid Crystal Light Valve", in Spatial Light modulators and Applications Technical Digest, 1993 (Optical Society of America, Washington, D.C., 1993), Vol.6, pp. 93-96.
6. N. Collings and W. Xue, "Optically Addressed SLM Performance Criteria Relevant to Neural Network Application", Presented at 7èmes journées d'études les fonctions optiques dans l'ordinateur, Brest, France, 19-20 September 1991.
7. W. Xue and N. Collings, "Dynamic behavior of a neural network using liquid crystal light valve", presented at ICO Topical Meeting, Kyoto, Japan, 3-8 April 1994.